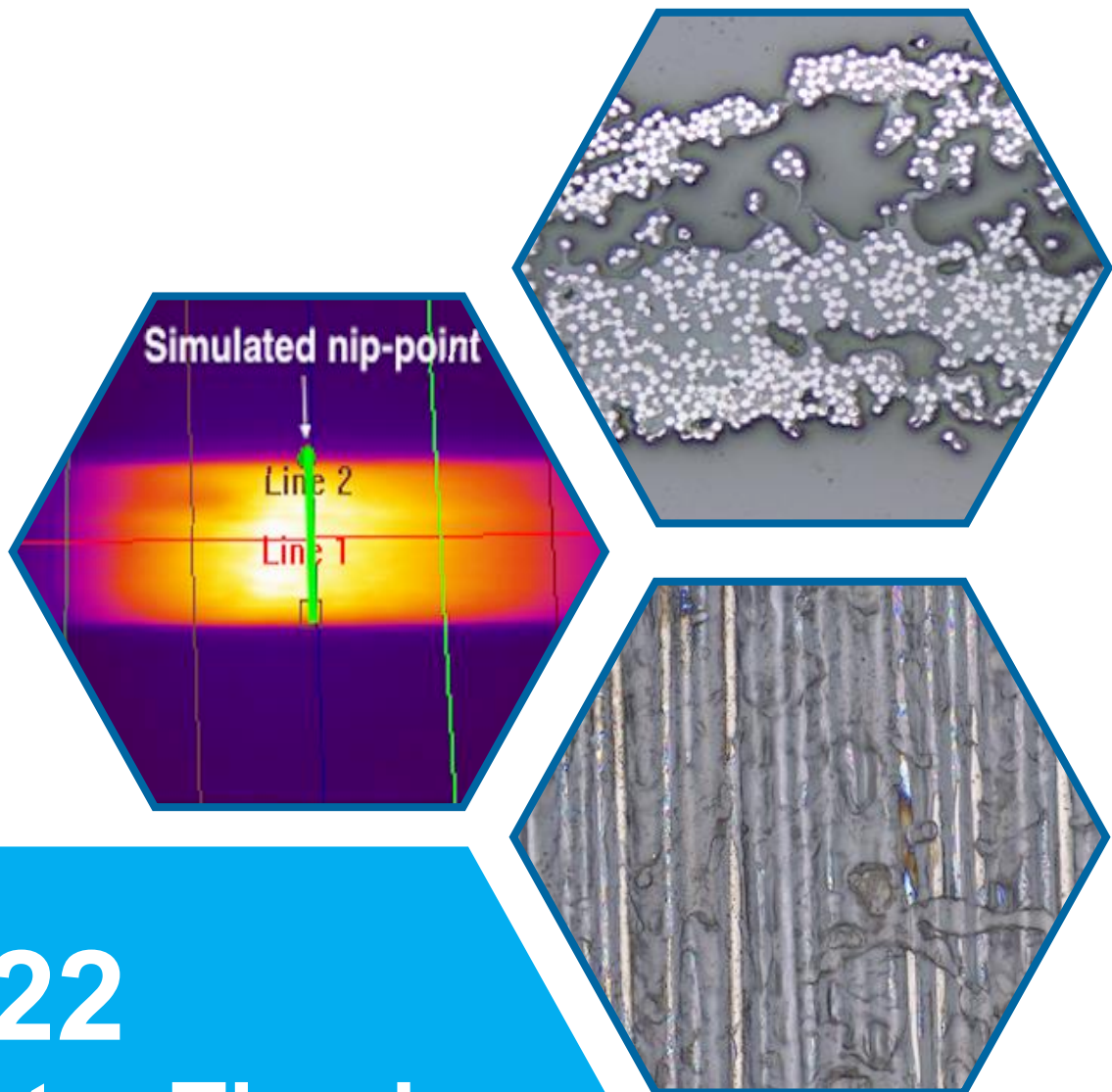


# Deconsolidation of thermoplastic prepreg tapes during the heating phase of LAFP

*An experimental investigation into the effect of a resin-rich surface and tape pre-tension*



**2022**  
**Master Thesis**

Yannick Michar Blommert



# Deconsolidation of thermoplastic prepreg tapes during the heating phase of LAFP

*An experimental investigation into the effect of a resin-rich surface and tape pre-tension*

by

**Yannick M. Blommert**

in partial fulfilment of the requirements for the degree of

**Master of Science**  
*in Aerospace Engineering*

at the Delft University of Technology.

To be defended publicly on Thursday 7 July 2022 at 14:00h.

Thesis committee:	Prof. Clemens Dransfeld	Chairholder, TU Delft
	Dr. ir. Julie Teuwen	Supervisor, TU Delft
	Dr. ir. Daniël Peeters	Supervisor, TU Delft
	Dr. ir. Otto Bergsma	External committee member, TU Delft
Secondary supervisor	Dr. Ozan Çelik	TU Delft

An electronic version of this thesis is available at <http://repository.tudelft.nl/>.



# DELFT UNIVERSITY OF TECHNOLOGY

FACULTY OF AEROSPACE ENGINEERING  
DEPARTMENT OF AEROSPACE MANUFACTURING TECHNOLOGIES

## GRADUATION COMMITTEE

Date of graduation: 7 July 2022

Chairholder:

---

prof. C.A. Dransfeld

Supervisor:

---

dr.ir. J.J.E. Teuwen

Supervisor:

---

dr.ir. D.M.J. Peeters

External:

---

dr.ir. O.K. Bergsma





# Abstract

Laser-assisted automated fiber placement (LAFP) is a promising additive manufacturing technique for the production of large aerospace components. Thermoplastic prepreg tapes will be placed ply-by-ply on top of a mould and in-situ consolidated. This is beneficial for higher production rates. The mechanical performance of thermoplastic composite laminates is highly dependent on the consolidation quality. One of the quality indicators is the maximum allowable void content after LAFP-manufacturing, which still exceeds the 1% limit for aerospace standards. Challenges remain before LAFP can be completely industrialized with the desired throughput and still obtaining the minimum required quality.

During the heating phase the material is heated to a processing temperature of around 400 °C within a very short heating time (0.2-0.8s) and no pressure application. As a result of rapid heating, interconnected mechanisms can occur which affect the final consolidation quality. These mechanisms and their relation with processing parameters need to be understood to achieve a high quality laminate manufactured by LAFP. Previous research at Delft University of Technology has shown that deconsolidation phenomena, such as decompaction of the fiber reinforcement network, waviness formation and void thermal growth occur during the heating phase. This will give rise to an increase in void content, surface roughness, out-of-plane deformation and dimensional changes. However, this research did not include tape pre-tension in the experimental setup which is the main component of a LAFP tape placement head. Also, thermoplastic prepreg tapes with a resin-rich surface have been suggested in literature to contribute to a higher consolidation quality of the final laminate. The effect on deconsolidation of thermoplastic prepreg tapes with resin-rich surface during the rapid heating phase is not known yet.

Therefore, the focus of this study is on the effect of a resin-rich surface and tape pre-tension on the deconsolidation response during the heating phase of LAFP. Deconsolidation was quantified through the following response variables (output): surface roughness, maximum out-of-plane deformation, void content, thickness increase and arc-length increase. The results showed that the processing parameters (heating time, heated spot length, resin-richness and tape pre-tension) affect the deconsolidation response through similar interlinked mechanisms as were observed before. However, it has been demonstrated that the mechanisms affecting the deconsolidation response are different due to the presence of a resin-rich surface and as a result of tape pre-tension.

Suprem resin-rich thermoplastic prepreg tapes have a great potential to be used together with the LAFP-process. It has been shown that a resin-rich surface contributes to significantly less decompaction of the fiber reinforcement network. This resulted in less surface roughness and less out-of-plane deformation after the heating phase. Because the fibers are surrounded by resin, no dry fibers are popping-out of the heated surface. The smoother and more resin-rich surface are beneficial for intimate contact development during the consolidation phase of LAFP. It is therefore expected that a higher degree of effective intimate contact can be reached with Suprem resin-rich tapes which is favourable for a higher final quality of a LAFP-manufactured laminate.

Laser heating experiments were performed with three levels of tape pre-tension: 5N, 10N and 15N. Increasing the level of tape pre-tension improved the contact between the tape and the surface of the tool. Since the tool worked as a heat sink in this case, it was shown that local heat absorption occurred only at locations where fiber clusters were present. Increasing the tape pre-tension level towards 10N and 15N seem to be disadvantageous for the LAFP-process. Large out-of-plane deformation was observed and the temperature data showed a highly non-uniform temperature across the simulated nip-point (for 10N and 15N) which is unfavourable for intimate contact development during the consolidation phase of the LAFP-process. It is therefore expected that the optimum pre-tension level lies around 5N. It is assumed that global out-of-plane decompaction and global surface roughness increase will remain lower if a low (5N) pre-tension force is applied.



# Contents

<b>List of Figures</b>	<b>ix</b>
<b>List of Tables</b>	<b>xiii</b>
<b>Nomenclature</b>	<b>xv</b>
<b>1 Introduction</b>	<b>1</b>
1.1 Background . . . . .	1
1.2 Motivation . . . . .	2
1.3 Objective . . . . .	3
1.4 Outline . . . . .	3
<b>2 Literature review</b>	<b>5</b>
2.1 Laser-assisted automated fiber placement . . . . .	5
2.2 Tape pre-tension . . . . .	6
2.3 Diode laser heating . . . . .	6
2.4 In-situ consolidation . . . . .	8
2.5 Bonding mechanism . . . . .	9
2.6 Heating phase parameters . . . . .	9
2.7 Effects of the heating phase on deconsolidation during LAFF . . . . .	11
2.7.1 Deconsolidation mechanisms . . . . .	11
2.7.2 Deconsolidation phenomena in the context of LAFF . . . . .	14
2.8 Conclusion . . . . .	16
<b>3 Research definition</b>	<b>17</b>
3.1 Research gaps identified in literature . . . . .	17
3.2 Research questions . . . . .	18
3.3 Hypothesis . . . . .	20
<b>4 Methodology</b>	<b>21</b>
4.1 Materials . . . . .	21
4.2 Experimental setup . . . . .	21
4.3 Characterization techniques . . . . .	23
4.3.1 Characterization of a resin-rich surface . . . . .	24
4.3.2 Temperature measurements . . . . .	25
4.3.3 Tape surface deformation measurements . . . . .	26
4.3.4 Surface roughness evaluation . . . . .	27
4.3.5 Cross-sectional microscopy . . . . .	28
4.3.6 Thickness measurements . . . . .	29
4.3.7 Void content evaluation . . . . .	29
4.4 As-received state tape material properties . . . . .	30
<b>5 Results: influence of heating time and heated spot length</b>	<b>33</b>
5.1 Test matrix . . . . .	33
5.2 Influence of heating time and heated spot length on the deconsolidation response of Toray-Ten Cate tapes. . . . .	34
5.2.1 Out-of-plane deformation . . . . .	34
5.2.2 Surface roughness . . . . .	35
5.2.3 Void content . . . . .	36
5.2.4 Arc-length increase . . . . .	37
5.2.5 Thickness increase. . . . .	37

5.3	Discussion . . . . .	38
5.4	Conclusion . . . . .	41
<b>6</b>	<b>Results: effect of a resin-rich surface on deconsolidation</b>	<b>43</b>
6.1	Test matrix . . . . .	43
6.2	Quantification of resin-richness. . . . .	44
6.3	Deconsolidation response of Suprem resin-rich tapes . . . . .	46
6.3.1	Surface roughness . . . . .	47
6.3.2	Out-of-plane deformation . . . . .	48
6.3.3	Void content . . . . .	50
6.3.4	Thickness increase . . . . .	52
6.3.5	Arc-length increase . . . . .	54
6.4	Discussion . . . . .	55
6.5	Conclusion . . . . .	58
<b>7</b>	<b>Results: effect of tape pre-tension on deconsolidation</b>	<b>61</b>
7.1	Test matrix . . . . .	61
7.2	Deconsolidation response of Ten Cate pre-tensioned tapes . . . . .	62
7.2.1	Out-of-plane deformation . . . . .	62
7.2.2	Surface roughness . . . . .	64
7.2.3	Width increase . . . . .	64
7.2.4	Void content . . . . .	66
7.2.5	Thickness change . . . . .	67
7.3	Discussion . . . . .	68
7.4	Conclusion . . . . .	70
<b>8</b>	<b>Conclusion</b>	<b>73</b>
<b>9</b>	<b>Recommendations</b>	<b>77</b>
<b>A</b>	<b>Conceptual design of a pre-tension setup</b>	<b>79</b>
<b>B</b>	<b>Load cell calibration</b>	<b>81</b>
<b>C</b>	<b>IR-camera calibration</b>	<b>83</b>
	<b>Bibliography</b>	<b>90</b>

# List of Figures

1.1	Left: schematic representation of the LAFP-process, right: LAFP tape placement head [7]	2
2.1	Tape tension control in a tape placement head [11]	6
2.2	Schematical representation of LAFP process [30]	6
2.3	VCSEL technology, building blocks from small single VCSEL to a scalable system [34]	7
2.4	Left: VCSEL module; Right: adjustable heating profile by separate control of emission zones [37, 36]	7
2.5	Heat intensity distribution for different target distances [36]	7
2.6	Steps involved in the in-situ consolidation process [14]	8
2.7	Bonding mechanism involves intimate contact development and autohesion (diffusion of polymer chains across the bond interface) [41]	9
2.8	Increased fixed area (more restrained tape) can be seen in the lower drawing	11
2.9	Thickness increases as a result of longer deconsolidation times: 0, 50, 200, 500 s. [49]	12
2.10	Migration of voids as a result of continuously void growth and void closure in the direction of the heat flux [58]	13
2.11	Left: as-received tape, Right: deconsolidated tape [17]	14
4.1	Experimental setup research parts A and B. Left: setup used from Choudhary [19], Right: schematic overview of setup equipment.	22
4.2	Overview of pre-tension experimental setup including schematical view	23
4.3	Attachments of load cell and weights to the pre-tension setup	23
4.4	Suprem CF/PEEK prepreg tape material, variations in gloss can clearly be seen (camera photograph)	24
4.5	Keyence VK-X1000 laser scanning confocal microscope	24
4.6	1: Gray scale top surface micrograph (50X magnification) 2: Histogram of grayscale top surface micrograph 3: Binary image (red is allocated to fibers and black to resin)	25
4.7	Simulated nip-point for rapid heating experiment with 30mm spot length.	26
4.8	Left: Temporal plot of mean nip-point temperature, Right: Temperature profile at the end of the heating phase Both measured at the simulated nip-point location, example from A80/800	26
4.9	In-situ tape deformation measured by LLS and corresponding waviness profile. Left: start of heating phase, Right: end of heating phase	27
4.10	Comparison of tape deformation profiles obtained from LLS and LSCM, examples of config. A80/800	27
4.11	Height map of the nip-point surface	28
4.12	Surface deformation profiles retrieved from LSCM Left: Total surface profile (raw measurements), Right: Surface roughness measured locally around 4 different locations, at 20%, 40%, 60% and 80% of the width at nip-point location	28
4.13	Steps taken for cross-sectional epoxy samples preparation. Left: Struers CitoVac, Mid: Struers Tegramin-20 Polishing machine, Right: Cross-sectional sample	29
4.14	Thickness locally measured at 4 locations along the width at nip-point location	29
4.15	Histogram of the grayscale cross-sectional image with thresholds indicated for void content measurement	30
4.16	Void content indicated by the red areas	30
5.1	Influence on out-of-plane deformation for several process configurations	34
5.2	Comparison between out-of-plane deformation at the start of heating and at the end of heating. Heating time = 500ms and heated spot length = 50mm	34
5.3	Temperature profile plotted together with deformation profile (from LLS) at the end of heating. Heating time = 800ms and heated spot length = 80mm	35

5.4	Influence on RMS roughness for several process configurations . . . . .	35
5.5	Influence on void content for several process configurations . . . . .	36
5.6	Voids present in the material for different heated spot lengths . . . . .	36
5.7	Influence on arc-length for several process configurations . . . . .	37
5.8	Out-of-plane deformation and waviness curves for a heating time of 350ms. Left: heated spot length = 30mm; Mid: heated spot length = 50mm; Right: heated spot length = 80mm . . . . .	37
5.9	Influence on thickness increase for several process configurations . . . . .	38
5.10	Temperature profile and deformation profile of the simulated nip-point at the end of heating, sample A30/350 . . . . .	39
5.11	Large roughness and out-of-plane decompaction shown at locations where peaks are shown in waviness profile, sample A30/350 . . . . .	39
5.12	Void formation phenomena . . . . .	40
5.13	Void coalescence takes place for longer heating times . . . . .	40
5.14	Polymer matrix movement towards the sides of the tape which can contribute to arc-length increase . . . . .	41
5.15	Void content has a major contribution to thickness increase, sample A30/800 . . . . .	41
6.1	Variation observed in the gloss of Suprem CF/PEEK prepreg tape (camera photograph) . . . . .	44
6.2	Close-up images taken from figure 6.1. I: Glossy surface, II: Combined glossy and matte surface, III: Matte surface . . . . .	45
6.3	Micrographs (captured with LSCM at 50X) corresponding to images shown in figure 6.2 I: Glossy surface, II: Combined glossy and matte surface, III: Matte surface . . . . .	45
6.4	Comparison of resin content on top surface. Resin is shown in black while red represent fibres on the top surface. I: Glossy surface, II: Combined glossy and matte surface, III: Matte surface . . . . .	45
6.5	Comparison between different top surface appearances of Suprem material . . . . .	46
6.6	Comparison between Suprem cross-sectional micrographs . . . . .	46
6.7	Comparison between top surface micrographs of Toray-Ten Cate and Suprem material . . . . .	46
6.8	Comparison between Toray-Ten Cate and Suprem cross-sectional micrographs . . . . .	46
6.9	Effect of resin-richness on surface roughness . . . . .	47
6.10	Difference in surface roughness observed after heating for resin-poor and resin-rich samples . . . . .	48
6.11	Effect of resin-richness on out-of-plane deformation . . . . .	48
6.12	Increasing warpage with heated spot length for a heating time of 350ms . . . . .	49
6.13	Temperature distribution in the nip-point at the end of heating . . . . .	49
6.14	Out-of-plane deformation and waviness profile fitted (end of heating) . . . . .	49
6.15	Increasing warpage with heated spot length for a heating time of 800ms . . . . .	50
6.16	Temperature distribution in the nip-point at the end of heating . . . . .	50
6.17	Out-of-plane deformation and waviness profile fitted (end of heating) . . . . .	50
6.18	Effect of resin-richness on void content . . . . .	51
6.19	Resin-rich layer in the middle of the tape (seen through-the thickness), low local fiber volume content . . . . .	51
6.20	Temperature below the melting temperature results in no void formation, sample B80/800 . . . . .	51
6.21	As-received resin-rich Suprem samples showing scatter in initial void content . . . . .	52
6.22	Effect of resin-richness on void content for several process configurations . . . . .	52
6.23	Effect of resin-richness on thickness increase . . . . .	53
6.24	Influence on thickness increase for several process configurations . . . . .	53
6.25	Local maximum indicated by blue arrow around 20% width, local minimums indicated by red arrows around 20% and 60% width, sample B80/800 . . . . .	54
6.26	Effect of resin-richness on arc-length increase . . . . .	54
6.27	Influence on arc-length for several process configurations . . . . .	55
6.28	More warpage observed for resin-rich sample with the same configuration 80mm/350ms . . . . .	55
6.29	Cross-sectional image (B30/800). Void formation can be seen mainly at the right-handside (between bracket). In the close-up image below the effect of voids on thickness increase . . . . .	56
6.30	Temperature profile at the end of heating for the corresponding sample (B30/800) shown in Fig. 6.29 . . . . .	57
6.31	Resin-poor Toray-Ten Cate material fibers evenly distributed through-the-thickness of the cross-section . . . . .	57

6.32 Resin-rich Sumprem material lower fiber volume content in the middle, seen through-the-thickness of the cross-section . . . . .	57
7.1 Variation in temperature profiles at the end of heating. Heated spot length = 30mm, heating time = 800ms Left: pre-tension = 5N; Mid: pre-tension = 10N; Right: pre-tension = 15N . . . . .	62
7.2 Out-of-plane deformation diagrams corresponding to the same samples as in Figure 7.1. Left: pre-tension = 5N; Mid: pre-tension = 10N; Right: pre-tension = 15N . . . . .	63
7.3 Normalized maximum out-of-plane deformation for several tape pre-tension levels and process configurations . . . . .	63
7.4 RMS roughness for several process configurations . . . . .	64
7.5 RMS roughness as a function of temperature . . . . .	64
7.6 Width increase measured before and after heating, sample from config. C30/800/10 . . . . .	65
7.7 Width increase for several pre-tension levels and process configurations . . . . .	65
7.8 Schematic representation of the edge of the tape . . . . .	66
7.9 Temperature profile of config. C30/800/10 . . . . .	66
7.10 Higher void content present at locations where temperatures above $T_m$ were reached, config. C30/800/10 . . . . .	67
7.11 Normalized void content for several pre-tension levels and process settings . . . . .	67
7.12 Thickness increase for different levels of pre-tension . . . . .	67
7.13 Measured thickness as a function of temperature . . . . .	67
7.14 Normalized thickness change for several pre-tension levels and process settings . . . . .	68
7.15 Fiber clusters located at the heated surface causing locally high temperatures, hence out-of-plane deformation . . . . .	69
A.1 Schematic preliminary design of pre-tension setup, top and side view . . . . .	79
A.2 Proof-of-concept tape pre-tension setup . . . . .	80
B.1 Load cell calibration setup . . . . .	81
B.2 Load cell calibration run . . . . .	82
B.3 Load cell calibration curve . . . . .	82
C.1 Calibration setup, VCSEL positioned orthogonal w.r.t. tool surface . . . . .	83
C.2 Thermal image captured by IR-camera during emissivity calibration . . . . .	84
C.3 Emissivity calibration curves Toray/Ten Cate thermoplastic prepreg CF/PEEK . . . . .	85
C.4 Emissivity calibration curves Sumprem thermoplastic prepreg CF/PEEK . . . . .	86



# List of Tables

4.1	Material properties of prepreg tapes used during the research . . . . .	21
4.2	As-received state prepreg tape properties, standard deviation between square brackets . . . . .	31
5.1	Configuration settings experimental research 0.5" Ten Cate prepreg tapes . . . . .	33
6.1	Configuration settings experimental research 0.5" resin-rich Suprem prepreg tapes . . . . .	43
6.2	Results of the top surface resin content measurements for different material types . . . . .	44
6.3	RMS roughness data, comparison between resin-rich and resin-poor samples . . . . .	47
7.1	Configuration settings experimental research 0.5" Ten Cate prepreg tapes, pre-tension: 5N . . .	61
7.2	Configuration settings experimental research 0.5" Ten Cate prepreg tapes, pre-tension: 10N . .	62
7.3	Configuration settings experimental research 0.5" Ten Cate prepreg tapes, pre-tension: 15N . .	62



# Nomenclature

A320	Airbus A320
AFP	Automated fiber placement
B737	Boeing 737
CF/PEEK	Carbon fiber / Polyetheretherketone
CF/PEI	Carbon fiber / Polyetherimide
CF/PEKK	Carbon fiber / Polyetherketoneketone
CF/PPS	Carbon fiber / Polyphenylenesulfide
DAQ	Data acquisition
DEIC	Degree of effective intimate contact
GF	Glass fiber
ILSS	Interlaminar shear strength
IR	Infrared
LAFP	Laser-assisted automated fiber placement
LLS	Laser line scanner
LSCM	Laser scanning confocal microscope
OHC	Open-hole compression strength
OOP	Out-of-plane
PAEK	Polyaryletherketone
PEEK	Polyetheretherketone
PEKK	Polyetherketoneketone
RMS	Root-mean-square
TC	Toray-Ten Cate
VCSEL	Vertical Cavity Surface Emitting Laser
A-samples	Toray-Ten Cate samples used for research question 1 (chapter 5)
B-samples	Suprem samples used for research question 2 (chapter 6)
C-samples	Toray-Ten Cate samples used for research question 3 (chapter 7)
NF	Normalization factor
$NF_{OOP}$	Out-of-plane deformation normalization factor
$NF_{void}$	Void content normalization factor
$R_q$	Root-mean-square roughness
$T_g$	Glass transition temperature
$T_{lm}$	Liquid melt temperature
$T_m$	Melting temperature





# Introduction

## 1.1. Background

Over the past decades composite materials have earned their way to the aerospace industry. Metallic structures are being replaced by fiber reinforced composite structures because they are lightweight and have a better specific strength and stiffness. The demand for larger structures does also require the use of fiber reinforced polymer composite materials. Significant weight reductions of 10-20% can be realized by the use of lightweight composite materials. Furthermore, due to the anisotropic nature of composite structures additional weight optimization is possible. This in turn will result in less fuel consumption. Costs, up to 18%, can be reduced due to energy savings [1, 2, 3].

Both Airbus and Boeing are working on redesigns for their A320 and B737 [4]. According to a forecast from Airbus, more than 28,000 new single-aisle aircraft will be needed by 2037 [5]. Boeing expects that more than 30,000 new single-aisle aircraft will be needed by 2037. Moreover, this demand for single-aisle type aircraft is about two thirds of the total demand. The desired production rate in order to meet this big demand will be 60 up to 100 aircraft per month (current: 30-50 per month), that is 2 to 3 aircraft every day [4, 6].

Looking towards the future, especially fiber reinforced *thermoplastic* composites are becoming increasingly interesting for aerospace applications. The aerospace industry demands highly automated and efficient processes with high repeatability in order to fulfil the requirements with respect to production rate. Automated placement techniques with thermoset composites are already present and are widely applied nowadays. However, the main disadvantage is that an additional autoclave curing cycle is required after the placement of the fibers has finished [3]. This curing process is a time-consuming processing step. Moreover, the autoclave limits the size of components that can be manufactured. Thermoset composites can be replaced by thermoplastic composites in order to get rid of the autoclave curing cycle. Thermoplastic composites allow for automated, and out-of-autoclave, processing through laying up prepreg tapes and consolidation in one processing step. Other benefits of using thermoplastic composites include indefinite shelf life, higher impact resistance, repair possibilities and the fusion bonding capability [3, 7].

On a molecular level, thermosets undergo a chemical reaction during curing. Cross-links will be formed in an environment of elevated temperature and pressure (autoclave). This is an irreversible process, a cured thermoset can therefore not be re-melted or reprocessed. Within a thermoplastic matrix the polymer chains are held together by physical entanglements, chemical cross-links are not present. An increased temperature causes chain mobility which allow a thermoplastic polymer to melt. Thermoplastic matrix composites can therefore be fusion bonded or welded. This makes them perfectly suitable for rapid automated manufacturing processes such as laser-assisted automated fiber placement (LAFP) [8].

Beyeler et al. [9] investigated the concept of laser-assisted consolidation already more than 30 years ago. A setup was developed for which continuous consolidation of thermoplastic matrix tapes has been made possible. Using a heat source, in this case a laser, the matrix of the incoming tape and the matrix of the laminate were locally melted. By applying pressure of the consolidation roller the polymer chains diffuse across the

bondline. Laser-assisted automated fiber placement is a manufacturing technology that makes use of the continuous consolidation concept of Beyeler et al. [9]. The process is described by the placement of unidirectional fiber reinforced thermoplastic matrix tapes and continuous consolidation directly during the tape placement process. The tapes are laid down ply-by-ply and a bond is formed through heating, consolidation and solidification across the layer interface. This process is referred to as '*laser-assisted automated fiber placement with in-situ consolidation*'. A tape placement head in combination with a gantry system or a robotic arm are used for the placement and orientation of the fibers. A schematic overview of the process and a picture of the robot with tape placement head can be seen in Figure 1.1. The prepreg tapes are stored on spools and fed through a delivery system to the tape placement head [7]. The tape placement head is a modular end-effector and includes the following main components: laser heating source with laser optics, fiber delivery system, compaction roller and thermal camera [10, 11]. The fiber delivery system controls the tape tension force which is typically in the range of 0-10N [12].

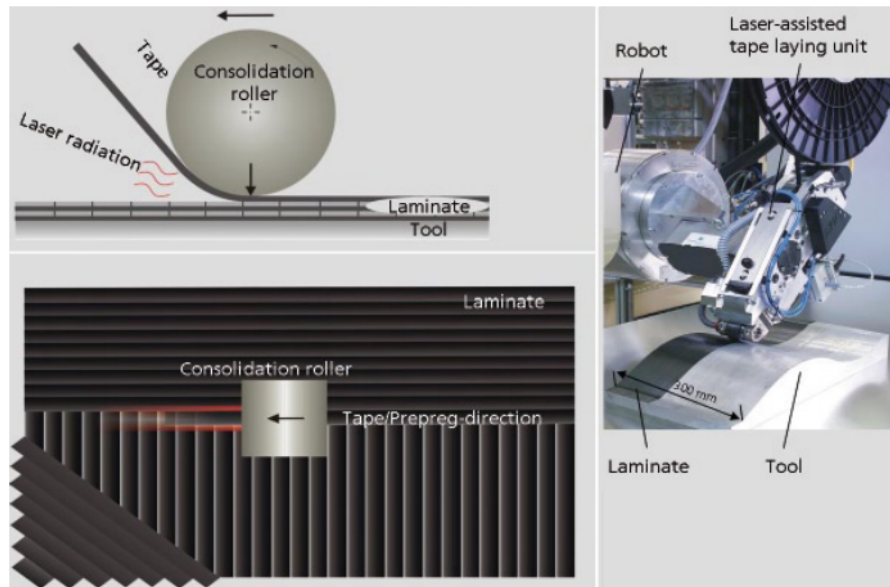


Figure 1.1: Left: schematic representation of the LAFP-process, right: LAFP tape placement head [7]

## 1.2. Motivation

Full in-situ consolidation has not been achieved (at the desired processing speed) so far with the LAFP-technique and the consolidation quality does not meet aerospace standards yet [13, 14]. Sufficient part quality with a feasible processing speed (400-800 mm/s) must be achieved before LAFP can be certified and used for the aerospace industry [15]. The mechanical performance of thermoplastic composite laminates is highly dependent on the consolidation quality [16]. One of the quality indicators is the maximum allowable void content after manufacturing, which still exceeds the 1% limit for aerospace standards [10]. Interlaminar voids can be characterized as LAFP-process induced defects, due to lack of intimate contact between the plies. Although the morphology of the 'as-received tape' plays also an important role here [17].

LAFP consists of three interconnected phases: heating, compaction and cooling. Heating is the first phase in the process and has a big impact on the final consolidation quality of the part. During heating the material is heated to a processing temperature of around 400°C without pressure application and within a very short heating time (0.2-0.8s). As a result of rapid heating interconnected deconsolidation mechanisms (decompaction of the fiber reinforcement network, void thermal growth, polymer movement in the melt phase and waviness formation) occur which affect the final consolidation quality. These underlying mechanisms and their relation with processing parameters need to be understood to achieve a high quality laminate manufactured by LAFP [15]. Previous research has shown that deconsolidation mechanisms during the heating phase will give rise to an increase in void content, surface roughness, fiber decompaction and dimensional changes [15, 17, 18, 19]. Therefore, the focus during this research will be on the heating phase of the in-situ consolidation process during LAFP.

### **1.3. Objective**

This thesis deals with an experimental research into the the heating phase of the in-situ consolidation process during LAFP. The aim is understanding the deconsolidation behavior during rapid laser heating and quantification of the consolidation state of thermoplastic prepreg tapes during heating and at the end of the rapid heating phase of LAFP by means of (in-situ) evaluation of the material behavior in terms of out-of-plane deformation, surface roughness, void content development, thickness increase and arc-length (width) increase.

The experimental research that was performed during this thesis project will help to identify the relevant mechanisms on deconsolidation formation during rapid laser heating and to understand the material state before compaction. The desired outcome will be given by qualitative and quantitative relationships between the input parameters (heating time and heated spot length) and the deconsolidation output parameters (maximum out-of-plane deformation, surface roughness, void content, thickness increase and arc-length (width) increase).

### **1.4. Outline**

This Master Thesis report will start with a deep-dive, in chapter 2, into relevant literature on the LAFP process, the heating phase and deconsolidation mechanisms in the context of LAFP. Based on the state-of-the-art LAFP technology found in literature, research gaps are identified, research questions and hypothesis are formulated. This can be read in chapter 3. The materials used during this research, the experimental setup and the characterization techniques will be described in chapter 4. After this, the results are presented in three separate chapters. In chapter 5, the influence of heating time and heated spot length on deconsolidation is presented. In chapter 6, the effect of a resin-rich surface on deconsolidation is described. In chapter 7, the effect of tape pre-tension on deconsolidation is described. Finally, the research conclusion will be formulated in chapter 8 and recommendations for future research will be given in chapter 9.



# 2

## Literature review

Automated fiber placement (AFP) is a widely applied automated manufacturing technique by which large and lightweight aerospace components can be manufactured in a cost-efficient way with a high accuracy and repeatability. [2]. LAFP is a closely related process (see schematical representation of the process in figure 2.2) which has the potential to offer even higher production rates by increasing the throughput. A lot of research has already been performed on LAFP, although remaining developments are needed in order to certify and commercialize this technology for the aerospace industry. This chapter gives an overview of the current state-of-the-art of the LAFP process as found in literature.

### 2.1. Laser-assisted automated fiber placement

LAFP has already been investigated in literature for more than 30 years, Beyeler et al. [9] started the basic concept in 1988. Comer et al. [10] performed different experiments using carbon fiber/polyetheretherketone (CF/PEEK) prepreg tapes and the laser-assisted automated tape placement manufacturing technique. The quality of laminates produced by the LAFP technique were compared to the ones consolidated in autoclave. From this research it can be concluded that the laminates produced by LAFP performed better in terms of interlaminar toughness (134%). However, in terms of flexural strength (68%), interlaminar shear strength (ILSS, 70%), flexural stiffness (88%) and open-hole compression strength (OHC, 78%) LAFP performed less compared to autoclave consolidation. The void content for LAFP-produced CF/PEEK laminates was found to be 2.8%<sup>1</sup>. Schledjewski and Miaris [20] obtained an interlaminar shear strength of 94% of the strength of autoclave-produced laminates. A fiber volume fraction of above 60% was obtained and an average void fraction just below 3.5%. Grouve et al. [21, 22] showed in their research on LAFP with CF/polyphenylsulfide (PPS) prepreg tapes that bond strength increases with increasing temperature and placement velocity. Laminates manufactured with LAFP outperformed press molded laminates in terms of fracture toughness. The short consolidation time is thus sufficient to achieve a good bonding, although due to the high cooling rate the PPS matrix remains amorphous.

Interesting observations were made with respect to the lower crystallinity of the laminates produced by LAFP. The optimal degree of crystallinity that is considered for good mechanical properties (strength, stiffness, fracture toughness) is 35% [23, 24]. Laminates manufactured by LAFP obtained 17.6% crystallinity of the PEEK matrix, whereas autoclave consolidated laminates obtained 40% crystallinity. Similar results were reported by Ray et al. [23], higher interlaminar toughness of LAFP-produced laminates can be attributed to the lower crystallinity. Low crystallinity can be either a result of high cooling rates or the interior laminate plies that are not heated above melting point. Gao and Kim [25] highlighted in their research that interlaminar toughness is a result of interactions between fiber-matrix interface bond strength and matrix ductility. Slow cooling is beneficial for fiber-matrix interface bond strength, strength and stiffness of the matrix. On the contrary, ductility of the PEEK matrix increases with increasing cooling rate which results in higher interlaminar fracture toughness and impact damage resistance. Thus, the composite properties can be adjusted as desired by changing processing conditions.

---

<sup>1</sup>2.8% void content was found for CF(IM7)/PEEK material [10]

## 2.2. Tape pre-tension

Fiber placement systems have the capability to feed individual tapes through a fiber delivery system into a fiber placement head [11]. Individual tapes will be fed through the placement head and compacted onto the substrate while controlling the tape tension, see figure 2.1. Tape pre-tension is an important parameter since it has an influence on the final quality of the manufactured laminate. Typical values for tape tension used in AFP machines range from around 2N (for low tack prepreg tapes) up to 10N [11, 12]. In order to achieve a high quality laminate the tapes must experience a constant force. Instability of tension control can lead to structural defects due to fiber wrinkling, misalignment of the tapes and void formation in between subsequent placed tapes. This can lead to delamination and a reduction of mechanical strength [26, 27]. Next to that, Wang et al [26] reported that too low pre-tension force (< 5N) can cause a low strength and fatigue resistance of the laminate. While a too large pre-tension force (> 15N) can affect the strength negatively due to fiber wear or breakage[28]. The effects just described all influence the final quality of the laminate in terms of mechanical properties, however it might influence LAFP processing already during the heating phase. Tape pre-tension can possibly affect the deconsolidation of the incoming tape as suggested by Celik [29], but this has not yet been clearly demonstrated in research.

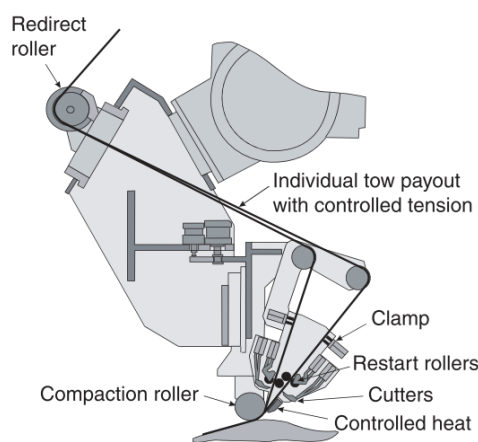


Figure 2.1: Tape tension control in a tape placement head [11]

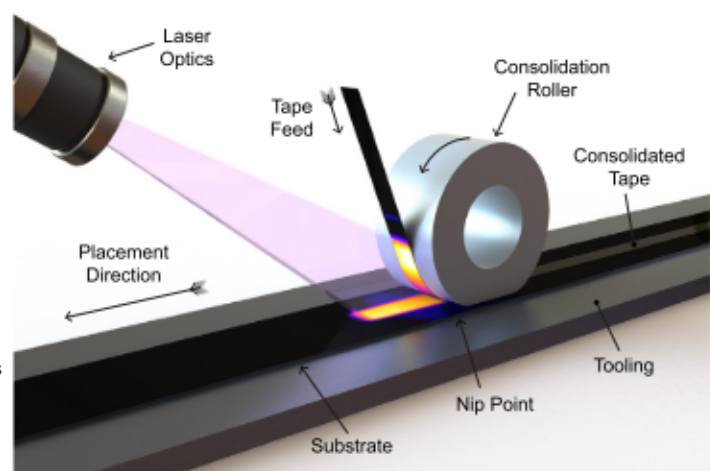


Figure 2.2: Schematical representation of LAFP process [30]

## 2.3. Diode laser heating

As found in literature laser heating provides a high heat intensity at a local point [9, 31]. The ability to focus a high heat intensity makes this heating method especially suitable for AFP, because it should heat the incoming tape and the substrate only locally in the nip point (location where the incoming tape and the substrate are consolidated together by the roller and a bond will be formed), see figure 2.2. Furthermore, Stokes-Griffin et al. [32] make use of laser optics in their research to create an enlarged rectangular spot of uniform density. A homogeneous heating is realized across the length and the width of the tape. The spot size is dependent on the distance of the laser source as a result of a diverging laser beam. Moreover, lasers are efficient, provide rapid heating and cooling rates (temperature gradients up to 1000 °C/s) and a fast response time which are favourable for a better temperature and process control [33]. It can be stated that laser heating has a great potential in terms of quality of the thermoplastic laminate, its ability to adapt to tape material and operating costs [20]. However, the main drawbacks are the high initial investment cost of laser equipment and the strict safety requirements.

Vertical Cavity Surface Emitting Lasers (VCSEL) offer the possibility to control the laser intensity distribution by individually controllable emitter lines. Independent heating of the tape and substrate can be made possible by adjustable heat intensity profiles both in width direction and placement direction [34]. A VCSEL consists of thousands of lasers, see figure 2.3. These 30  $\mu\text{m}$  wide lasers are high-densely packed in VCSEL arrays with packing densities up to 600 VCSELs per  $\text{mm}^2$ , one single  $2 \times 2 \text{ mm}^2$  chip contains therefore 2205 VCSELs. An emitter contains 56 array chips equally divided over 2 individual controllable lines of 28 chips connected in series. The 56 array chips in one emitter are placed in 4 columns of 14 chips [34, 35].

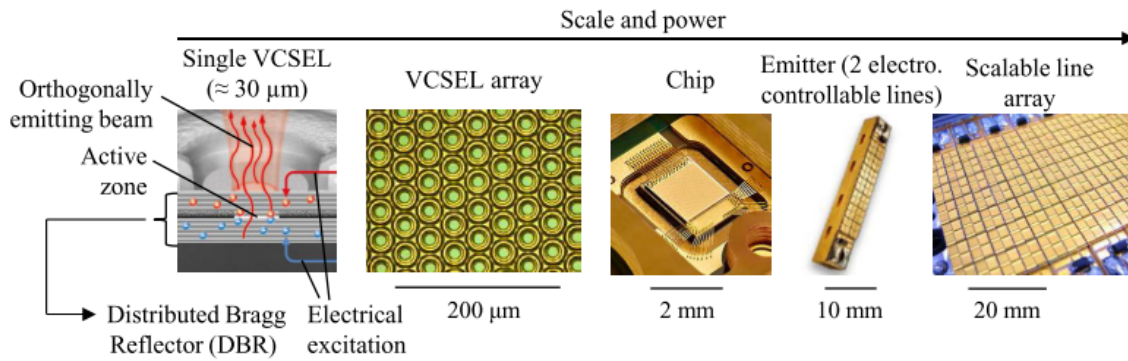


Figure 2.3: VCSEL technology, building blocks from small single VCSEL to a scalable system [34]

VCSELs are capable of separating emitter zones into distinct sections which allow for an adjustable control of the heating profile, see figure 2.4. This is reachable due to the fact that those systems are powered by an electronic driver unit, which contains separate driver channels [36]. For each individual zone the desired current level can be adjusted from zero to the maximum value. Even dynamically varying heating profiles during operation are possible. A VCSEL module is shown in figure 2.4, the PPM412-12-890-24 type [37] that will be used has 12 distinct emitter zones and is able to deliver an optical power between 0.1 and 2.4 kW.

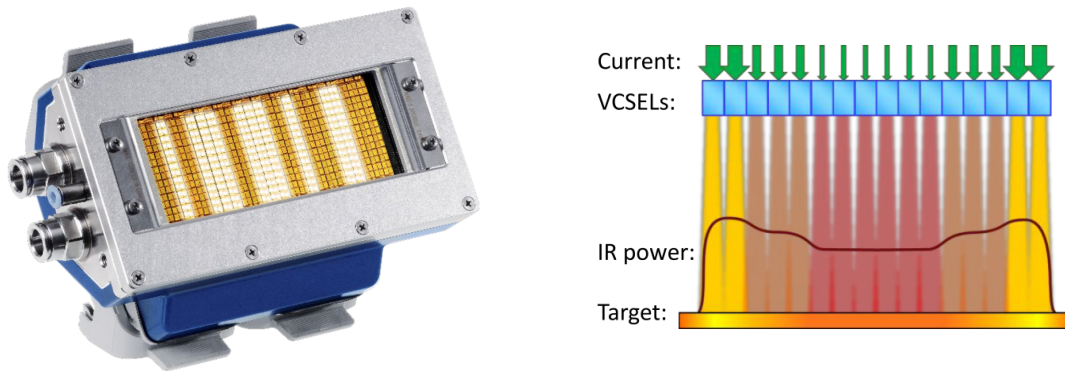


Figure 2.4: Left: VCSEL module; Right: adjustable heating profile by separate control of emission zones [37, 36]

Diode laser heating by a VCSEL is capable of generating uniform temperature profiles, although the uniformity decreases as the distance between the emitter and the target increases as can be seen in figure 2.5. Heating, by radiation, occurs primarily due to absorption of the laser light by the carbon fibers, especially at the wavelength of the electromagnetic infrared radiation. At this wavelength of about 980 nm light transmits through the resin. The high thermal conductivity of carbon fibers will help to distribute heat through the prepreg tape in a uniform and controllable manner [38].

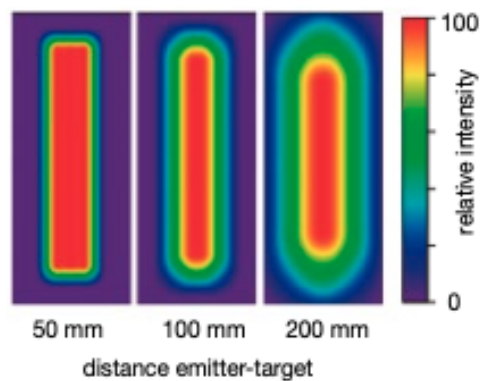


Figure 2.5: Heat intensity distribution for different target distances [36]

According to Schledjewski and Miaris [20] four laser adjustment parameters are important which might influence the efficiency of the fiber placement process.

- The **laser power** which affects the heat input in the prepreg tapes during the process. A too low laser power can cause insufficient intimate contact development, hence insufficient consolidation as a result of a high matrix viscosity due to insufficient heating. A high laser power can cause thermal degradation due to overheating.
- The **power distribution** between the incoming tape and the substrate can be adjusted. Both the incoming tape and the substrate should have enough power (temperature) input in order to achieve low matrix viscosities such that intimate contact development and a good consolidation quality can be facilitated. The power distribution is defined by the laser beam area ratio of the portion projected onto the incoming tape over the portion projected onto the substrate.
- The laser beam **angle of attack** (angle of the laser beam with respect to the incoming tape and the substrate, see figure 2.2) which affects the magnitude of the shaded areas should be as close to  $0^\circ$  as possible in order to minimize the size of shadow areas.
- The **laser beam cross section** (see figure 2.5) is affected by the distance between the emitter and the target. The heat intensity input will change as a result of a changing laser beam cross section as could also be concluded from Moench and Derra [36].

## 2.4. In-situ consolidation

In-situ consolidation is described by the process of simultaneously applying heat and pressure to thermoplastic matrix composite material in order to remove volatiles and interface boundaries. New bonds will be created through polymer healing. The in-situ consolidation process can be divided into three different physical steps: heating, consolidation and cooling according to Narnhofer et al. [39]. Several mechanisms play a role during these steps, which will affect the state of the thermoplastic prepreg tape and quality of the final part. In figure 2.6 the three consecutive steps are shown (with the cooling step the same is meant as with solidification). The mechanisms that occur during each processing step are described in more detail below.

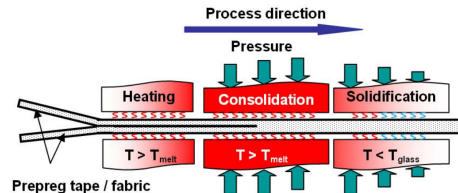


Figure 2.6: Steps involved in the in-situ consolidation process [14]

During the **heating step**, the tape and substrate will be heated to the processing temperature of the thermoplastic matrix. The processing temperature for semi-crystalline thermoplastic polymers is just above their melting temperature. The laser heat source plays a key role in achieving the desired final quality and the efficiency of the process. Several mechanisms play a role during rapid heating that negatively affect the consolidation state. For instance, release of residual stresses resulting in decompaction of the fiber reinforcement network, growth of voids, dimensional changes of the tape and an increase in surface roughness. It is therefore important to have understanding of the heating phase since it is the first step in the process and it directly changes the state of the as-received tape.

In the next step, **consolidation**, the incoming tape and substrate will be brought together and the tape is fused onto the substrate by applying heat and pressure in the nip-point. The consolidation step consist of 2 main processes: first intimate contact development between the tape and substrate and secondly polymer healing across the interface, this will be further explained in the next section 2.5.

The final step is **solidification** during which the material is cooled down below the glass transition temperature, the pressure is released and finally the temperature will cool down to ambient temperature. During cooling residual stresses can be built up because elastic energy will be stored again due to mismatch in coefficients of thermal expansion between the fibers and matrix.

## 2.5. Bonding mechanism

The bonding mechanism is the source of interlaminar strength development and is dictated by two principles, intimate contact development and autohesion. The aim is to achieve a high quality bond, a uniform bondline, which will be created by intimate contact development and subsequently interdiffusion of the polymer molecules across the bondline interface. Autohesion can only occur if two surfaces are in intimate contact, therefore the bonding mechanism is often referred to as the coupled intimate contact and autohesion mechanism [40].

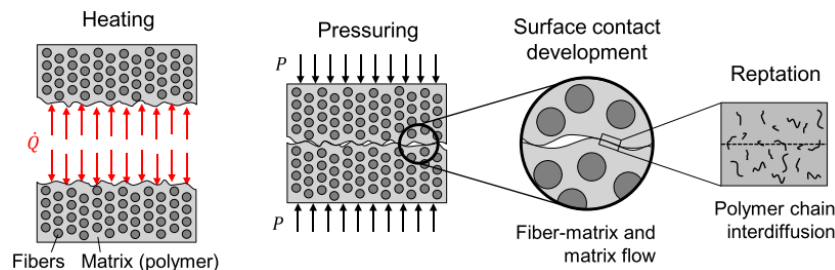


Figure 2.7: Bonding mechanism involves intimate contact development and autohesion (diffusion of polymer chains across the bond interface) [41]

The degree of effective intimate contact describes the portion of the total resin-rich surface area that is actually in contact [42]. As can be seen in figure 2.7 intimate contact development is initially limited due to the presence of surface asperities. During the heating phase heat is applied to the bond interfaces. Due to an increase in temperature of thermoplastic polymer matrix it becomes soft and starts to flow. In the next step, pressure will be applied such that the surfaces become in increased degree of intimate contact [40]. The bonding time required to achieve intimate contact depends on the surface roughness, pressure and the viscosity of the polymer matrix which is temperature dependent [43]. The most important parameters affected by the heating phase are surface roughness and viscosity, both dependent on temperature. The viscosity decreases as a result of an increasing temperature. An increased surface roughness at the heated surface is an effect of the heating phase, deconsolidation mechanisms play an important role here which will be further discussed in section 2.7.

Autohesion or healing is the interdiffusion of the thermoplastic polymer chains across the bond interface which is promoted by effective intimate contact. Autohesion is highly dependent on temperature. When the temperature is above  $T_g$  for amorphous polymers or above  $T_m$  for semi-crystalline polymers, interdiffusion can occur [44]. Polymer chains of the incoming tape will entangle with polymer chains of the substrate when both are in contact. The initial interface will be erased with increasing amount of crossed chains. The degree of healing is proportional to the interlaminar bond strength of the interface. Full bond strength can only be achieved when the last increment of effective intimate contact has developed and has subsequently healed completely [40, 43]. Although autohesion does occur during the consolidation phase it is highly dependent on intimate contact development and the heat input during the heating phase.

## 2.6. Heating phase parameters

LAFP is a multivariable process and therefore challenging to optimize for a high final product quality. Several parameters play a key role during the heating phase. Further assessment of the parameters is needed to gain understanding of their influence on deconsolidation during the heating phase. The relevant material properties and processing variables are discussed below.

The **initial tape quality and resin-richness** determine the final laminate quality and the laminate mechanical properties after processing. Due to high requirements for the final quality of LAFP-produced parts in aerospace industry, high demands should be set for the initial quality of as-received tapes [3]. A key factor to achieve a high consolidation quality and autoclave-level mechanical properties is the availability of high quality prepreg tapes. Material manufacturers have improved their quality and offer tapes with a low void content and a smooth surface in order to improve processability [17]. Initial tape properties that are important include void content, fiber volume fraction and dimensional tolerances [10]. During the heating phase

several physical changes to the state of the tape affect the final quality. Even the same tapes from different manufactures could behave different since the manufacturing process of the as-received prepreg has an impact as was shown by Kok [17]. Furthermore, variations in types of tapes (both fibers and matrix materials) could have a different response. Although, similar deconsolidation behavior was observed by Choudhary [19] for CF/PEEK and CF/PEKK from the same manufacturer. The composition of tapes in terms of fiber matrix distribution at the surface could have a significant influence on the deconsolidation behavior. Various authors have suggested that a resin-rich surface should facilitate a smoother surface which is beneficial for in-situ consolidation during AFP processing [19, 45, 46]. It is expected that the lower surface roughness for resin-rich tapes will result in better intimate contact development [17]. It is therefore interesting to perform research on how tapes with a difference in resin-richness will behave as a result of rapid heating. Another motivation for this research parameter is that in general less research has been performed so far on different material types. This will contribute to the understanding whether deconsolidation mechanisms are material specific or occur for all kinds of thermoplastic tapes.

The heat input into the tape material is determined by the **power** delivered by the laser. The required intensity of the heat input depends on several parameters such as material deposition rate, laser angle with respect to the tape and substrate, tool temperature and heated spot length. The achieved tape temperature, laser power input, heated spot length and heating time are interdependent on each other. This means that the same tape temperature could be achieved by different configurations of laser power, heating time and heated spot length. It is therefore convenient to control the process using the nip-point temperature as a reference and adjusting process settings (laser power, heating time and heated spot length) according to the desired nip-point temperature [17]. Heating the tape to the processing temperature of the matrix will melt the matrix and decreases its viscosity. This is required in order to achieve a good consolidation quality since flattening of surface asperities will become easier for a lower viscosity.

The **heating time** is determined by the material deposition rate of the LAFP-process and defines the productivity of the machine. The time available for heating and consolidation are dependent on the material deposition rate. The heating time at the nip-point is therefore determined by the deposition rate and the heated spot length. Typical material deposition rates are in the order of 100-400 mm/s (75-300ms heating time for 30mm heated spot length) [8, 44], but nowadays maximum rates of 800 mm/s (37.5ms heating time for 30mm heated spot length) can be reached for AFP. However, a deposition rate of 25-100 mm/s (300-1200ms heating time for 30mm heated spot length) is more typical in order to achieve a good in-situ consolidation quality [47, 48]. Simulation of the material deposition rate, using a static setup, can be performed by adjusting the heating time corresponding to typical deposition rates while keeping the heated spot length constant.

It was shown that the heating time significantly affects deconsolidation behavior. Wolfrath [49] reported less thickness increase for shorter heating times for glass mat thermoplastics. Kok [17] suggested that shorter heating times reduce the available time for deconsolidation, hence reduce the amount of deconsolidation. Choudhary [19] found that a shorter heating time with higher intensity (in order to aim for the same nip-point temperature in all cases) reduces the amount of increase in surface roughness, void content and thickness at the nip-point.

The **heated spot length** (order of magnitude 30-80mm) or size of the laser spot is a function of the laser distance to the tape and the activated laser zones. A larger heated spot length results in a longer heating time for the same material deposition rate. The laser angle with respect to the tape affects the reflection and absorption of laser light, therefore the temperature distribution [17].

In actual LAFP systems the **tape pre-tension** is applied and controlled in the tape placement head [11], as was shown in section 2.2. Tape pre-tension is assumed to contribute to diminish deconsolidation effects. Preliminary research has shown that a more restrained tape reduces deconsolidation effects [19]. Changing the fixed tape length (see figure 2.8 will change the degree of deconsolidation. Less warpage and out-of-plane decompaction were observed for the case of a larger fixed area. As a result, less surface roughness and width increase were observed. It is assumed here that increasing the fixed area increases the tape pre-tension. The actual tape pre-tension was not measured, it remains therefore to be experimentally verified whether these effects were observed due to larger tape pre-tension and if deconsolidation effects could be minimized for a certain optimum value of tape pre-tension.

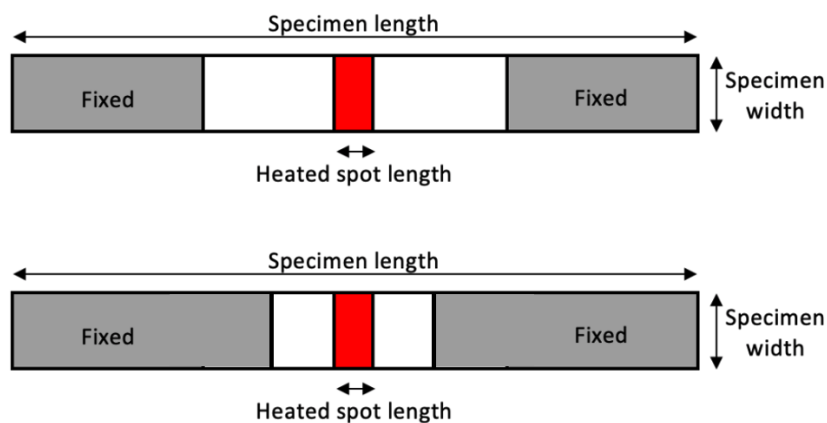


Figure 2.8: Increased fixed area (more restrained tape) can be seen in the lower drawing

## 2.7. Effects of the heating phase on deconsolidation during LAFP

The heating phase has a large impact on the consolidation quality of thermoplastic composite structures manufactured by LAFP. Especially the high heating rates together with the limited consolidation time are responsible for the difficulty to reach a good consolidation quality. Recent literature has shown that the tape deconsolidates during the short rapid heating phase [17]. Deconsolidation mechanisms play an important role in the material behavior during the heating phase. Therefore, the link between process parameters and deconsolidation during the heating phase needs to be understood very well. One of the main reasons for the high void content is deconsolidation. Furthermore, deconsolidation mechanisms cause an increased surface roughness and a matrix poor surface which are disadvantageous for intimate contact development, hence consolidation quality [18].

Deconsolidation phenomena are also found during conventional manufacturing processes for thermoplastic composites such as autoclave or hot press consolidation, mainly during post-processing when heating without any external pressure applied. Although, these processes are associated with low heating rates it can help to understand deconsolidation behavior during LAFP (high heating rates).

### 2.7.1. Deconsolidation mechanisms

Deconsolidation during the heating phase, prior to the nip-point is undesired since it significantly affects the consolidation state of the as-received tape during the process. It will negatively affect intimate contact development which results in a poor bonding quality between the plies. A rough fiber-rich outer surface, of an initially smooth tape, has been observed. Furthermore, an increase in void content, an increase in width and thickness of the tape occur due to deconsolidation at the end of the heating phase [17, 18, 19].

Ye et al. [50] reported two imported phenomena as a result of thermal deconsolidation, decompaction of the fiber network and migration of the resin melt. Therefore, deconsolidation could be considered as the inverse process of consolidation. According to Ye et al. [50] thermal deconsolidation can be described with the following definition: "meso-structure disintegration as well as the resulting deterioration in macro-performance of the initially well-consolidated composite during post-thermal processing." Similarly Henninger et al. [51] define deconsolidation as: "The tendency of a composite to loose consolidation upon re-heating, hence as a structural degradation. The degradation is associated with an increase in void content."

An increase in void content is often used in literature as a measure for the degree of deconsolidation. The presence of voids in laminates will lead to a decrease of mechanical properties, such as a significant loss of strength and stiffness [50]. Beehag and Ye [52] reported a drop ( 50%) in transverse flexural performance as well as a drop in mode I (of around 35%) and mode II (of around 45%) interlaminar fracture properties for a commingled CF/PEEK unidirectional fabric as a result of cooling at ambient pressure. It can be concluded that deconsolidation effects can occur during two particular moments, heating and cooling phase, when the temperature remains above the processing temperature in absence of any external pressure applied. An external applied pressure of 0.2 MPa maintained during cooling is enough to achieve a good consolidation

quality [52]. Similar results were found by Ageorges et al. [53] during resistance welding of CF/PEI laminates. A welding pressure of 0.5 MPa appeared to be optimal, while a pressure of 0.2 MPa is already enough to achieve a good consolidation quality and prevent thermal expansion deconsolidation phenomena. However, deconsolidation during the cooling phase is not relevant for the LAFP process due to the high heating and cooling rates the temperature will not remain at processing temperature during cooling.

Several mechanisms have been identified in literature that affect deconsolidation each associated with different causes in the micro-structure. Brzeski and Mitschang [54] reported four main causes for deconsolidation behavior as summarized below. Note here, these have been investigated for conventional manufacturing processes mainly during post-processing. Conventional processes are associated with heating rates in the order of 20 °C/s, while the heating rate for LAFP can exceed 1000 °C/s [32]. More research is therefore needed in order to investigate if these mechanisms will also occur during rapid heating of the LAFP-process.

1. Decompaction of the fiber reinforcement network as a result of residual stress release.
2. Thermal expansion and viscoelastic behavior of the thermoplastic matrix material due to heating (above  $T_g$ ).
3. Void expansion due to thermal gas expansion and internal void pressure.
4. Void shrinkage and coalescence of smaller voids into larger voids due to surface tension.

Decompaction of the fiber network is affected by the energy that is stored during compaction in the form of residual stresses. As the consolidated laminate is reheated and the matrix is remelted, the initially stored residual stresses tend to release [54, 55]. Wolfrath et al. [49] attributed deconsolidation mainly to the elastic behavior of the fiber preform in case of glass mat reinforced thermoplastics. The elastic release of stresses in the fiber preform is referred to as "springback effect" in their research. It was shown that voids are formed in the liquid matrix and grow under tensile stresses imposed by the moving preform which contributes to the springback effect. Moreover, void formation due to tensile forces induced by the springback effect is dependent on matrix viscosity. A lower viscosity is more prone to formation and growth of voids. Besides this effect of temperature a time dependency was shown as well. A longer reheating time results in more deconsolidation as shown in Figure 2.9. According to Ye et al. [50] decompaction of the fiber reinforcement network is associated with a significant increase in thickness. This indicates that decompaction and void growth associated with migration of the resin melt must take place simultaneously. Deconsolidation occurs if the externally applied pressure is less than the so-called critical decompaction pressure. In this specific case, the fiber reinforcement network is able to decompact. This results in growth of voids, initially present in the matrix, due to interaction between the reinforcement and resin melt. Another study by Ye et al. [55] points out that decompaction pressure is the driving force for void growth. The decompaction pressure is dependent on the elastic fiber properties, configuration of the fiber reinforcement network and on the fiber volume fraction. However, void growth is also strongly dependent on the behavior of the thermoplastic matrix.



Figure 2.9: Thickness increases as a result of longer deconsolidation times: 0, 50, 200, 500 s. [49]

Viscoelastic behavior of the matrix is another major contributor to the void content development. Semi-crystalline polymers (such as the PAEK family) exist of both amorphous and crystalline phases below their melting temperature. As the temperature increases above  $T_g$  the viscosity decreases rapidly. A temperature of about  $T_g + 60-100$  °C can be taken as the onset of a truly liquid melt ( $T_{lm}$ ) [56]. Between the  $T_g$  and  $T_{lm}$  the amorphous part of the polymer has both elastic and viscous properties. For a semi-crystalline polymer this means that as the temperature remains between  $T_g$  and  $T_{lm}$ , the polymer melt is able to store elastic energy and deforms under stress [57]. Upon release of the stress the elastic deformation may be recovered. This can lead to growth of microscopic voids, initially present in the matrix. This occurs due to elasticity of the matrix melt enabling voids in the matrix to grow due to traction. Formation of new voids can also occur due to tension as a result of a cavitation in the matrix [55].

Subsequent research by Lu et al. [58] has shown that if the temperature exceeds beyond  $T_m$ , such that the matrix melt is in full liquid state and the elastic behavior disappears, migration of voids appears during deconsolidation. Migration of voids is a continuous process of void growth in the previous phase (temperature was between  $T_g$  and  $T_m$ ). It is shown that migration of voids is not actually movement of voids throughout the matrix, but rather a continuous process of void growth and void closure. When the matrix reaches a full liquid state (low viscosity) the elasticity of the matrix disappears. As a result the driving force for void growth will vanish and voids can collapse, hence deconsolidation disappears in a particular region [55, 58]. This process proceeds continuously with time in the direction of the heat flux and therefore voids seem to migrate as can be seen in figure 2.10.

Furthermore, thermal expansion of the composite laminate results in a volume expansion due to increased temperature. As the temperature increases a material usually expands and contracts when the temperature decreases. For semi-crystalline polymers another physical mechanism plays an important role. The crystalline part has a higher density compared to the amorphous part of the semi-crystalline polymer. During melting, the crystals change to an amorphous structure which leads to an increase in the total volume of the matrix [54].

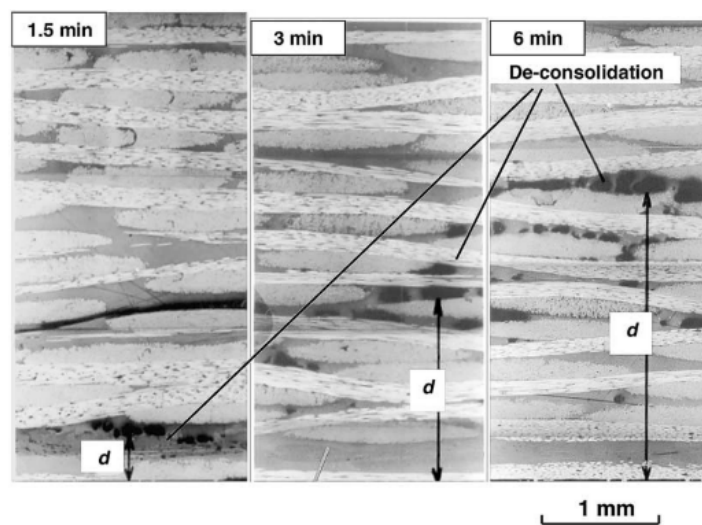


Figure 2.10: Migration of voids as a result of continuously void growth and void closure in the direction of the heat flux [58]

Brzeski and Mitschang [54] reported that the internal void pressure can decrease deconsolidation, while thermal gas expansion increases deconsolidation. Internal void pressure originates from the pressure introduced by the consolidation roller (during the consolidation step in the process) causing a reduction in void volume hence an increase internal void pressure [59]. Thermal void expansion is often neglected in research on the mechanisms causing deconsolidation since the contribution of thermal expansion of the gas is small. Ye et al. [55] found an increase of around 0.7 times in volume (upper bound calculation) due to thermal gas expansion. The total volume of voids due to deconsolidation has been reported as at least 10-20% of the total volume of the composite laminate. Therefore, one can conclude that thermal expansion of the voids does not have a major contribution in void growth and the final void content.

The surface tension has an influence on shrinkage and coalescence of voids. Surface tension can decrease the deconsolidation effects. Many small voids have a larger surface area than less large voids with the same amount of void content. The surface energy is therefore higher for a lot of small voids which can diminish the effect of deconsolidation. As the thickness of a laminate increases due to deconsolidation effects, voids become larger and can coalesce. This decreases in turn the inhibiting influence of surface tension on deconsolidation [54]. Although the number of voids reduces as small voids coalesce into larger voids, the global void content does not increase. Therefore, coalescence of smaller voids into larger voids does not have a major contribution to the total void content formation. A requirement for coalescence of voids is contact between the voids [55].

### 2.7.2. Deconsolidation phenomena in the context of LAFP

Limited literature is available on thermal deconsolidation in the context of LAFP. Kok et al. [17, 18] have put effort in quantifying CF/PEEK tape deconsolidation during LAFP. More recently, Choudhary [19] has performed preliminary research, at Delft University of Technology, into the deconsolidation effects during the rapid heating phase of LAFP using CF/PEEK tapes. Confirmatory experiments were performed with CF/PEEK tapes. The results obtained are very useful and promising for further research into this topic in an attempt to diminish deconsolidation effects. This section will present an overview of the most important observations so far in the context of LAFP, which are relevant for the research that is presented in this thesis.

Deconsolidation phenomena during LAFP will lead to undesired behavior of the tape: increase in surface roughness, out-of-plane decompaction, increase in void content and dimensional changes [19]. This causes a reduction in consolidation quality and mechanical performance after manufacturing. A tape with a reduced consolidation quality can be seen in figure 2.11 on the right and is characterized by a high void content, a rough fiber-rich outer surface and an increased tape thickness. At the end of the heating phase, prior to the nip-point, the tape is heated above its melting temperature without applying external pressure. Voids and volatiles, already present in the tape, can therefore expand. Furthermore, a fiber-rich and rough outer surface is the result of deconsolidation. According to Kok et al. [18] deconsolidation effects are visible up to 20  $\mu\text{m}$  from the heated surface, which is approximately 20% of the entire tape thickness. The rough outer surface is characterized by an increased void content, a higher fiber volume content than in the middle and a lower matrix volume content than in the middle of the tape. A low amount of matrix is available to wet the fibers and for healing of the tapes resulting in an increased local fiber-matrix distribution. To summarize: tape deconsolidation during the heating phase will hinder intimate contact development, hence resulting in interlaminar voids [60]. Both the surface morphology and the changed consolidation state affect intimate contact development.

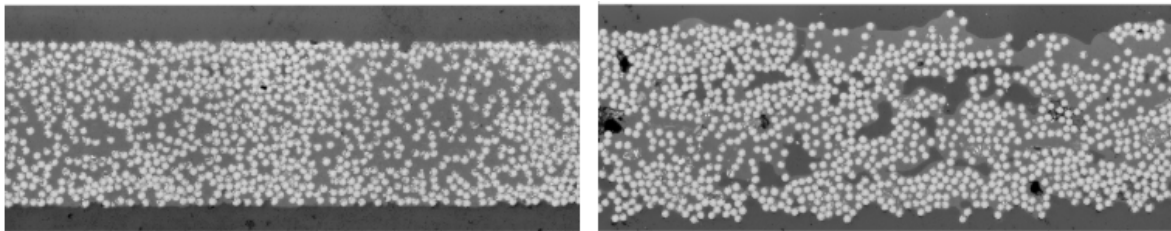


Figure 2.11: Left: as-received tape, Right: deconsolidated tape [17]

The source of deconsolidation can be attributed to fiber bed decompaction causing an increase in void content due to cavitation in the matrix, expansion of voids and subsequently coalescence of voids [17]. Furthermore, it was reported that tape deformation during the heating phase is mainly a function of tape temperature. The process settings, laser power, heated spot size and heating time (defined by placement rate), determine the tape temperature. It was suggested that shorter heating times will reduce deconsolidation effects [17]. Recent work from Celik [15] confirmed that reducing the heated spot length or increasing the placement speed (equivalent to shorter heating time) will result in less surface roughness and dry fibers at the heated surface after rapid heating. This indicates that deconsolidation responses are a function heated spot length, placement speed and temperature. However, more research is required to investigate the deconsolidation response variables as a function of resin-richness of the surface, tape pre-tension and several process configurations (heating time and heated spot length).

Choudhary [19] investigated thermal deconsolidation during the rapid heating phase of LAFP at Delft University of Technology. The following observations were reported as a result of deconsolidation:

**Decompaction of the fiber reinforcement network in the out-of-plane direction** occurs due to release of residual stresses introduced during manufacturing. This results in a rougher surface and a larger deformation in the out-of-plane direction. Indirectly, tape warpage and voids near the surface are created due to traction and cavitation in the matrix as a result of decompaction.

**Void thermal growth** is primarily caused by thermal expansion of voids already present in the as-received prepreg tapes when the temperature approaches processing temperature (between  $T_g$  and  $T_m$ ). This results in an high void content and an increase in tape thickness. Furthermore, it was found that the high void content does also contribute to an increase in width of the tape during rapid heating.

**Thickness increase** occurs mainly due to the increase in void content. A large increase in void content was observed in the cross-section after heating, which has a major contribution to the thickness increase. However, the out-of-plane fiber decompaction has also a minor contribution.

**Polymer matrix chain movement and void coalescence resulting in a change in tape width** primarily due to polymer matrix chain movement in the melt phase. A minor contribution is observed due to the increased void content. Void coalescence results in lesser tape width increase as a result of longer time spent above the melting temperature. However, the latter seems to be counter-intuitive and needs to be experimentally confirmed because the global void content does not change due to coalescence of voids as was stated in Section 2.7.1.

**Tape warpage** is caused by non-uniform temperature distribution along the fiber direction as well as transverse to the fiber direction. This will cause a variation in tape waviness (transverse to the fiber direction) at different longitudinal locations resulting in warpage of the tape.

**Influence of polymer type and quality** have been suggested by Kok [17] to affect the deconsolidation behavior. However, similar trends were observed by Choudhary [19] for CF/PEEK and CF/PEKK from the same manufacturer. The observation of warpage due to fiber decompaction and subsequently non uniform heating could be an indication that a tape with a different fiber matrix composition will behave differently. More research is required in order to verify how differences between tape manufacturing processes and tape composition might affect the deconsolidation behavior.

**Fixed tape length** is found to have an influence on the deconsolidation behavior. An unknown tension force was applied to the tape by completely fixing the non-heated part of the tape to the tool surface. It was observed that less fiber decompaction in the out-of-plane direction, warpage and width increase occurred. Additional research is required in order to determine the pre-tension force that would minimize deconsolidation phenomena.

Current models (for the consolidation phase) assume that the tape has not changed during the heating phase and that sufficient resin is present for consolidation. Celik [15] reported that several models [61, 62, 63] for tape consolidation, intimate development and void reduction have been used to predict the final state of the laminate after manufacturing. Material properties (initial roughness, dimensions, void content) are needed as input for these models. The input parameters are retrieved from the initial state of the tape in these models. It was shown (in previous literature) that the as-received consolidation state of the tape does significantly change (increase in surface roughness, thickness, width, void content and out-of-plane deformation) during the heating phase. This means that current models do not predict the consolidation behavior (intimate contact development) and the final state of the tape correctly. More research is needed to better understand the change in consolidation state during the heating phase prior to the nip-point. This can be used as an input for better intimate contact models and it can improve the final quality of a LAFP-produced part. It is suggested that more research should be performed on different types of tapes (with respect to resin-richness of the surface) from different manufacturers, since the manufacturing process of the tape itself could have an effect on the change in morphology during the heating phase [60].

## 2.8. Conclusion

A literature review on LAFP has been performed. This promising additive manufacturing technique has been widely investigated in literature. Most work has been focussing on the consolidation phase of the process and was performed on CF/PEEK prepreg tapes. A fiber placement system in combination with the application of tape pre-tension has been discussed as one of the variables during the AFP process. The working principle of laser diode heating was discussed in detail, the heat source for this process. The quality of LAFP-produced laminates does not meet aerospace standards yet, since the void content exceeds the 1% aerospace limit. Challenges remain before LAFP can be completely industrialized with the desired throughput and still obtaining the minimum required quality.

Research at Delft University of Technology on LAFP has shown that several thermally induced mechanisms occur due to the rapid heating phase [15, 19]. These mechanisms affect the consolidation state of the tape negatively such that the quality of the 'as-received' has significantly decreased after heating prior to the nip point. It is usually referred to as thermal deconsolidation and is also observed by Kok [17] and quantified by Kok et al. [18] for LAFP. Deconsolidation has been found to occur during conventional manufacturing processes as well, although in contrast to LAFP these processes are associated with low heating rates.

Deconsolidation during the heating phase gives rise to an increase in surface roughness, void content and waviness, larger out-of-plane deformation and dimensional changes. The problem is that the quality of the as-received tape has significantly decreased and that the aforementioned deconsolidation responses will lead to a lower final part quality. The increased surface roughness at the end of the heating phase, prior to the nip-point, is disadvantageous for intimate contact development during the consolidation phase (the next step in the process after heating). A high degree of effective intimate contact development is required to achieve a high bond strength and a low interlaminar void content, hence high final part quality. It can be concluded that the heat input during the heating phase plays a key role in obtaining a high final laminate quality.

In general less research has been performed on deconsolidation during LAFP. Kok et al. [18] emphasized the importance of the heating phase of LAFP, but measurements were only performed after the tape cooled down. A knowledge gap can be identified about the state of the tape at the end of heating, prior to the nip-point. Next to that, current consolidation models lack input on the reduced consolidation state of the tape after heating. Therefore, more research is required to understand and quantify the change in consolidation state during the heating phase prior to the nip-point. More specifically, the influence of polymer type (quality and composition, in terms of resin-richness) and tape pre-tension were suggested to affect deconsolidation behavior. Both (resin-richness surface and tape pre-tension) are considered to be beneficial for intimate contact development, hence higher final laminate quality. However, this remains to be experimentally verified. Research into both topics will contribute to a better understanding of the deconsolidation mechanisms during the heating phase. Further discussion of the research gaps that were identified and the research questions that have been formulated on the effect of resin-rich surface tapes and tape pre-tension will follow in chapter 3.

# 3

## Research definition

### 3.1. Research gaps identified in literature

Since not much research has been performed on deconsolidation phenomena during the heating phase of LAFP, prior to the nip-point, this can be considered as a general research gap. Particularly on the heating phase of LAFP more specific research gaps can be identified.

#### **Resin-rich surface tapes**

Thermoplastic tapes with a resin-rich surface have been suggested in literature to be beneficial for higher in-situ consolidation quality, a reduction in void content and an increase in interlaminar shear strength [46, 45]. Kok [17] suggested in his research that resin-rich surfaces might be beneficial for intimate contact development and healing, resulting in better interlaminar bonding. Furthermore, a smooth surface, facilitated by a resin-rich area, should make intimate contact easier and will result in a reduction of interlaminar voids. This should however be experimentally confirmed, hence a research gap is identified here.

#### **Tape pre-tension system**

Earlier research has been performed at Delft University of Technology on thermal deconsolidation during LAFP[19], however this thesis research did not include tape pre-tension (a main component of a LAFP tape placement head) in the test setup. Preliminary experiments did indicate that less fiber decompaction in the out-of-plane direction occurs due to more a restrained tape which resulted in a lower surface roughness. Moreover, a more uniform temperature distribution at the nip-point has been observed due to reduced tape waviness. Although the actual tape pre-tension was not measured, it is expected that tape pre-tension might be beneficial for minimizing the degree of deconsolidation. Hence, a research gap can be identified here as well and research can be performed on quantifying the pre-tension force required to minimize the degree of deconsolidation.

#### **Different different types of tape material**

Most of the research on LAFP has been performed on CF/PEEK prepreg tapes. Also confirmatory experiments were often performed by using the same material. In order to fully commercialize LAFP, it should be capable of being used with a wide variety of different materials [44]. Different types of tape material can have different material response as a result of rapid heating. The same prepreg material from different manufacturers could lead to a difference in final quality, since the processing conditions of the as-received tape could affect material behavior during LAFP. Choudhary [19] performed confirmatory experiments on CF/PEKK and found results similar to CF/PEEK from the same manufacturer. Kok [17] found some similarities in material response of CF/PEEK from different manufacturers, but also some significant differences. Therefore, more research is needed to understand the effect of: type of fiber, type of matrix material, resin-richness of the tape, fiber-matrix distribution throughout the tape and prepreg tapes from different manufacturers (difference in processing conditions). This will help to investigate if the material behavior due to deconsolidation is material specific.

### **Change in consolidation state and surface morphology of the tape**

Kok et al. [60] performed research on the change in consolidation state and surface morphology during the heating phase of LAFP. Current intimate contact models assume that the consolidation state of the tape at the end of the heating phase is the same as the as-received state. However, research has shown that the tape deconsolidates during the heating phase resulting in a higher void content and a changed surface morphology. Intimate contact models are based on the surface morphology of the tape, although the changing surface morphology during the heating phase is not yet incorporated. More research should be performed in order to capture the changing consolidation state and morphology, in-situ, during the heating phase. This helps to get a better understanding of the changing state of the tape such that current intimate contact models can be improved.

## **3.2. Research questions**

Gaps were identified in the current understanding of deconsolidation effects during the heating phase of LAFP as described in the previous section 3.1. The most important gaps to address in this research are *resin-rich surface tapes* and *tape pre-tension systems*.

First of all, research into thermoplastic prepreg tapes with a resin-rich surface does contribute to a better understanding of the deconsolidation mechanisms with respect to difference in material composition (in terms of a resin-rich surface). Moreover, it is expected that a resin-rich surface is beneficial for intimate contact development which is advantageous for the final laminate quality. This is therefore an interesting research direction and the expected outcome (effect of a resin-rich surface on deconsolidation during the heating phase) does add value to the future goal of minimizing deconsolidation effects.

Secondly, research into tape pre-tension systems is important since this has not been taken into account during previous research into the heating phase of LAFP. Actual LAFP machines include tape pre-tension systems, however this was lacking in an experimental setup so far. To mimic the actual LAFP machine and the process better, tape pre-tension needs to be incorporated in the experimental setup. Next to that, it is expected that tape pre-tension will minimize deconsolidation effects (this remains to be experimentally verified). Therefore, this can contribute to further optimizing LAFP-manufactured laminates with respect to quality by adjusting the level of pre-tension.

The research questions can be divided into three main questions. Research question 1 is a repetition of the research of Choudhary [19]. Research questions 2 and 3 deal with research gaps identified in literature, hence novel research. Therefore, subquestions were formulated for research questions 2 and 3.

### **1. Influence of heating time and spot length**

What is the influence of varying heating time and heated spot length on deconsolidation response parameters (surface roughness, void content development, out-of-plane deformation, thickness and arc-length increase) of thermoplastic prepreg tapes during the rapid heating phase of LAFP?

### **2. Effect of a resin-rich surface on deconsolidation**

What is the effect of a resin-rich surface on deconsolidation response parameters (surface roughness, void content development, out-of-plane deformation, thickness and arc-length increase) of thermoplastic prepreg tapes during the rapid heating phase of LAFP?

- (a) How can the resin-richness of thermoplastic prepreg tapes be defined and characterized?
- (b) Which experimental methods and equipment can be used to quantify and characterize the presence of the resin-rich surface of thermoplastic prepreg tapes?
- (c) What is the qualitative and quantitative effect of a resin-rich surface, for several process settings, on deconsolidation response parameters (surface roughness, void content development, out-of-plane deformation, thickness and arc-length increase) of thermoplastic prepreg tapes during the rapid heating phase of LAFP?

**3. Effect of pre-tension on deconsolidation**

What is the effect of tape pre-tension on deconsolidation response parameters (surface roughness, void content development, out-of-plane deformation, thickness and width increase) of thermoplastic prepreg tapes during the rapid heating phase of LAFP?

- (a) How can a static diode laser setup be designed (to simulate the rapid heating phase of LAFP) and used to study the link between controlled tape pre-tension and its effect on deconsolidation mechanisms during the rapid heating phase of LAFP?
- (b) Which equipment or devices can be used to apply (force controlled) and measure pre-tension to thermoplastic prepreg tapes?
- (c) What is the qualitative and quantitative effect, for several process settings, of tape pre-tension on deconsolidation response parameters (surface roughness, void content development, out-of-plane deformation, thickness and width increase) of thermoplastic prepreg tapes during the rapid heating phase of LAFP?

### 3.3. Hypothesis

The deconsolidation behavior is measured in terms of five deconsolidation response parameters: maximum out-of-plane deformation, surface roughness, void content, thickness increase and arc-length increase (width increase instead of arc-length increase for research question 3). Arc-length represents the arc-length of the waviness curve. The difference between the the arc-length at the start and end of the heating phase gives the change in arc-length. This is used as a representative measure for the deformation of the tape in width direction.

Hypothesis are formulated for all research questions presented in the previous section. Based on the knowledge gathered from current literature the propositions below are made. The hypothesis given for research question 1 (influence of heating time and spot length) are based on results reported by Choudhary [19].

#### 1. Influence of heating time and spot length

- (a) Fiber decompaction has a strong influence on the magnitude of out-of-plane deformation. More out-of-plane deformation is expected for shorter heating times and for larger heated spot lengths.
- (b) Surface roughness is expected to increase with heating time and heated spot length. It is hypothesized that out-of-plane decompaction contributes to an increase in surface roughness.
- (c) Increase in void content at processing temperature is primarily due to thermal void growth in the cross-section of the prepreg tape. An increase in void content with heating time is expected to be seen.
- (d) Arc-length increase during the heating phase occurs primarily due to polymer movement (transverse to the fiber direction) in its melt phase and is also influenced by void coalescence and out-of-plane deformation during deconsolidation. It is expected that less arc-length increase will be observed for longer heating times while an increase is expected with larger heated spot lengths.
- (e) Thickness increase occurs mainly due to void content increase during the rapid heating phase. Therefore, an increasing trend with heating time is expected to be seen.

#### 2. Effect of a resin-rich surface on deconsolidation

- (a) As-received prepreg tapes with a more resin-rich surface will result in a smoother surface (less surface roughness compared to a resin-poor surface) after rapid heating.
- (b) A resin-rich surface facilitates a smoother surface resulting in less decompaction of the fiber reinforcement hence less maximum out-of-plane deformation will be measured.
- (c) Resin-rich surface tapes will show a lower final void content at the heated surface of the tape due to less out-of-plane deformation compared to the reference tape (resin-poor tape).
- (d) Void content increase is the main contributor to thickness increase, however less thickness increase is expected to be observed for resin-rich surface tapes due to a lower final void content.
- (e) Arc-length increase will occur mainly due to polymer matrix movement in the melt phase and to a lesser extent as a result of void content increase. Less arc-length increase will be observed for resin-rich tapes due to a lower fiber volume fraction at the heated surface.

#### 3. Effect of tape pre-tension on deconsolidation

- (a) For higher tape pre-tension a more uniform temperature distribution in width direction is expected to be seen at the nip-point location and the amount of out-of-plane deformation is expected to be less severe.
- (b) Increased tape pre-tension will diminish the surface roughness due to less out-of-plane decompaction of the fiber reinforcement network and a more uniform temperature distribution.
- (c) More width increase will be observed for pre-tensioned prepreg tapes since out-of-plane decompaction will be hindered. If the tape can deform less in the out-of-plane direction then it should deform in width direction.
- (d) Void content development is expected to become less with increasing pre-tension force since the tape will be hindered to decompact.
- (e) Thickness increase will be expected to be less severe since less void content development is expected for higher pre-tension levels.

# 4

## Methodology

The research was divided into three research questions. The first research question deals with the influence of heating time and heated spot length on deconsolidation of thermoplastic prepreg tapes. The second research question deals with the effect of resin-rich surface tapes on the deconsolidation behavior. The third research question deals with the influence of tape pre-tension on deconsolidation behavior. In this chapter the materials, experimental setups and characterization techniques that were used along the three research lines will be discussed in detail.

### 4.1. Materials

The materials that were used for the research are summarized in table 4.1. The fiber volume content was measured (with standard deviation between brackets) and compared with the specification given by the manufacturer. For the first research question Toray/Ten Cate 0.5" thermoplastic prepreg tapes were used with a length of 10cm. For the second research question resin-rich Suprem 0.5" thermoplastic prepreg tapes were used with a length of 10cm. For the third research question Toray/Ten Cate 0.5" thermoplastic prepreg tapes were used with a tape length of 60cm in order to be able to fix the tape on one end and apply tape pre-tension on the other end.

Table 4.1: Material properties of prepreg tapes used during the research

Material type	Fiber vol. data sheet(%)	Measured fiber vol.(%)	$T_g$ (°C)	$T_m$ (°C)
Toray/Ten Cate TC-1200 (resin-poor) CF AS4D/PEEK [64]	55 <sup>1</sup>	50.8 [4.9]	143	343
Suprem (resin-rich) CF AS4/PEEK-150 [65]	55 <sup>2</sup>	44.3 [2.3]	143	343

### 4.2. Experimental setup

To simulate the LAFP-process a static experimental setup was build to perform laser heating experiments. Two different experimental setups were used during stages of the research. Both setups consist at least of a Vertical Cavity Surface Emitting Laser (VCSEL) unit, Laser Line Scanner (LLS), a thermal camera (IR-camera) and an aluminium tool to align and attach the prepreg tape specimen underneath the VCSEL. The VCSEL type that was used is a PPM412-12-890-24 [37] which has 12 distinct emitter zones and is able to deliver an optical power between 0.1 and 2.4 kW. Details on the working principle of a VCSEL were already provided in chapter 2. The LLS that was used is a MicroEpsilon ScanCONTROL 2950-25 which has a measurement range between 53.5 mm and 78.5 mm of the sensor. It was required to install it at a fixed position within the measurement range and more important perpendicular to the tape such that the measurement line of the LLS was perfectly aligned with the nip-point. The maximum measuring speed of the LLS equals 2000 Hz, however a sampling

<sup>1</sup>Material is on-spec. However, fiber volume content is still measured for comparison with Suprem material

<sup>2</sup>Material is off-spec. 55% is reported by manufacturer, 44.3% is measured

frequency of 100 Hz was used such that it could be matched with thermal data. A FLIR A655sc IR-camera with FOL25 lens was used to capture thermal data at a sampling frequency of 50 Hz during the rapid heating phase.

For the first and second research questions, the experimental setup from Choudhary [19] was used as shown in figure 4.1. Here the VCSEL was positioned at angle of  $45^\circ$  with respect to the surface of the tape. Individual heating zones along the length of the VCSEL were activated depending on the required heated spot length. This allowed for achieving a relatively uniform temperature over the width of the tape at the simulated nip-point. Since all measurements and material characterizations were performed only locally at the simulated nip-point this was the most important requirement. Along the fiber direction the goal was to achieve an as uniform temperature distribution as possible. However, due to the inclination angle of the VCSEL this was more difficult. The distance from an individual heating zone to the tape varies causing a gradient in the heat input into the material. The IR-camera was positioned at an inclination angle of  $55^\circ$  and the LLS was positioned perpendicular to the tape at the simulated nip-point. For the third research question it was needed to apply and measure tape pre-tension. The current setup did not allow to fit all the required equipment.

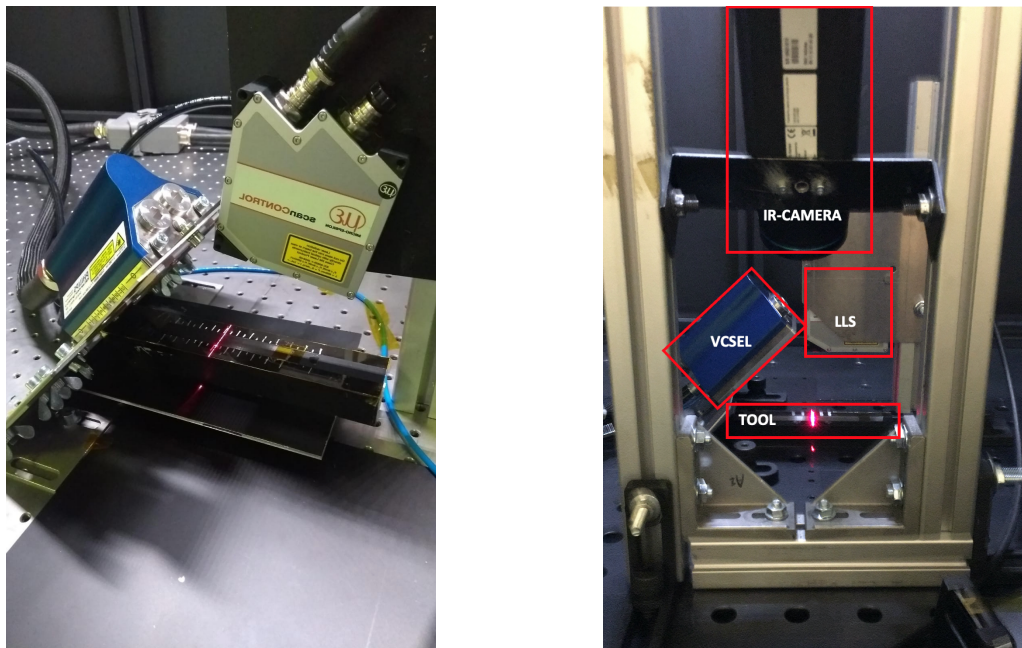


Figure 4.1: Experimental setup research parts A and B.  
Left: setup used from Choudhary [19], Right: schematic overview of setup equipment.

To provide an answer to the third research question, it is necessary to apply and measure tape pre-tension. For this a novel experimental setup had to be developed and built. Since the objective is to study the effect of tape pre-tension on the deconsolidation behavior the setup should allow for applying a pre-tension force in a controlled manner. The design freedom of the pre-tension setup is limited mostly by two factors. First of all, the entire setup should fit within the laser enclosure (for safety reasons). Secondly, all measurement equipment has to fit at a similar location with respect the tool and nip-point in the tape as compared to the setup used for the first and second research questions. An initial design as well as the proof-of-concept are included in Appendix A. The final pre-tension setup is shown in figure 4.2. As can be seen the entire setup is positioned at elevated height through aluminium profiles. This makes the setup suitable for application of pre-tension using weights and adding a load cell to measure the pre-tension force.

An in-house made load cell was used to measure the pre-tension force experienced by the tape as a result of applying a weight at the other end of the tape. Calibration of the load cell was done outside of the laser safety enclosure before using it in the pre-tension setup, see appendix B. As can be seen in figures 4.3 the load cell was fixed at the laser table. A loop of thermoplastic prepreg tape went through to the ring on top load cell in order to attach the load cell to the tape. The load cell was made to have a measurement range of 0 - 50 N, with an accuracy of 0.5%. The pre-tension measurements were captured by a data acquisition module (DAQ).

Three different levels of tape pre-tension have been chosen for the experimental research, namely 5 N, 10 N and 15 N. The lower value was experimentally determined and based on the minimum force required to let the tape make contact with the tool surface. The other two values were based on reference values in literature [26, 28] and the fact that LAFP systems often make use of low tape pre-tension values to allow for manufacturing of complex structures [27, 29]. For each of the three sets of pre-tension experiments (for 5N, 10N and 15N) the same set of weights was used throughout the two repetitions.

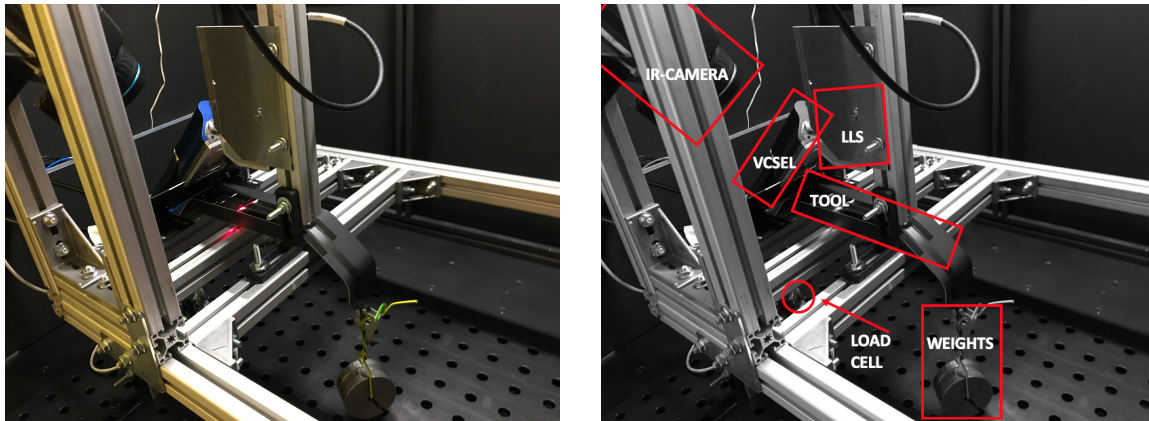


Figure 4.2: Overview of pre-tension experimental setup including schematical view

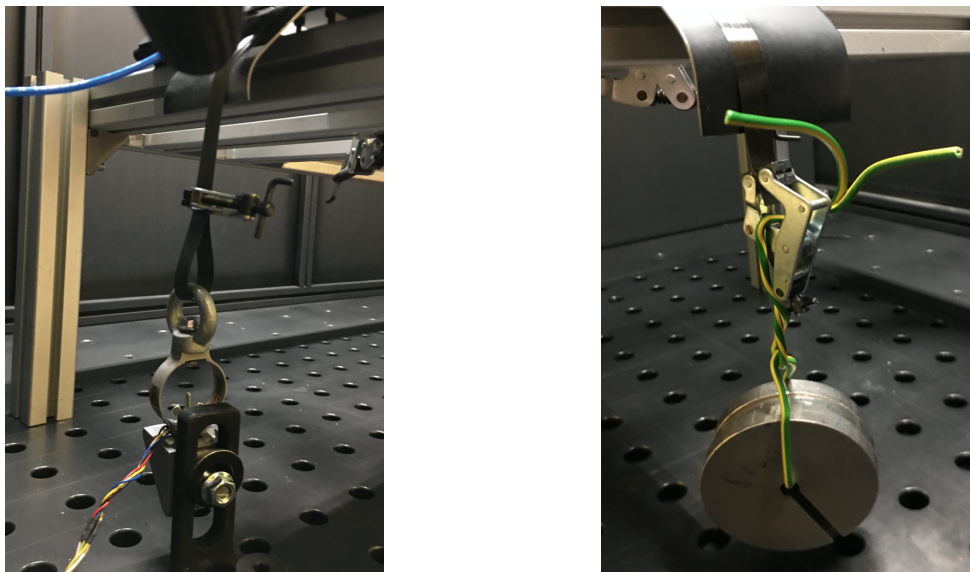


Figure 4.3: Attachments of load cell and weights to the pre-tension setup

### 4.3. Characterization techniques

Deconsolidation behavior as a result of the rapid heating phase is characterized by five different deconsolidation response variables during this research. These response variables are surface roughness, thickness increase, arc-length increase, out-of-plane deformation and void content development. Next to that, the temperature achieved in the simulated nip-point plays an important role in affecting the deconsolidation responses. The characterization techniques that were used are described in detail in the sections below. Furthermore, a new characterization technique was initiated for determining the so-called "resin-richness" of the top surface of the tape.

### 4.3.1. Characterization of a resin-rich surface

The Suprem material used for the second research question can be observed in figure 4.4. As can clearly be observed from this photograph variation exist in the gloss of the top surface of the material. Investigation was performed at different locations such that the different surface characteristics (with respect to the level of gloss) were captured and quantified. It was expected that the variation in the gloss of the top surface is linked to the resin-richness of the top surface. The methodology that was developed to analyze the resin-richness of the top surface of thermoplastic prepreg tapes was derived from Celik [42] and is based on the concept of degree of effective intimate contact (DEIC).



Figure 4.4: Suprem CF/PEEK prepreg tape material, variations in gloss can clearly be seen (camera photograph)

A Keyence VK-X1000 laser scanning confocal microscope (LSCM) was used to analyze and perform measurements on the top surface of Suprem resin-rich tapes and for comparison on Ten Cate resin-poor tapes. The Keyence VK-X1000 LSCM can be seen in figure 4.5 and was moreover also used for surface roughness characterization and cross-sectional microscopy.

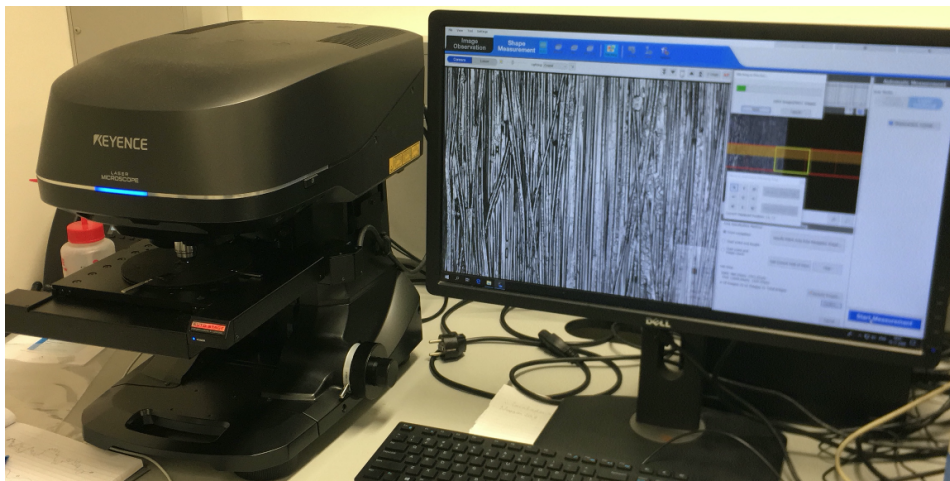


Figure 4.5: Keyence VK-X1000 laser scanning confocal microscope

Prepreg tapes with a width of 0.5" were extracted from the material shown in figure 4.4. Three different material variations can be distinguished here: samples with an entire glossy surface, a matte surface and both glossy and matte characteristics (see figure 4.4). Top surface images were captured with the Keyence LSCM at 50X magnification, see image 1 in figure 4.6. Three local measurements were performed per sample, at 30%, 50% and 70% along the width of the 0.5" specimen. This was done to account for variations within a specimen. Three repetitions were performed for each of the material variations. In total, 9 resin-richness measurements were performed (3 repetitions at 3 locations) per material type.

The steps taken to quantify the resin-richness from a top surface micrographs can be best explained with figure 4.6. The image size of a locally captured top surface micrograph (see figure 4.6) is 2048 by 730 pixels and the resolution is  $3.6 \mu\text{m}/\text{pixel}$  for all images. Grayscale intensity histograms were generated by using a MATLAB script for each micrograph separately. As can be seen in figure 4.6 a large peak exist in the middle of the histogram (around 130). They grayscale related to this peak can be allocated to pixels that are associated with resin. A small peak can be observed at the right-hand-side of the histogram (around 220). In between, a local minimum is indicated in figure 4.6, this is the location in the histogram that is used as the threshold. The pixels with a grayscale lower than the threshold belong to resin, while pixels with a grayscale higher than the threshold value belong to fibers. Binary images were created from the top surface micrograph and with the threshold from the histogram as separation between fibers and resin. A binary image can be seen in the third image of figure 4.6, with red areas fibers are indicated and the black area belongs to resin. The resin-richness is quantified (from the third image in figure 4.6) as the resin area content expressed in percentages of the total image area.

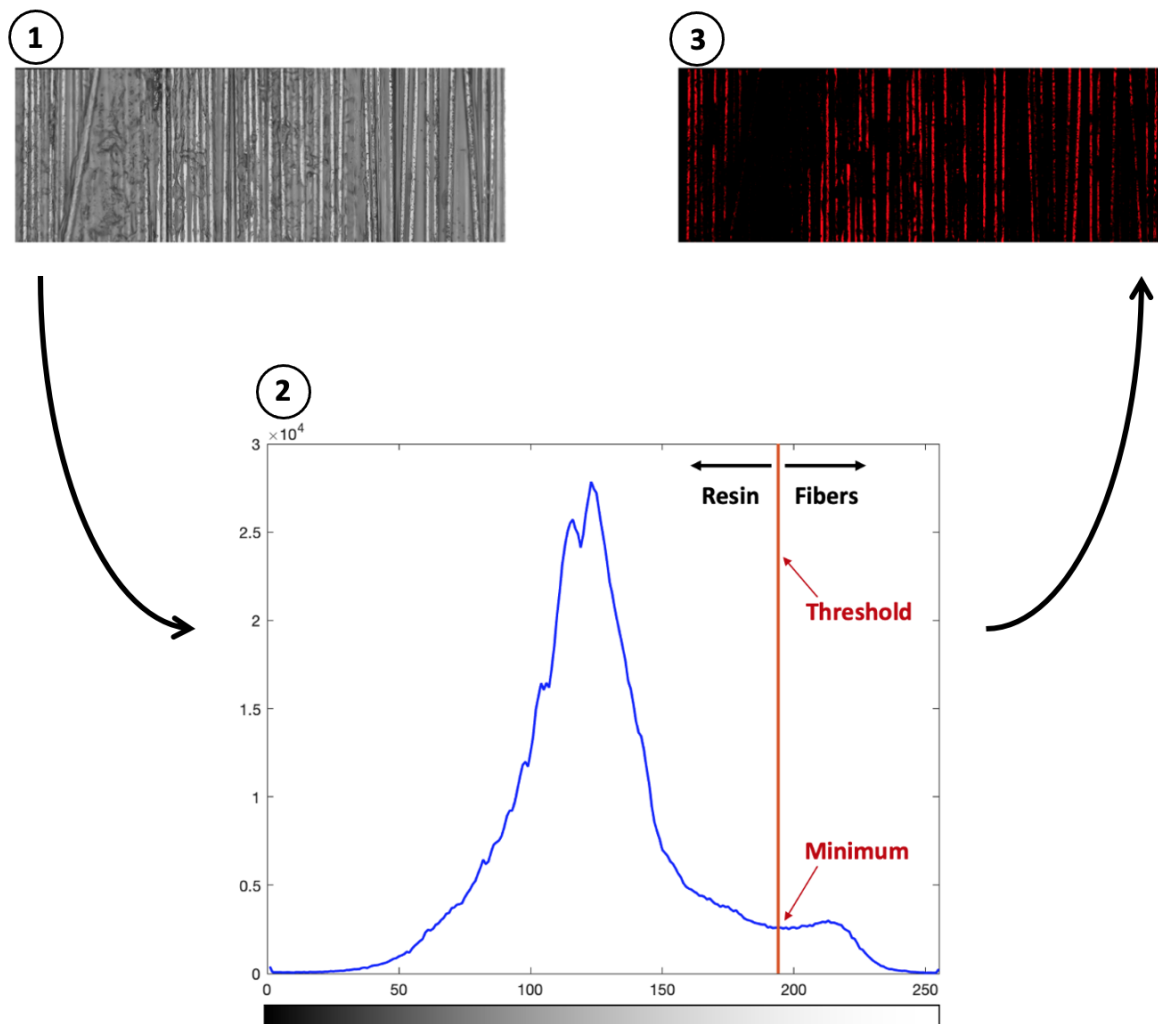


Figure 4.6:

- 1: Gray scale top surface micrograph (50X magnification)
- 2: Histogram of grayscale top surface micrograph
- 3: Binary image (red is allocated to fibers and black to resin)

#### 4.3.2. Temperature measurements

In-situ temperature measurements were performed to monitor the material behavior during the rapid heating phase. First of all, the temperature was continuously measured by using the FLIR A655sc IR-camera. In figure 4.7 the simulated nip-point is indicated as a line across the width of the tape. The average nip-point

temperature was measured as the average temperature across this line. The laser settings (activated zones and power per zone) of the VSCEL were adjusted such that it was aimed for a mean nip-point temperature of around 360-400 °C.

The IR-camera needed to be calibrated before executing the actual temperature measurements during de-consolidation experiments. The emissivity was experimentally determined in order to account for the inclination angle of the IR-camera and variation in emissivity due to different prepreg tape materials. Details on the IR-camera calibration can be found in Appendix C. For Toray/Ten Cate CF/PEEK tape material an emissivity of 0.80 was found and for Suprem CF/PEEK an emissivity of 0.81 was found.

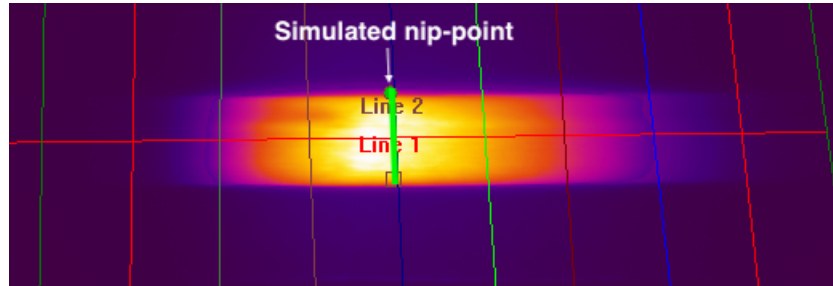


Figure 4.7: Simulated nip-point for rapid heating experiment with 30mm spot length.

In figure 4.8 a graphical representation of the temperature measurements can be seen that was retrieved from the raw temperature data. In the left graph the simulated nip-point mean temperature can be seen as a function of the heating time. In this example, a maximum average nip-point temperature of 385°C was reached at the end of the heating phase. The right graph represents the temperature distribution across the width of the tape at the nip-point location at the end of heating.

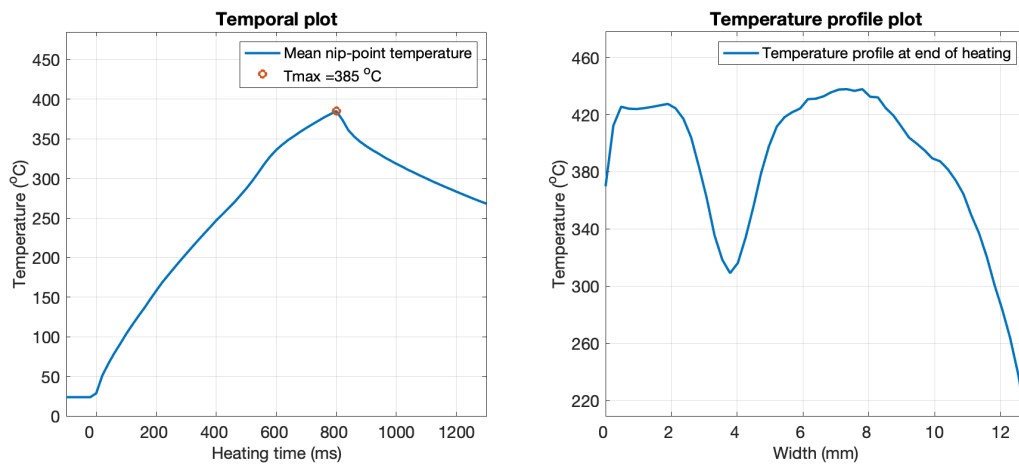


Figure 4.8: Left: Temporal plot of mean nip-point temperature, Right: Temperature profile at the end of the heating phase Both measured at the simulated nip-point location, example from A80/800

### 4.3.3. Tape surface deformation measurements

The deformation of the surface of the tape, in width and out-of-plane direction, was measured at the nip-point location with a LLS. In figure 4.9 the surface deformation profiles are shown by the blue curves at the start (left graph) and end of heating (right graph). The red curves represent the waviness profiles. A cut-off wavelength of 0.8mm was used here to extract the global waviness profiles from the raw measurement data.

Arc-length increase is one of the 5 main deconsolidation response variables and is calculated from the waviness profiles. The difference between the the arc-length at the start and end of the heating phase gives the change in arc-length. This is used as a representative measure for the deformation of the tape in width direction.

Maximum out-of-plane deformation is retrieved from the LLS measurement data as well. The maximum out-of-plane deformation is determined by the average of three data points around the global maximum at the end of heating. It is calculated with respect to the as-received state of the tape. That means, the average deformation of the initial state of the tape was determined and subtracted from the maximum out-of-plane deformation at the end of heating. This ensures that for every sample the maximum out-of-plane deformation is determined in the same manner and relative to the initial state of that specific sample. Moreover, in this way the data is corrected for variation in the initial thickness of the tape.

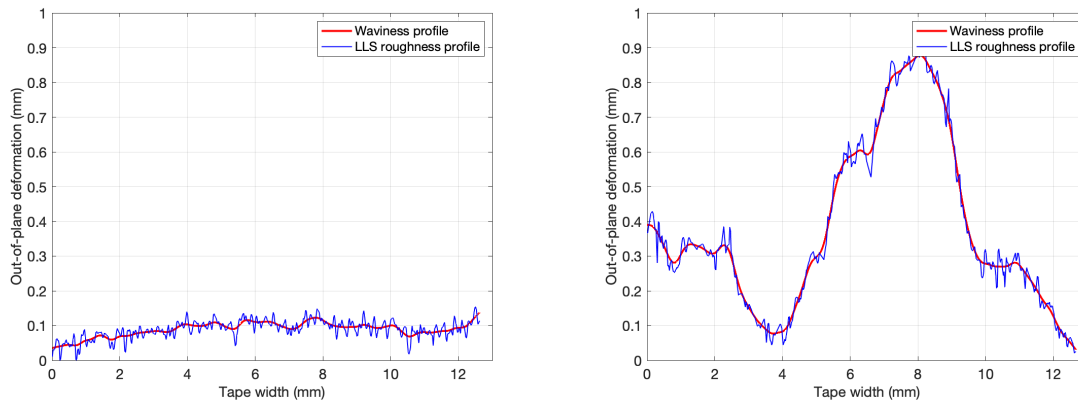


Figure 4.9: In-situ tape deformation measured by LLS and corresponding waviness profile. Left: start of heating phase, Right: end of heating phase

The validation of the LLS was done by a comparison with surface deformation measurements obtained from the Keyence VK-X1000 LSCM. As can be seen in figure 4.10 the data from the LLS does not perfectly match the data from the LSCM. This is due to several reasons. First of all, the tape specimen is not exactly the same mounted to the LSCM table as it is mounted to the tool. Secondly, a deviation in the scale of both measurements exist because the LSCM measurements were performed at 20X magnification. Thirdly, the LLS data is retrieved right at the end of heating while the LSCM data is retrieved after cooling down to atmospheric conditions (room temperature). Nevertheless, at least the same deformation trends could be observed for both measurements.

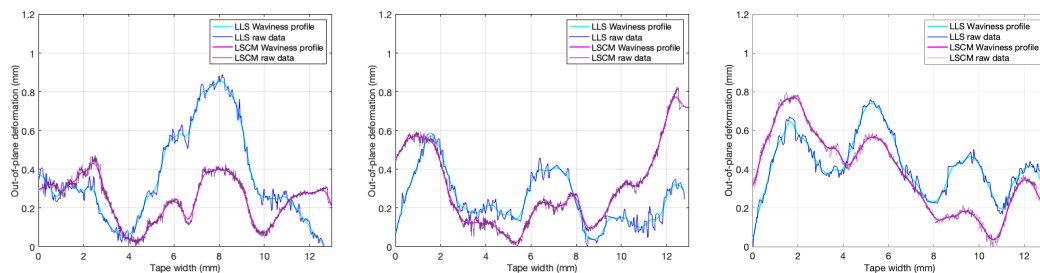


Figure 4.10: Comparison of tape deformation profiles obtained from LLS and LSCM, examples of config. A80/800

#### 4.3.4. Surface roughness evaluation

The surface roughness was measured from the top surface images that were captured with the Keyence VK-X1000 LSCM at 20x magnification. These images were captured over the entire width and automatically stitched together by the LSCM. In figure 4.11 the height map (3D plot of surface deformation) of a top surface measurement can be seen. In figure 4.12 the total 2D surface profile can be seen in the left image as well as the roughness profile that is extracted from that in the right image. Two important observations can be made here. Firstly, variation exists in global deformation pattern of the tape, this can be best observed in figure 4.11 and figure 4.12 (left). Secondly, variation in local roughness exist as can be seen from figure 4.12 (right).

This variation in roughness over the width of the tape is dependent on the global deformation pattern. It was found that the highest roughness is measured at local extremes in the waviness curve.

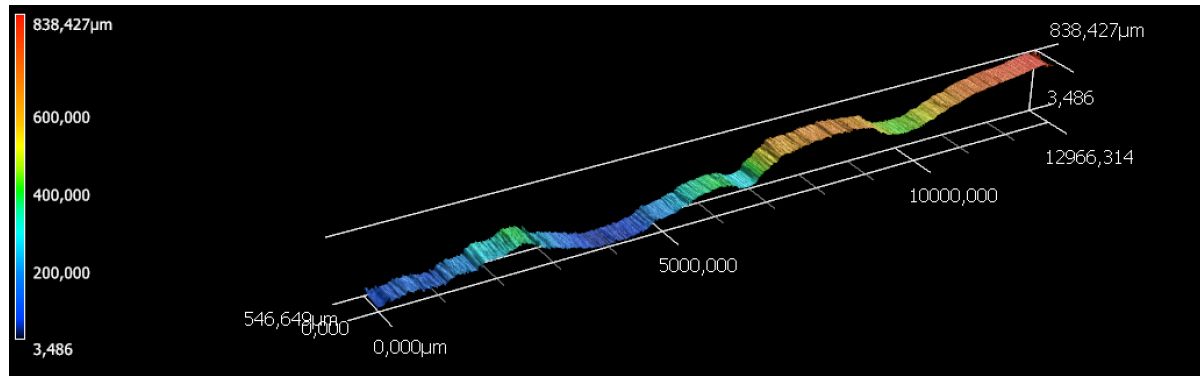


Figure 4.11: Height map of the nip-point surface

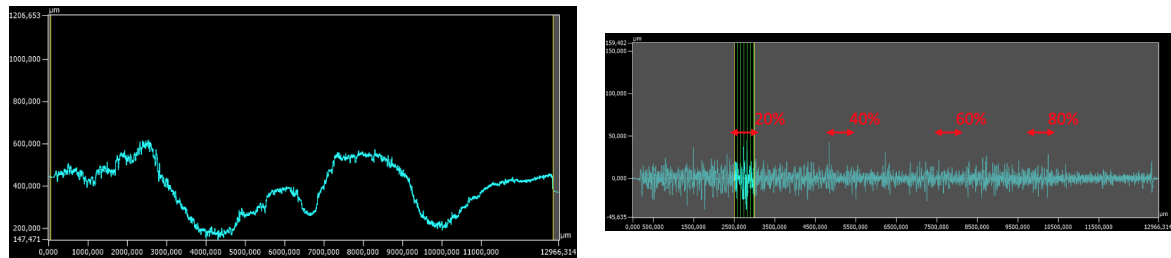


Figure 4.12: Surface deformation profiles retrieved from LSCM

Left: Total surface profile (raw measurements), Right: Surface roughness measured locally around 4 different locations, at 20%, 40%, 60% and 80% of the width at nip-point location

Because of the large variation in roughness across the width, it was decided to measure the surface roughness response variable locally at 4 different locations. In figure 4.12 it can be seen that the surface roughness is determined around 20%, 40%, 60% and 80% of the width. Local measurements at different distinct locations ensures that the data is not driven by just an extreme being present in the material.

The local roughness measurements were captured over a width of  $500\mu\text{m}$ . Based on ISO-4287 a minimum of 5 sampling lengths should be used within an evaluation length. A cut-off length of  $0.08\text{mm}$  was used, which means 6 samplings within  $500\mu\text{m}$  evaluation length. The multi-line roughness tool was used within the Keyence Multi-File Analyzer software to determine the root-mean-square (RMS) surface roughness value ( $R_q$ ). The tool evaluates the roughness over 11 line measurements in width direction. The 11 lines are equally divided within the evaluation area in length direction of the tape. The RMS roughness that the software reports is the average over 11 lines. An average RMS roughness over the 4 measurement points per sample (at 20%, 40%, 60% and 80%) is presented in the results Chapters 5-7.

### 4.3.5. Cross-sectional microscopy

In order to analyze the cross-section at the nip-point location, samples were prepared at first. The 10 cm prepreg samples were cut at the nip-point location with an offset of a few millimeters to allow for grinding and polishing of the surface. Small pieces of prepreg specimen were subsequently embedded into epoxy resin. Next, these cross-sectional samples were prepared and cured in the Struers CitoVac, see left image in Figure 4.13. The surface was then grinded and polished with the Struers Polishing machine, see middle image in Figure 4.13. The final state of a cross-sectional sample can be seen in the right image of Figure 4.13.



Figure 4.13: Steps taken for cross-sectional epoxy samples preparation. Left: Struers CitoVac, Mid: Struers Tegramin-20 Polishing machine, Right: Cross-sectional sample

These fully prepared samples were used to analyze with the Keyence VK-X1000 LSCM. Cross-sectional images at the nip-point location were captured at 20X magnification and the images were automatically stitched together over the entire width and height of the cross-section of the tape. An example of a cross-sectional image can be seen in Figure 4.14. These images were used to measure the thickness increase and the global void content of the tape as a result of deconsolidation during rapid laser heating.

#### 4.3.6. Thickness measurements

The thickness was measured locally at 4 distinct locations (20%, 40%, 60% and 80%) along the width of the tape using the Multi-File Analyzer software of Keyence. To account for local variation in thickness, three observations were performed at each location and the average of three observations was taken as local thickness measurement, see Figure 4.14. The thickness is given by the perpendicular distance between the top and bottom surface, loose fibers separated from the surface not taken into account. Since surface roughness was measured locally (from top surface micrographs), thickness was measured (from cross-sectional micrographs) at corresponding locations for the same reason. This is beneficial because the five consolidation variables could not be analyzed separate from each other. The thickness of as-received samples is determined in exactly the same manner as for deconsolidated samples. Thickness increase is therefore measured with respect to the average of multiple as-received state samples.

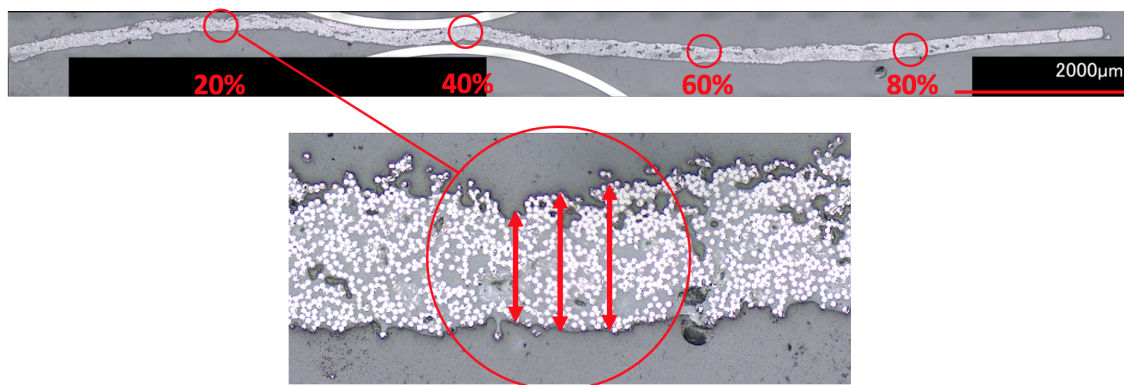


Figure 4.14: Thickness locally measured at 4 locations along the width at nip-point location

#### 4.3.7. Void content evaluation

The global void content was determined by the method described here. The background of the images (that contains the epoxy resin for embedding) needed to be removed using Adobe Photoshop. It can be seen in figure 4.16 that the background of the image is entirely black. The image was then converted in MATLAB to a grayscale image first and subsequently the histogram of the grayscale image was plotted as can be seen in figure 4.15. This helped in determining the thresholds for the pixels that can be attributed to the global void content. The peak around 250 (white pixels) in the histogram can be attributed to fibers in the cross-sectional

image. The peak around 180 (light gray pixels) can be attributed to the PEEK matrix. The peak around 0 can be attributed to the interface between the tape and embedding epoxy resin and is therefore not counted as voids. Since the method is not completely perfect, the void content is given as a range from a minimum to a maximum threshold as can be seen in figure 4.15. With the minimum threshold a best approximation for the lower bound on the actual void content is performed, with the maximum threshold a best approximation for the upper bound on the actual void content is given. In the results the void content is presented as the average of the minimum threshold and maximum threshold and expressed as an area percentage of the total cross-sectional tape surface area. In Figure 4.16 the voids are indicated by the red areas.

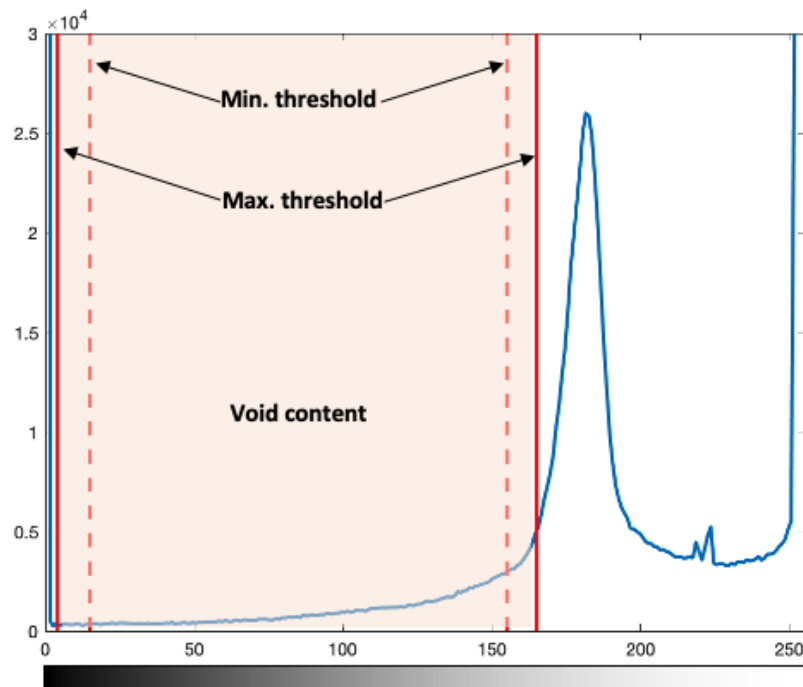


Figure 4.15: Histogram of the grayscale cross-sectional image with thresholds indicated for void content measurement

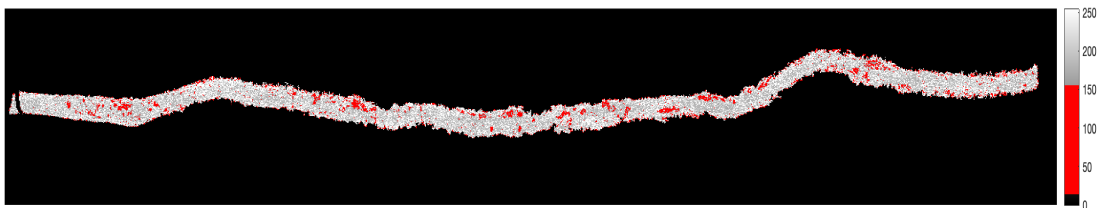


Figure 4.16: Void content indicated by the red areas

#### 4.4. As-received state tape material properties

The characterization methods described in the previous sections were used to characterize the as-received state of the tape material, both for Toray-Ten Cate (TC) and Suprem. In Table 4.2 the results can be observed.

The RMS roughness of Toray-Ten Cate material is determined from the average measurement over 9 different as-received samples. For Suprem material the RMS roughness is determined from the average over 11 different samples. The difference in amount of samples arises from the difference in process configurations. For Toray-Ten Cate the RMS roughness was measured on only one as-received sample per configuration. For

Suprem the as-received RMS roughness was measured on all valid samples (11) due to larger variations between as-received samples (off-spec material). The standard deviation in Table 4.2 is given between square brackets. As can be seen the standard deviation is almost 2.5 times as large for Suprem material in terms of RMS roughness. Therefore, the roughness increase is also reported in the results (Section 6.3.1) per sample for Suprem material.

The as-received width is determined from the average over 5 samples for both Toray-Ten Cate and Suprem. It is measured by the distance between the two edges of a sample (perpendicular to the fiber direction) in top surface micrograph images. The large standard deviation for Suprem is due the fact that samples were cut in-house from 150mm width tapes to 0.5" tapes by an automated cutting machine, whereas Toray-Ten Cate material was already delivered from the supplier to 0.5" tapes.

Finally, the thickness and void content of as-received samples are determined from the cross-sectional images as explained in Section 4.3.5. For Toray-Ten Cate 3 cross-sectional samples were used because all seem to be quite similar in terms of thickness and void content. For Suprem 5 samples were used as more variation can be observed between as-received samples looking at the cross-sectional micrographs. This is an important observation because it can affect the deconsolidation behaviour and will be explained in more detail in Chapter 6.

Table 4.2: As-received state prepreg tape properties, standard deviation between square brackets

<b>Material</b>	<b>RMS roughness (<math>\mu\text{m}</math>)</b>	<b>Width (<math>\mu\text{m}</math>)</b>	<b>Thickness (<math>\mu\text{m}</math>)</b>	<b>Void content (min-max, %)</b>
TC AS4/PEEK	1.939 [0.213]	12751 [21]	166.92 [7.34]	0.47 - 0.65 [0.18]
Suprem AS4/PEEK	1.726 [0.503]	12939 [483]	173.79 [10.1]	0.39 - 0.87 [0.28]



# 5

## Results: influence of heating time and heated spot length

Chapter 5 presents the results on the influence of heating time and heated spot length on deconsolidation behavior of thermoplastic prepreg tapes. This chapter will provide an answer to the first research question: *"What are the effects of varying heating time and heated spot length on deconsolidation response parameters (surface roughness, void content development, out-of-plane deformation, thickness and arc-length increase) of thermoplastic prepreg tapes during the rapid heating phase of LAFP?"*. The main goal of this chapter is to investigate the influence of varying heating time and heated spot length on the deconsolidation behavior. Next to that, a comparison can be made with an earlier study of Choudhary [19] because no statistical data was gathered during that study. A verification of the findings can therefore be performed especially for the results that were found to be statistically insignificant. The test matrix for the experiments is shown in section 5.1. The results in terms of the five deconsolidation response variables will be given in section 5.2. After which a discussion of the results including a comparison to the study of Choudhary [19] will follow in section 5.3.

### 5.1. Test matrix

For the first research question heating times of 350ms, 500ms and 800ms were used and heated spot lengths of 30mm, 50mm and 80mm. These variables were chosen such that the results could be compared to the study of Choudhary [19]. The only deviation here is the lower limit for the heating time. During this research 350ms was used as the lower limit for the heating time, while Choudhary [19] used 200ms as the lower limit for the heating time. It was experimentally determined that it was impossible for the VCSEL to heat the material to the processing temperature for a heating time of 200ms and a heated spot length of 30mm. This was most likely caused by degradation of the laser emitters.

The process configurations can be seen in table 5.1. The activated zones of the VCSEL and the laser power (and power per individual zone) are given as well. It was aimed for a processing temperature of 360-400 °C. Three repetitions were performed for each of the process configurations.

Table 5.1: Configuration settings experimental research 0.5" Ten Cate prepreg tapes

Process config.	A30/350	A30/500	A30/800	A50/350	A50/500	A50/800	A80/350	A80/500	A80/800
Spot length (mm)	30	30	30	50	50	50	80	80	80
Heating time (ms)	350	500	800	350	500	800	350	500	800
VCSEL zones active	4-6	4-6	4-6	3-8	3-8	3-8	1-11	1-11	1-11
Power per zone (%)	100	70	44	58	45	30	52	40	28
Total power (W)	600	420	264	696	540	360	1144	880	616

## 5.2. Influence of heating time and heated spot length on the deconsolidation response of Toray-Ten Cate tapes

The results in terms of the influence of varying heating time and heated spot length on the deconsolidation response are given in sections 5.2.1-5.2.5. For each response variable the results are given in a separate section. The scatter diagrams will show the average results over 3 repetitions, while the error bars represent the minimum and maximum of the 3 repetitions. Since all the response variables and their underlying mechanisms interact with each other, the results will be discussed together in section 5.3. A comparison of the results obtained during this research and the results shown in the study of Choudhary [19] will be made here as well.

### 5.2.1. Out-of-plane deformation

The results in terms of maximum out-of-plane deformation are shown in figure 5.1. In the left graph (figure 5.1a) the effect of heating time is shown. As can be seen no significant trend with heating time can be observed. In the right graph (figure 5.1b) no effect of spot length on the maximum out-of-plane deformation is observed. In general, an increase in the out-of-plane deformation can be noticed as a result of heating the heating phase, see figure 5.2. However, no significant difference can be observed in the magnitude of the maximum out-of-plane deformation despite the several process configurations.

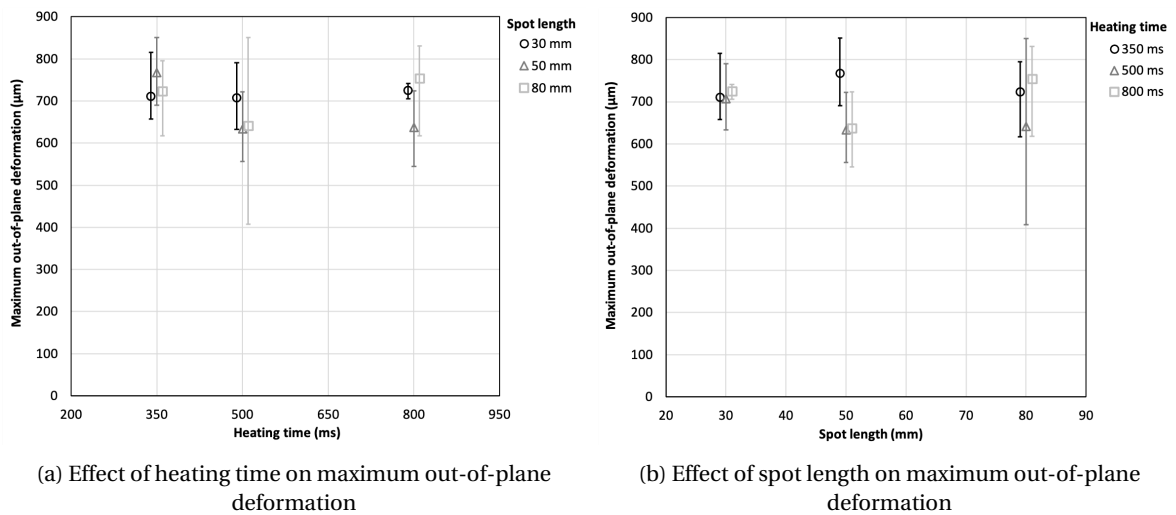


Figure 5.1: Influence on out-of-plane deformation for several process configurations

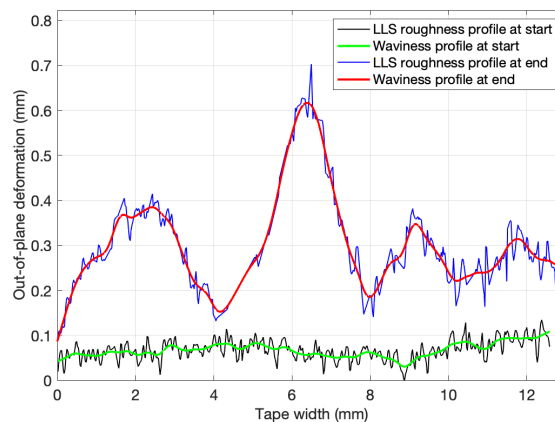


Figure 5.2: Comparison between out-of-plane deformation at the start of heating and at the end of heating. Heating time = 500ms and heated spot length = 50mm

Another observation that was done is shown in figure 5.3. The temperature profile at the end of heating is plotted together with the deformation profile retrieved from the LLS at the end of heating. It can be seen that at the valley in the temperature profile the out-of-plane deformation remains lower. The out-of-plane deformation is highest at the locations where the temperature is also at its maximum value. This implies that the way the tape deforms has an effect on the temperature distribution over the width which was also observed during the study of Choudhary [19].

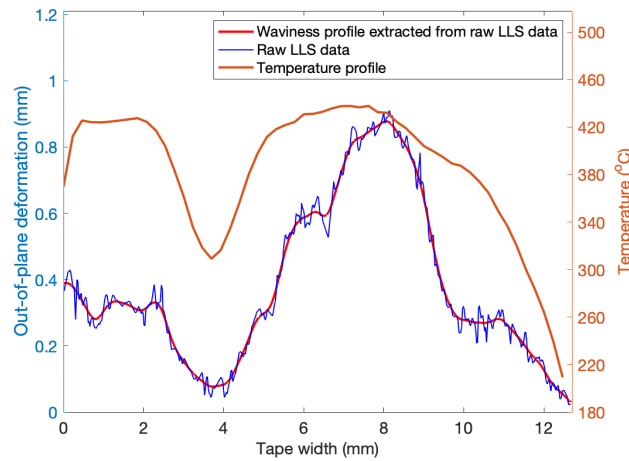
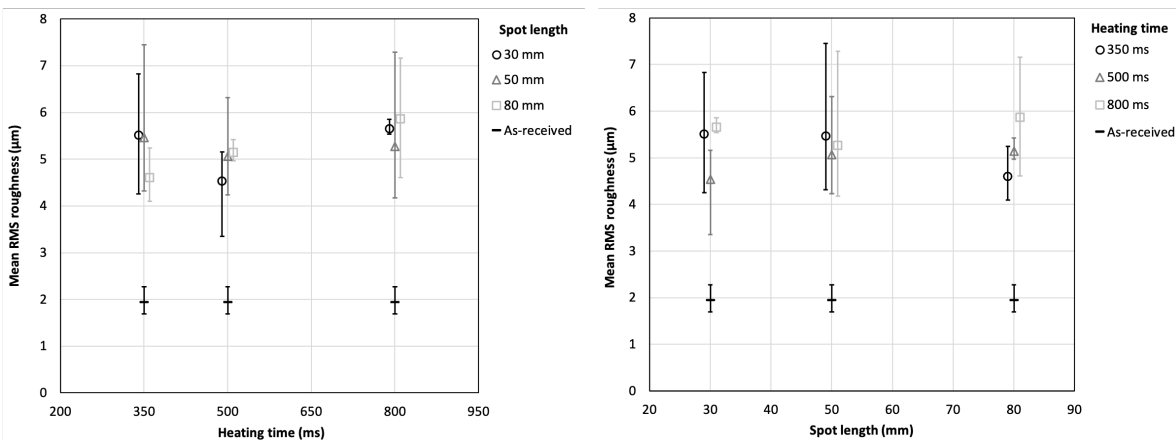


Figure 5.3: Temperature profile plotted together with deformation profile (from LLS) at the end of heating. Heating time = 800ms and heated spot length = 80mm

### 5.2.2. Surface roughness

The results for surface roughness are shown in figure 5.4. The mean RMS roughness for as-received samples (measured for 9 samples) is indicated by the black dash around  $2 \mu\text{m}$ . An increase in mean RMS roughness can be observed for all process configurations due to rapid heating. In the left graph (figure 5.4a) the mean RMS roughness is shown as a function of heating time. As can be seen no significant effect of heating time on mean RMS roughness can be observed. In the right graph (figure 5.4b) no significant effect of heated spot length of mean RMS roughness can be noticed. Due to relatively large scatter in the results, no significant difference in the magnitude for mean RMS roughness after heating can be noticed between different process configurations.



(a) Effect of heating time on RMS roughness

(b) Effect of spot length on RMS roughness

Figure 5.4: Influence on RMS roughness for several process configurations

### 5.2.3. Void content

In figure 5.5 the results for the void content are presented. In general it can be stated that a significant increase in void content occurs due to rapid heating (initial void content is <1%). No clear trend with respect to heating time can be observed in the left graph (figure 5.5a). The effect of heated spot length on void content development can be seen in the right graph (figure 5.5b). As can be observed the void content is decreasing with larger spot length.

It has to be taken into account that scatter in the results for void content exists mainly due to the characterization method. An error is made with regards to the exact location of the nip-point since grinding and polishing of the cross-sectional samples can cause a slight offset (of a few millimeters) from the actual simulated nip-point location.

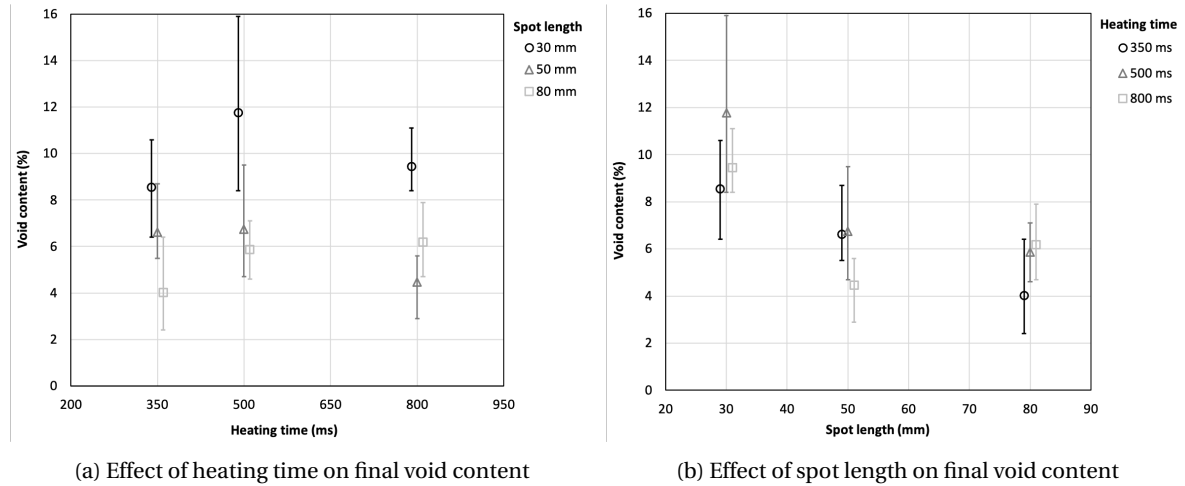


Figure 5.5: Influence on void content for several process configurations

From the cross-sectional micrographs (figure 5.6) it can be concluded that mainly large voids near the heated surface are causing the high void content for 30mm heated spot length. From figure 5.5 it can be concluded that 30mm samples exhibit the largest void content. A typical example can be seen in the top image of figure 5.6. For 50mm spot length voids are typically present in the middle of the material (through-the-thickness). The large voids near the heated surface are not observed for 50mm and 80mm heated spot length. For 80mm it is a combination of large and smaller voids present in the middle of the material.

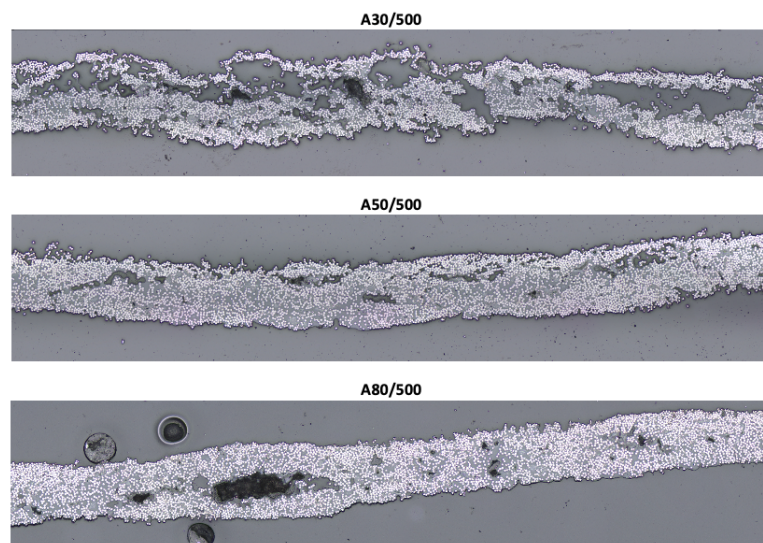


Figure 5.6: Voids present in the material for different heated spot lengths

### 5.2.4. Arc-length increase

The results for the arc-length increase are shown in figure 5.7. Heating time seems to have a decreasing effect on the arc-length increase as can be seen in the left graph (figure 5.7a). Next to that, samples with 80mm spot length show a significant larger arc-length increase for all three heating times. In the right graph (figure 5.7b) the effect of heated spot length on the arc-length increase is given. An increasing trend with heated spot length can be observed for 350ms samples. For 500ms and 800ms samples the data seem to suggest an increasing trend with respect to heated spot length as well, however it is less obvious than for 350ms samples.

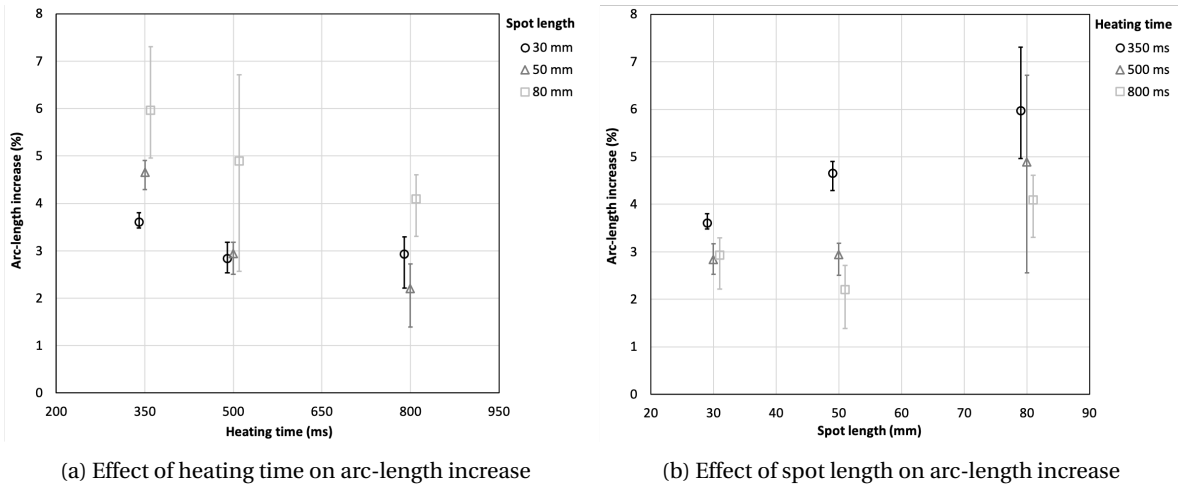


Figure 5.7: Influence on arc-length for several process configurations

The decreasing trend with heating time for arc-length increase can be explained by a combination of effects. Void coalescence (small voids merge together into larger voids) can occur for longer heating times resulting in less deformation in the width direction of the tape. Next to that, the global waviness profile seems to decrease for longer heating times. This will be further discussed in section 5.3.

The arc-length increase is determined by the arc-length of the waviness curve. More variation in out-of-plane deformation (larger waviness) was observed for larger heated spot lengths, this explains the larger arc-length increase for larger heated spot lengths. This can be seen in figure 5.8, a large difference exists between the peaks and valleys in the waviness curve for 80mm heated spot length.

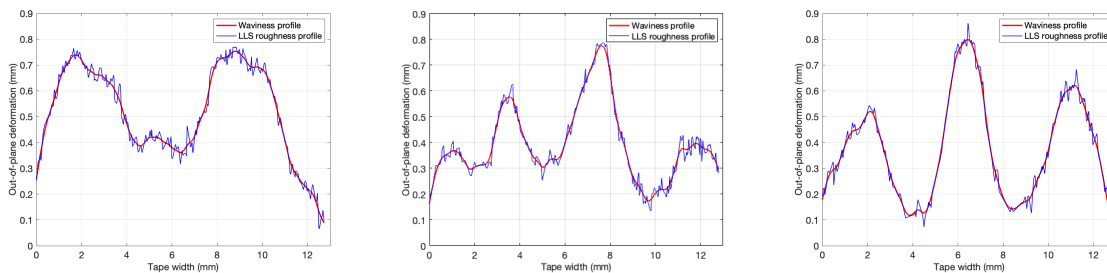


Figure 5.8: Out-of-plane deformation and waviness curves for a heating time of 350ms. Left: heated spot length = 30mm; Mid: heated spot length = 50mm; Right: heated spot length = 80mm

### 5.2.5. Thickness increase

In figure 5.9 the results for the thickness increase are presented. The error bars represent the measurement of the minimum and maximum sample from 3 repetitions (average measurement per sample, i.e. average of the 4 measurements at 4 locations along the width). The large scatter that is observed in the results is caused by the measurement method. The global mean thickness increase is determined from four local measurements. Due to large variations in thickness over the width of the tape the results are affected and show large variations.

The left graph (figure 5.13a) seems to show an increase for mean thickness increase with increasing heating time (except for data point 50mm, 800ms). However, it has to be emphasized that large scatter is observed in the results and this trend is not significant. From the right graph (figure 5.13b) no clear statement can be made with respect to the effect of the heated spot length. The main contributor to thickness increase is void content development, this will be further discussed in section 5.3.

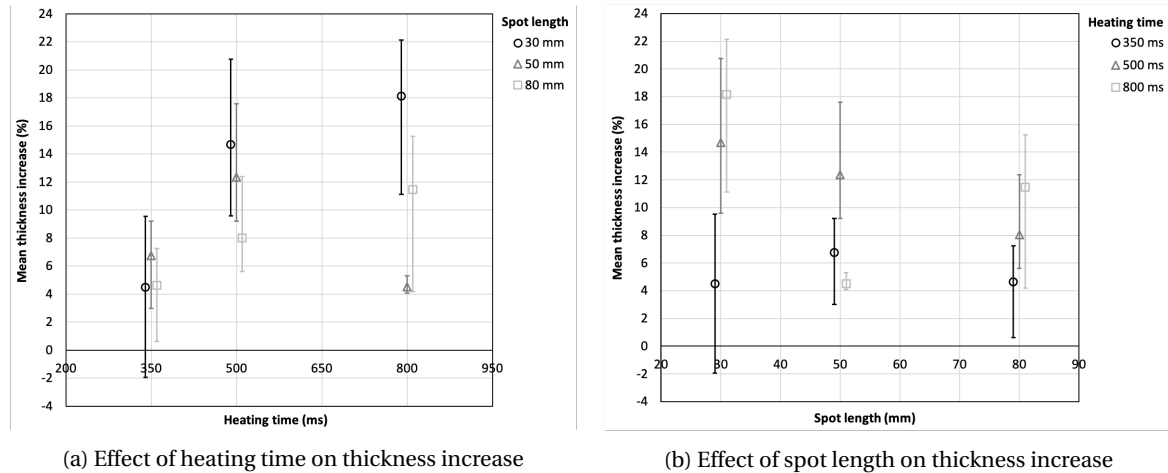


Figure 5.9: Influence on thickness increase for several process configurations

### 5.3. Discussion

The hypotheses that were given after the first research question in chapter 3 are based on findings and trends with respect to heating time and heating spot length observed by Choudhary [19]. A comparison can therefore be made between the results found in this research and the study of Choudhary in the discussion below.

The results in section 5.2.1 suggest that the temperature plays an important role for out-of-plane deformation. As will be shown that the temperature profile at the nip-point dominates the out-of-plane deformation and surface roughness. Both deconsolidation response parameters show a significant increase due to rapid heating, but no dependency with heating time or heated spot length. No effect is seen of variation in process configurations on the magnitude of maximum out-of-plane deformation and surface roughness. As was already shown the out-of-plane waviness formation at the simulated nip-point influences the temperature profile at the end of heating. This is an indication that the temperature achieved at the simulated nip-point is the most dominant factor affecting out-of-plane deformation and surface roughness. Moreover both parameters are interlinked through the same underlying mechanism: decompaction of the fiber reinforcement network (see figures 5.10-5.11). Large surface roughness is observed at locations with a local peak in the out-of-plane waviness profile. These peaks can be linked to peaks in the temperature profile (figure 5.10).

Choudhary [19] reported a significant decreasing trend for out-of-plane deformation with heating time and a significant increasing trend with heated spot length. The hypothesis was also based on these findings: "*fiber decompaction has a strong influence on the magnitude of out-of-plane deformation. More out-of-plane deformation is expected for shorter heating times and for larger heated spot lengths*". It can be concluded that the first part of the hypothesis is supported by the data: fiber decompaction has a strong influence on the magnitude of out-of-plane deformation. However, the trends with heating time and spot length are not observed because the temperature at the simulated nip-point is the most dominant factor as explained before. The maximum out-of-plane deformation is determined by a local point at the end of heating. Similar temperatures (of around 420-440°C) were found at the location of maximum out-of-plane deformation during this study, resulting in a similar magnitude of maximum out-of-plane deformation for all configurations. Therefore, it is assumed that more variation exists in the temperatures that Choudhary [19] measured at the location of maximum out-of-plane deformation for different configurations. In other words, more maximum out-of-plane deformation is measured at locations with higher temperatures. This can cause the trends that were observed with heating time and heated spot length.

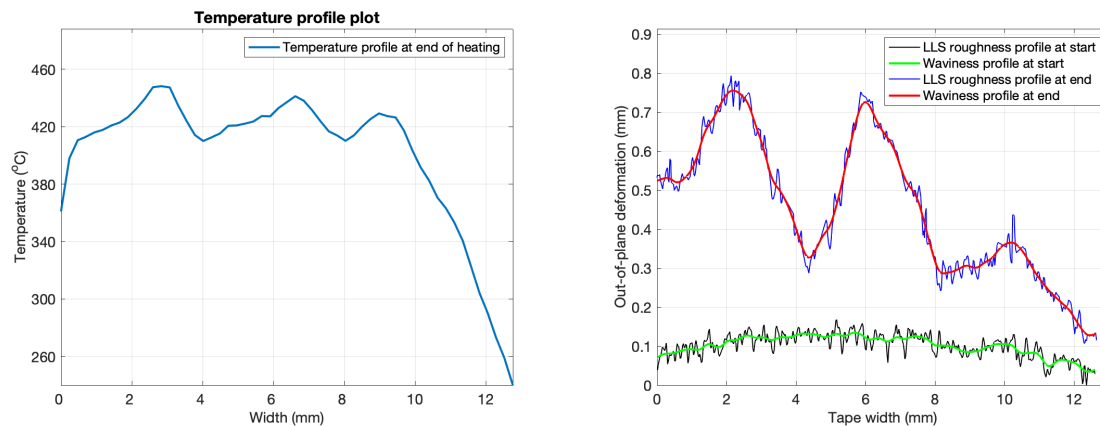


Figure 5.10: Temperature profile and deformation profile of the simulated nip-point at the end of heating, sample A30/350

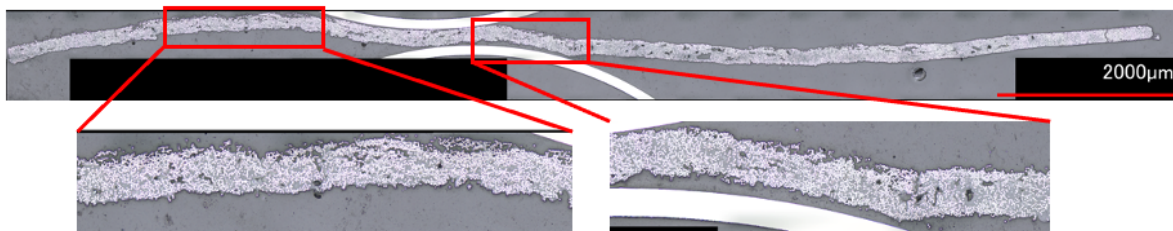


Figure 5.11: Large roughness and out-of-plane decompaction shown at locations where peaks are shown in waviness profile, sample A30/350

An increase with heating time and heated spot length was expected for surface roughness. The following hypothesis was formulated: *"Surface roughness is expected to increase with heating time and heated spot length. It is hypothesized that out-of-plane decompaction contributes to an increase in surface roughness"*. The second part of the hypothesis is supported by the data as was shown in figures 5.10 and 5.11. Large surface roughness and out-of-plane decompaction can be observed at locations where a peak is present in the waviness curve. Choudhary [19] observed significant increasing trends with heating time and heated spot length for surface roughness, however this could not be confirmed during this research. It is expected that this is due to the same cause as just described for out-of-plane deformation.

The void content results show two possible mechanisms of void formation: void formation due to traction and cavitation at the heated surface as a result of decompaction and void thermal growth. This can be seen in figure 5.12. Void formation due to traction and cavitation is mainly present in samples with the short heated spot length (30mm) and occurs primarily as a result of decompaction of the fiber reinforcement network. As can be seen in figure 5.12a these voids are present close to the heated surface where large out-of-plane decompaction is present. As a result of decompaction fibers are popping-out of the surface and fiber rearrangement occurs, hence creating large voids near the heated surface. This is an indication that out-of-plane decompaction plays a major role in void formation when the heat is concentrated on a small area (higher local heat flux for heated spot length = 30mm). Next to this, void growth occurs as a result of void thermal expansion of voids already present in the as-received material. Void growth due to thermal expansion during the rapid heating phase does occur especially for 50mm and 80mm samples, an example of these voids can be seen in figure 5.12b.

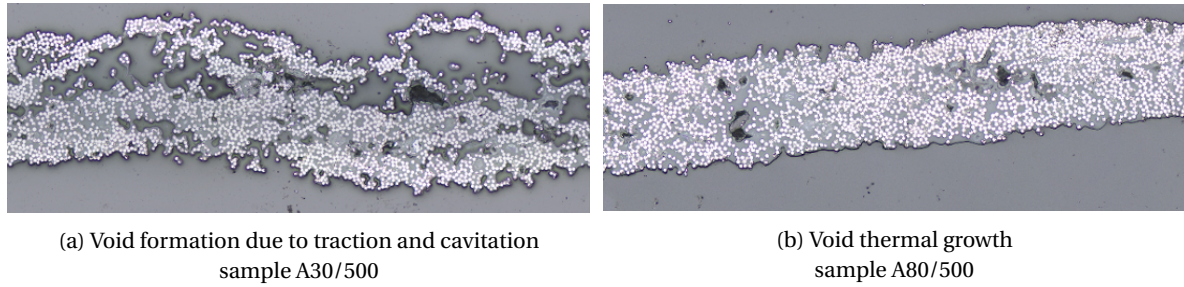


Figure 5.12: Void formation phenomena

Another mechanism that plays an important role for void content development is void coalescence. For longer heating times, the temperature remains above the melting temperature for a longer period of time. Small voids can coalesce together and form larger voids as can be seen in figure 5.13. This does not significantly change the total global void content, however it can affect the appearance of the void content in the 2D plane of the cross-section that is captured.

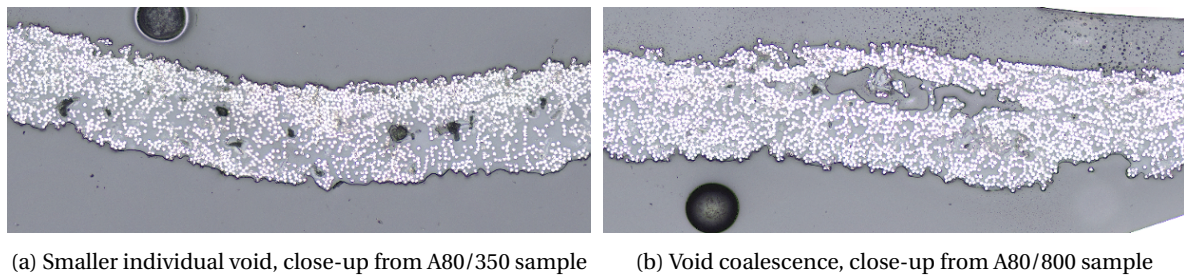


Figure 5.13: Void coalescence takes place for longer heating times

The following hypothesis was formulated for void content: *"increase in void content at processing temperature is primarily due to thermal void growth in the cross-section of the prepreg tape. An increase in void content with heating time is expected to be seen."* Based on the results it can be concluded that heating time does not play a significant role in the global void content that was measured. The significant increase of void content with heating time as observed by Choudhary [19] can therefore not be confirmed. It is believed that an effect of heating time on void formation exist, but this is mainly in the form of void coalescence. Small voids can coalesce together into larger voids, while the global void content does not significantly change. The first part of the hypothesis is supported by the data: increase in void content occurs as a result of void thermal growth. This is the main mechanism for samples with a heated spot length of 50mm and 80mm. However, the large void content for shorter heated spot lengths (30mm) can be mainly attributed to large voids near the heated surface. Here, the main mechanism for void formation is traction and cavitation due to decompaction. This is a result of the high heat flux for short heated spot lengths. It has to be acknowledged that the most important trend for void content is the decreasing trend with respect to heated spot length. It is expected that this has to do with the decreasing heat flux (total amount of power per unit spot length) for larger heated spot lengths.

Based on the results of arc-length increase and maximum out-of-plane deformation it can be stated that the arc-length increase is not affected by the maximum out-of-plane deformation. More importantly, the arc-length increase is determined by the waviness profile. Hence, variation in the out-of-plane deformation is most dominant factor affecting arc-length increase. Therefore, the void content development does not seem to have a major impact on the increase in arc-length. Moreover, the observed trends for arc-length and void content are in contradiction with each other.

It was hypothesised that *"arc-length increase during the heating phase occurs primarily due to polymer movement (transverse to the fiber direction) in its melt phase and is also influenced by void coalescence and out-of-plane deformation during deconsolidation. It is expected that less arc-length increase will be observed for longer heating times while an increase is expected with larger heated spot lengths"*. It can be concluded that

the trends observed by Choudhary [19], a decreasing trend for arc-length with respect to heating time and an increasing trend with respect to heated spot length, are supported by the data. It seems that the observed trends occur mainly due to global out-of-plane deformation. Void content development and void coalescence might also affect the deformation of the tape in width direction. Next to this, polymer movement in the melt phase was observed in the study of Choudhary [19] as the main contributor. This observation is expected to be true since resin-rich areas at the sides of the tape were seen after heating (see figure 5.14), however the contribution to the total arc-length increase could not be measured from the available data. Moreover, since various mechanisms play a role in the deformation of the tape in width direction and the magnitude of the mechanisms is not measured the data is inconclusive.

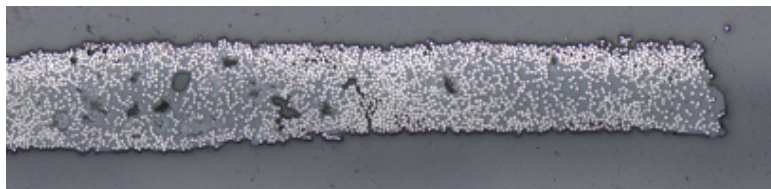


Figure 5.14: Polymer matrix movement towards the sides of the tape which can contribute to arc-length increase

From the cross-sectional images it can be concluded that void content development plays a major role in thickness increase, see figure 5.15. This corresponds with the hypothesis: *"thickness increase occurs mainly due to void content increase during the rapid heating phase. Therefore, an increasing trend with heating time is expected to be seen"*. The increasing trend with respect to heating time seems to be supported by the data, however due to large scatter in the results this statement is inconclusive. Choudhary [19] reported no significant trends for thickness increase with respect to heating time and heated spot length. Next to that, it seems that decompaction in the out-of-plane direction also plays a role in thickness increase since this has an impact on void content development as was shown in figure 5.12a.

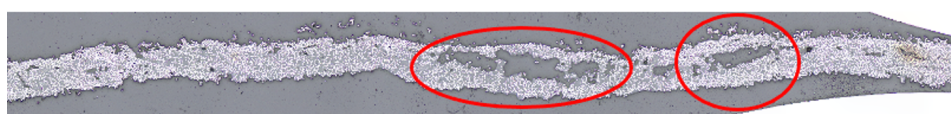


Figure 5.15: Void content has a major contribution to thickness increase, sample A30/800

## 5.4. Conclusion

The effect of varying the heating time and heated spot length on the deconsolidation response during the heating phase of LAFP was investigated. The results showed that the laser heating input variables (heating time and heated spot length) have an effect on the deconsolidation response through various interlinked mechanisms. Deconsolidation was quantified through the following response variables (output): maximum out-of-plane deformation, surface roughness, void content, arc-length increase and thickness increase.

It can be concluded that out-of-plane decompaction is the mechanism behind surface roughness development and out-of-plane deformation. Next to that, it contributes to void content development and thickness increase, mainly for the short heated spot length of 30mm. No significant effects of heating time and heated spot length were found on surface roughness and maximum out-of-plane deformation. The temperature achieved at the nip-point has been shown to be the most dominant factor causing local out-of-plane deformation and surface roughness. The non-uniform temperature profile at the end of heating is linked to waviness formation, peaks in the temperature profile do correspond to peaks in the waviness profile and larger roughness was found at local peaks in the waviness curve.

Void content development has shown two possible mechanisms: void formation due to traction and cavitation and void thermal growth of voids already present in the as-received material. Next to that, void coalescence can occur for larger heating times. Void content development was found to contribute to arc-length increase and thickness increase. No significant trend of heating time on void content was measured and larger void content was found for shorter heated spot length. The latter is a result of decompaction which

plays an important role in void formation for short heated spot lengths of 30mm for which heat flux is higher (total amount of power per unit spot length).

Various mechanisms were found to contribute to arc-length increase. Since arc-length is determined by the waviness profile, it is expected that the variation in waviness is the main contributor. Next to that, it was demonstrated that void coalescence and polymer matrix movement can play a role however the magnitude of each of the contributions was not measured. The data has shown that increasing heating time has a decreasing effect on arc-length, while increasing the heated spot length has an increasing effect on arc-length. It is expected that these observed trends occur mainly due to global waviness formation.

Thickness increase occurs primarily due to void content increase however out-of-plane decompaction does also contribute to thickness increase. It can not be concluded from the data that significant effects of heating time and heated spot length exist which affects thickness increase due to large scatter.

To conclude, this research did reveal that undesired deconsolidation behavior does occur during the heating phase of LAFP in terms of out-of-plane decompaction, waviness formation, void formation due to traction and cavitation and void thermal growth. The most important deconsolidation responses (increase in surface roughness, maximum out-of-plane deformation, void content, thickness and arc-length) have been quantified due to waviness formation and out-of-plane decompaction of the fiber reinforcement network. Waviness formation is undesirable because it will lead to non-uniform heating across the simulated nip-point causing locally higher out-of-plane decompaction and a rough fiber-rich surface. Mainly, the fiber-rich surface with an increased surface roughness is disadvantageous for the LAFP-process. Increased surface roughness at the end of the heating phase will lead to a lower degree of effective intimate contact, which is required for a good bond strength and a high final laminate quality, during the consolidation step in the LAFP-process.

No ideal process configuration, with respect to heating time and heated spot length for the LAFP-process, could be distinguished from the results to diminish the increase in surface roughness. To keep the waviness formation as small as possible it seems to be beneficial to use a large heating time (800ms) and a small heated spot length (30mm). This corresponds to a placement rate of 37.5 mm/s which is still 10-20x slower than the desired placement speed (approximately 400-800 mm/s). Based on the results a small heated spot length is, however, disadvantageous for decompaction. Nonetheless, the results gathered during this research did contribute to a better understanding of the heating phase of LAFP. The changed state of the tape with respect to initial as-received state (outcome of this research) can be used as input for consolidation models for LAFP. With the improved model it should be better possible to predict the material behaviour during the consolidation phase and to model the final quality of LAFP-manufactured laminates.

# 6

## Results: effect of a resin-rich surface on deconsolidation

Chapter 6 discusses the results on the effect of a resin-rich surface on the deconsolidation behaviour of thermoplastic prepreg tapes. It will therefore formulate an answer to the second research question: *"What is the influence of thermoplastic prepreg tapes with a resin-rich surface compared to reference tapes (without resin-rich surface) on the deconsolidation behavior during the rapid heating phase of LAFP?"*. The main goal in this chapter is to show the effect of resin-rich surface tapes on deconsolidation and to make a comparison with resin-poor surface tapes. The interaction effects with heating time and heated spot length are of secondary importance here. The test matrix for this part of the research is given in section 6.1. Secondly, the quantification results of resin-rich samples are presented in section 6.2. Three different Suprem material types and Toray-Ten Cate material are compared here to each other regarding the resin-rich top surface. The results in terms of five response variables are presented in section 6.3. The resulting deconsolidation interaction effects and the driving physical mechanisms are discussed in section 6.4 and the conclusion is given in section 6.5.

### 6.1. Test matrix

For the second research question 30mm and 80mm heated spot length were used and heating times of 350ms and 800ms. These variables were chosen such that the extreme configurations (in terms of heating time and heated spot length) were captured during this part of the research. Next to that, the results in this chapter can be compared to the results presented in chapter 5.

The process configurations can be seen in table 6.1. Again it was aimed for the same processing temperature between 360 - 400 °C. Three repetitions were done for each of the process configurations. However, for configurations B30/800 only 2 samples were taken into account during processing of the results. Sample 1 failed during the laser heating experiment. The processing temperature was not reached and therefore this particular sample did not show representative deconsolidation behavior.

An important remark can be made here regarding the total power in tables 5.1 and 6.1. It can be observed that for the Suprem samples (resin-rich) more total power was needed in comparison to the Toray-Ten Cate samples (resin-poor). It is suspected that this difference in total power is due to the resin-rich top surface layer, but the underlying reasoning will be discussed later on in this chapter in more detail, in section 6.4.

Table 6.1: Configuration settings experimental research 0.5" resin-rich Suprem prepreg tapes

Process configuration	B30/350	B30/800	B80/350	B80/800
Spot length (mm)	30	30	80	80
Heating time (ms)	350	800	350	800
VCSEL zones activated	4-6	4-6	1-11	1-11
Power per zone (%)	100	50	54	32
Total power (W)	600	300	1188	704

## 6.2. Quantification of resin-richness

The Suprem tape material used for the second research question can be observed in figure 6.1. As can be observed from this photograph differences exist in the gloss of the top surface of the material. The hypothesis is that this is linked to whether the top surface exhibits a resin-rich layer or not. To test this hypothesis further investigation was needed into the material characteristics. Furthermore, quantification of the resin-richness was needed to perform research into the effect of resin-richness on deconsolidation. For understanding and interpretation of the results it was also needed to quantify the differences between Toray-Ten Cate material and Suprem material in terms of resin-richness.

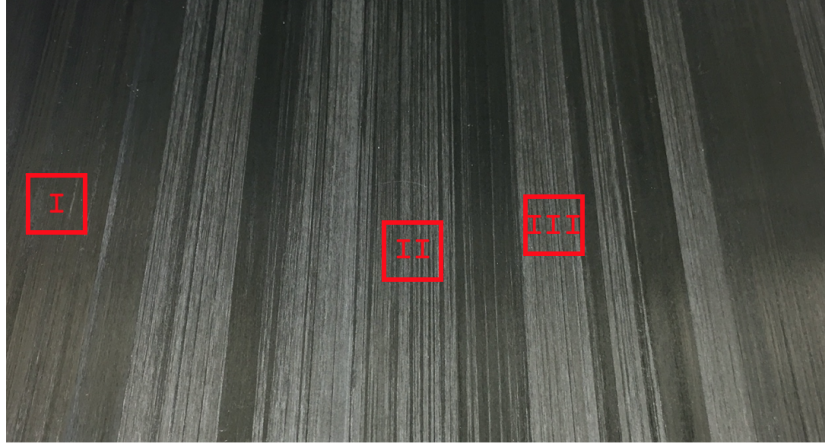


Figure 6.1: Variation observed in the gloss of Suprem CF/PEEK prepreg tape (camera photograph)

Close-up photographs that are shown below in figure 6.2 correspond to the locations I, II and III in figure 6.1. Top surface micrographs were captured at the corresponding locations with the Keyence LSCM at 50X magnification. These micrographs were further processed by the method described in section 4.3.1 to quantify the resin-richness of the various Suprem material compositions. The top surface micrographs can be seen in figure 6.3, here the white areas can be characterized as fibers while the grayish area is typically considered as resin. To the authors knowledge dry fibers at the top surface reflect more light than resin and appear therefore as white while the surrounding resin appears as gray. In figure 6.4 the corresponding converted binary images can be seen, this makes the distinction between fibers and resin at the top surface better visible. Red is characterized here as fibers at the top surface, while black is characterized as resin. Table 6.2 summarizes the results gained from figures 6.2 - 6.4. It can be concluded that glossy surface tapes have the least amount of resin on the top surface while the matte surface can be characterized as the most resin-rich. An overview of all the exact measurement values can be seen in table 6.2.

Table 6.2: Results of the top surface resin content measurements for different material types

Material type	Sample #	Resin content (%) At location along width			Avg. resin content (%)
		30%	50%	70%	
Toray-Ten Cate	1	81.6	82.6	79.4	81.2
	2	80.7	85.1	87.4	84.4
	3	78.0	74.1	72.0	74.7
Suprem Glossy surface	1	84.1	95.4	88.8	89.4
	2	94.7	97.2	91.5	94.5
	3	92.6	86.7	79.8	86.4
Suprem Matte surface	1	95.8	93.1	93.9	94.3
	2	96.2	95.5	97.2	96.3
	3	96.1	92.8	93.7	94.2
Suprem combined glossy and matte surface	1	91.2	94.4	93.8	91.2
	2	96.6	91.0	95.6	94.4
	3	92.3	93.8	95.4	93.8

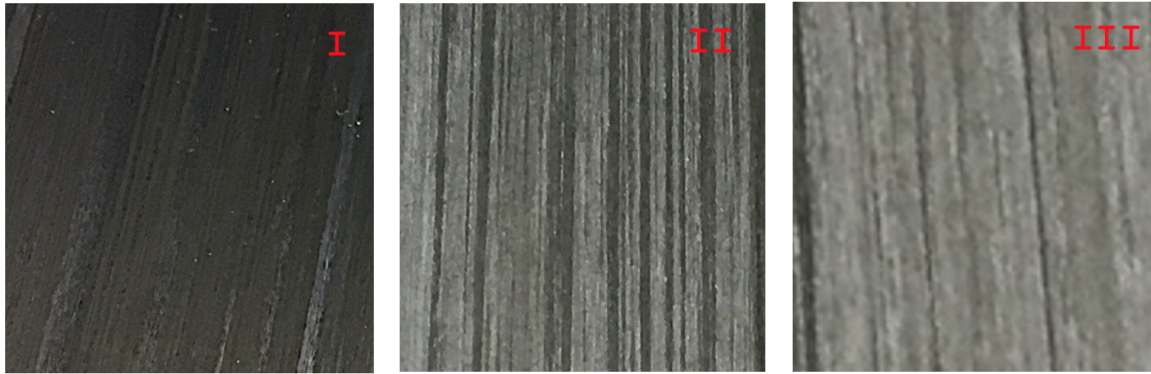


Figure 6.2: Close-up images taken from figure 6.1.  
I: Glossy surface, II: Combined glossy and matte surface, III: Matte surface

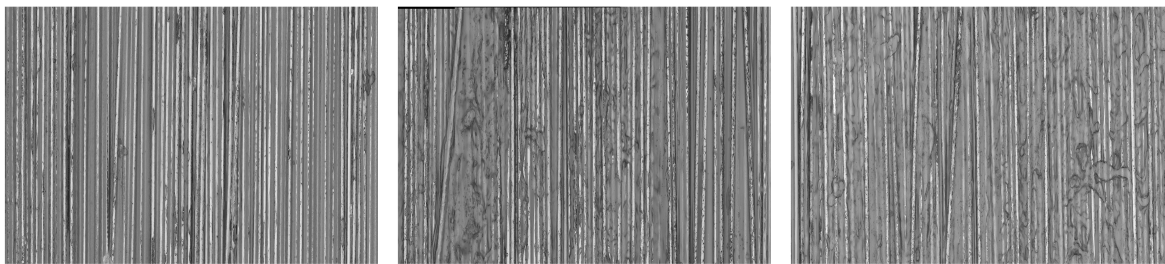


Figure 6.3: Micrographs (captured with LSCM at 50X) corresponding to images shown in figure 6.2  
I: Glossy surface, II: Combined glossy and matte surface, III: Matte surface

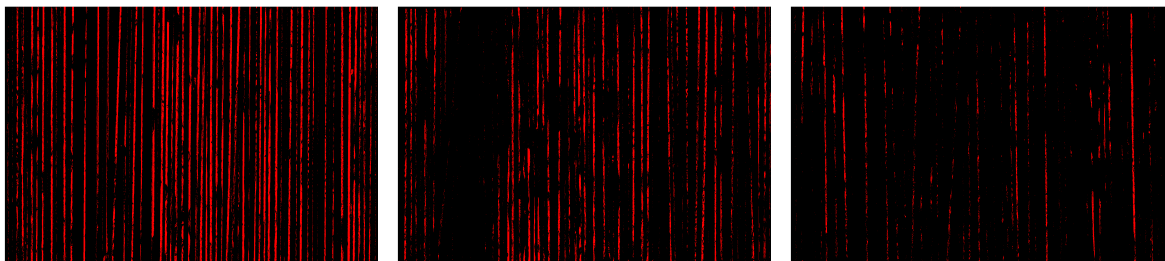
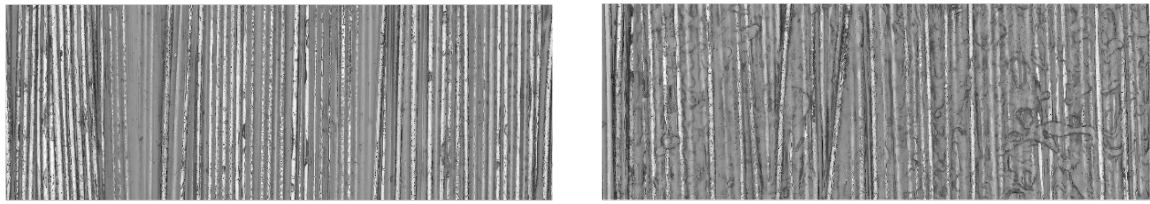


Figure 6.4: Comparison of resin content on top surface. Resin is shown in black while red represent fibres on the top surface.  
I: Glossy surface, II: Combined glossy and matte surface, III: Matte surface

It has already been shown that the appearance (glossy or matte) of the top surface can be linked to the amount of resin that is measured from top surface images. Next to that, the presence of the resin-rich layer as could be seen on cross-sectional images could also provide additional information and will also help in validating the measurements in table 6.2. In figures 6.5-6.6 below the top surface micrographs are matched with the cross-sectional micrographs at their corresponding locations. As can clearly be seen the sample with a glossy surface (resin content only 79.8%, see Table 6.2 Suprem glossy surface sample #3 measured at 70% width) has a fiber-rich top surface. The sample with a matte surface (resin content 97.2%, see Table 6.2 Suprem matte surface sample #2 measured at 70% width) has a resin-rich layer on the top surface. Although a cross-sectional image is only representative for a single line over the width, this qualitative observation (visual comparison) could give a confirmation that the resin-richness of the top surface can be characterized from top surface micrographs.



(a) Glossy top surface, resin content = 79.8%

(b) Matte top surface, resin content = 97.2%

Figure 6.5: Comparison between different top surface appearances of Suprem material

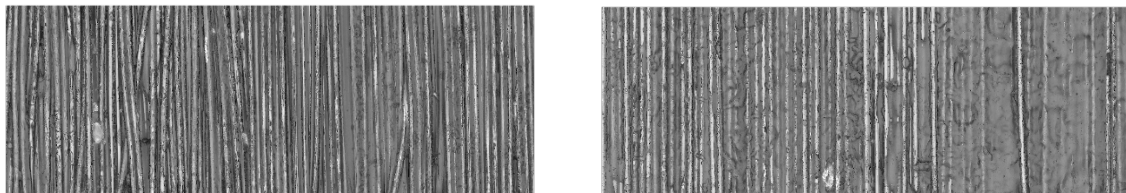


(a) Glossy top surface exhibits fiber-rich top surface

(b) Matte top surface exhibits resin-rich top surface

Figure 6.6: Comparison between Suprem cross-sectional micrographs

Because of the large variation within the Suprem tape material (material is off-spec), samples were used that were the most consistent with each other (looking visually as similar as possible). These samples can be characterized by the category *combined glossy and matte surface* samples in table 6.2, i.e. mostly matte sample with small glossy portions in between. From the measurements (in table 6.2) it can be concluded that the top surface of Suprem tapes that were used during the research contain on average 13% more resin in comparison with Toray-Ten Cate tapes. In the figures 6.7-6.8 below a comparison between Toray-Ten Cate and Suprem samples (used for the second research question) can be seen. In figure 6.8b it can be seen that the top surface of Suprem material contains a resin-rich layer. This is different from Toray-Ten Cate material which has more fibers on the outer top surface (fiber-rich) as can be seen in figure 6.8a. The effect of a resin-rich surface on the deconsolidation response variables will be discussed in detail in the next sections 6.3 and 6.4.



(a) Toray-Ten Cate sample, resin content = 82.6%

(b) Suprem sample, resin content = 95.4%

Figure 6.7: Comparison between top surface micrographs of Toray-Ten Cate and Suprem material



(a) Toray-Ten Cate sample with a fiber-rich top surface

(b) Suprem sample exhibits resin-rich top surface

Figure 6.8: Comparison between Toray-Ten Cate and Suprem cross-sectional micrographs

### 6.3. Deconsolidation response of Suprem resin-rich tapes

All results and observations in terms of the deconsolidation response for resin-rich surface tapes will be presented in the next sections 6.3.1-6.3.5, for each single response variable in a separate section. However, the five response variables can not be seen separate from each other since the underlying mechanisms all in-

teract with each other. It is therefore convenient to discuss the underlying mechanisms and the interlinks between the different response variables all together in section 6.4.

### 6.3.1. Surface roughness

In Table 6.3 the surface roughness measurements are given. The second column shows the RMS roughness for the sample before heating while the third column shows the RMS roughness for the same sample after heating. In columns 4 and 5 the increase in RMS roughness is given as absolute increase and as percentage change. For comparison resin-poor samples (A-samples, Toray-Ten Cate material) are added to table 6.3 per process configuration. The values given in the table represent the average over 3 measurements with the standard deviation between brackets. For the B-samples (corresponding to resin-rich Suprem samples) all single samples are included. The number between brackets in the first column corresponds to the number of the sample (repetition).

Large variations exist in the RMS roughness change (see last column) for the B-samples even for samples with the same process configuration. This can be mainly attributed to variations in the pre-process RMS roughness (off-spec material) as the B-samples show comparable post-process RMS roughness values.

Table 6.3: RMS roughness data, comparison between resin-rich and resin-poor samples

Process configuration	Pre-process RMS roughness ( $\mu\text{m}$ )	Post-process RMS roughness ( $\mu\text{m}$ )	RMS roughness increase ( $\mu\text{m}$ )	RMS roughness change (%)
<b>A30/350</b>	1.939 (0.213)	5.514 (1.286)	3.575	184
<b>B30/350 (1)</b>	2.415	2.682	0.267	11
<b>B30/350 (2)</b>	2.568	3.618	1.050	40
<b>B30/350 (3)</b>	1.256	3.054	1.799	143
<b>A30/800</b>	1.939 (0.213)	5.656 (0.175)	3.718	192
<b>B30/800 (2)</b>	1.848	2.726	0.878	47
<b>B30/800 (3)</b>	1.842	3.567	1.725	93
<b>A80/350</b>	1.939 (0.213)	4.602 (0.586)	2.664	137
<b>B80/350 (1)</b>	1.952	2.976	1.023	52
<b>B80/350 (2)</b>	1.242	2.624	1.382	111
<b>B80/350 (3)</b>	1.217	2.331	1.114	91
<b>A80/800</b>	1.939 (0.213)	5.867 (1.277)	3.929	203
<b>B80/800 (1)</b>	1.251	2.675	1.424	113
<b>B80/800 (2)</b>	1.304	2.740	1.436	110
<b>B80/800 (3)</b>	2.122	2.367	0.245	11

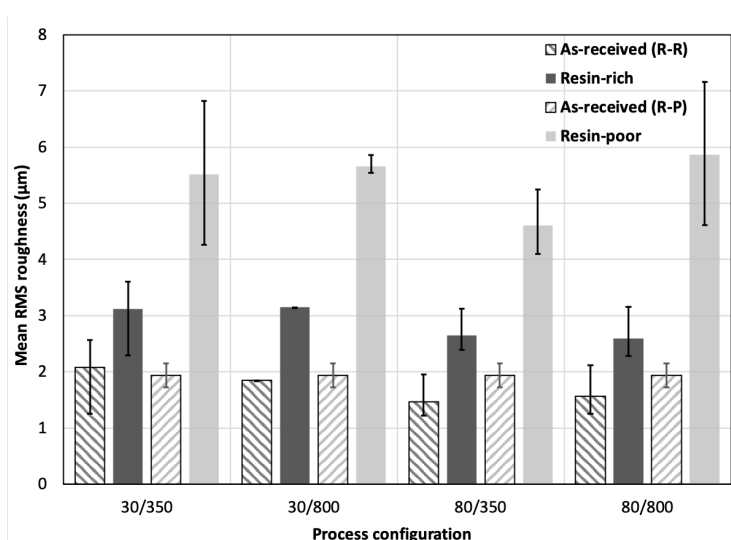


Figure 6.9: Effect of resin-richness on surface roughness

A graphical overview of the increase in RMS roughness can be seen in the bar diagram in figure 6.9. First of all, it can be observed that both resin-poor and resin-rich samples show an increase in RMS roughness as a result of rapid heating. Secondly, it can be concluded that resin-rich samples show significantly lower RMS roughness after rapid heating compared to resin-poor samples. Since there is no significant difference in as-received roughness between resin-poor and resin-rich samples, this will not be the dominant factor causing lower surface roughness after heating for resin-rich samples. Furthermore, no significant trend can be observed with heating time and heated spot length for both resin-poor and resin-rich samples.

From the cross-sectional images after heating a clear distinction in material behavior can be made between resin-poor and resin-rich samples, see figure 6.10. In case of resin-poor samples it can be seen in figure 6.10a that fibers have popped-out from the heated top surface due to deconsolidation. This is typically not seen for resin-rich samples, see figure 6.10b.

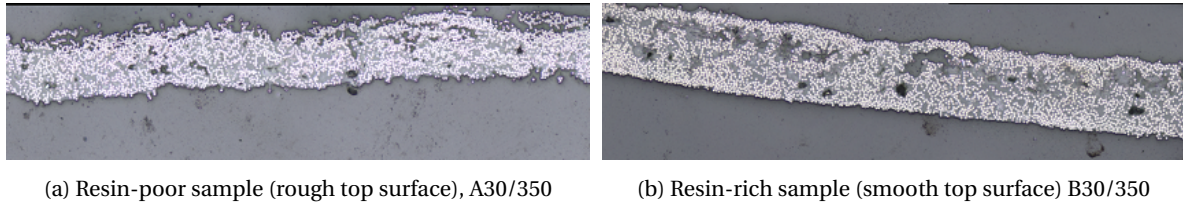


Figure 6.10: Difference in surface roughness observed after heating for resin-poor and resin-rich samples

### 6.3.2. Out-of-plane deformation

The main driver for out-of-plane deformation is expected to be decompaction of the fiber reinforcement network. However, warpage of the tape also contributes to deformation in the out-of-plane direction. Warpage in the width direction is mainly a result of non-uniform temperatures in the nip-point as was shown by the study of Choudhary [19]. Resin-rich samples do show warpage as will be discussed in the next paragraphs.

Figure 6.11 shows the results in terms of maximum out-of-plane deformation. Two important observations can be made. First of all, it can be seen that resin-rich samples have significantly less out-of-plane deformation compared to resin-poor samples. This can be explained by the fact that less decompaction is observed for resin-rich samples. Further discussion of this result will follow in section 6.4 as surface roughness and out-of-plane deformation are linked to the same underlying mechanisms: decompaction of the fiber reinforcement network and tape warpage does also play a significant role.

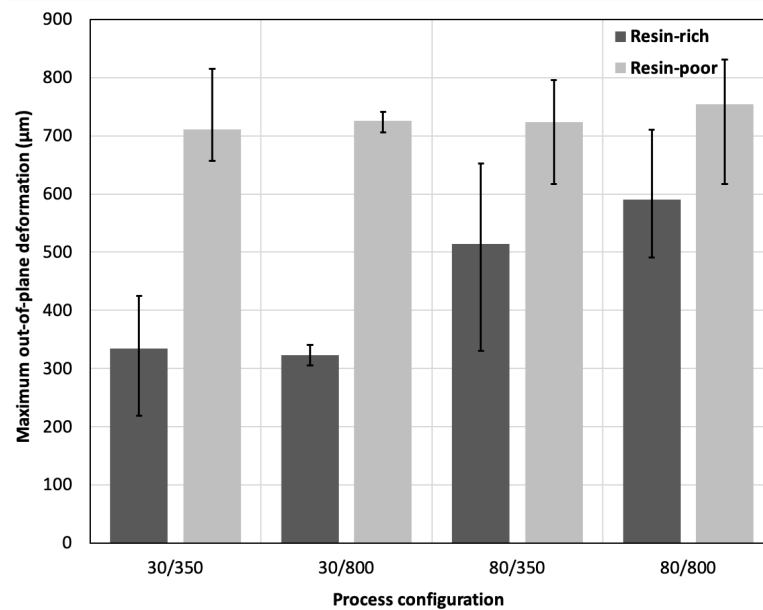


Figure 6.11: Effect of resin-richness on out-of-plane deformation

Secondly, resin-poor samples do not show any trend with heating time and heated spot length, while resin-rich samples show an increase in out-of-plane deformation with heated spot length. This can be explained by the larger warpage that is observed for samples with 80mm heated spot length for both heating times (350ms and 800ms). Figures 6.12-6.14 show the comparison for 350ms heating time and figures 6.15-6.17 show the comparison for 800ms heating time. As can be seen for both cases (heating time of 350ms and 800ms) the temperature is less uniform over the width for 80mm spot length. This leads to a larger variation in out-of-plane deformation (figures 6.14 and 6.17). As a result, samples with 80mm spot length exhibit more warpage.

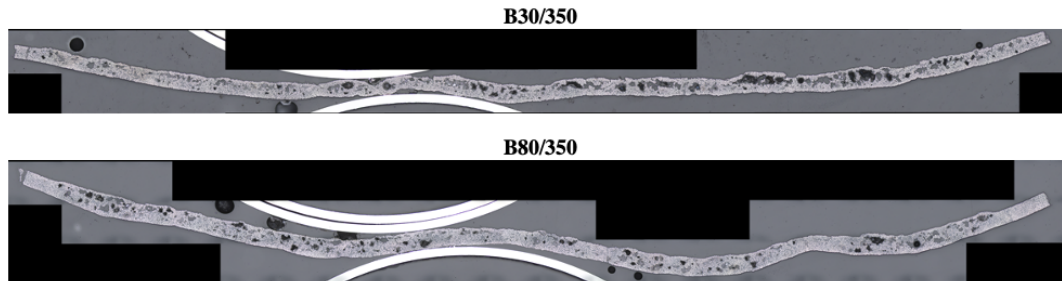


Figure 6.12: Increasing warpage with heated spot length for a heating time of 350ms

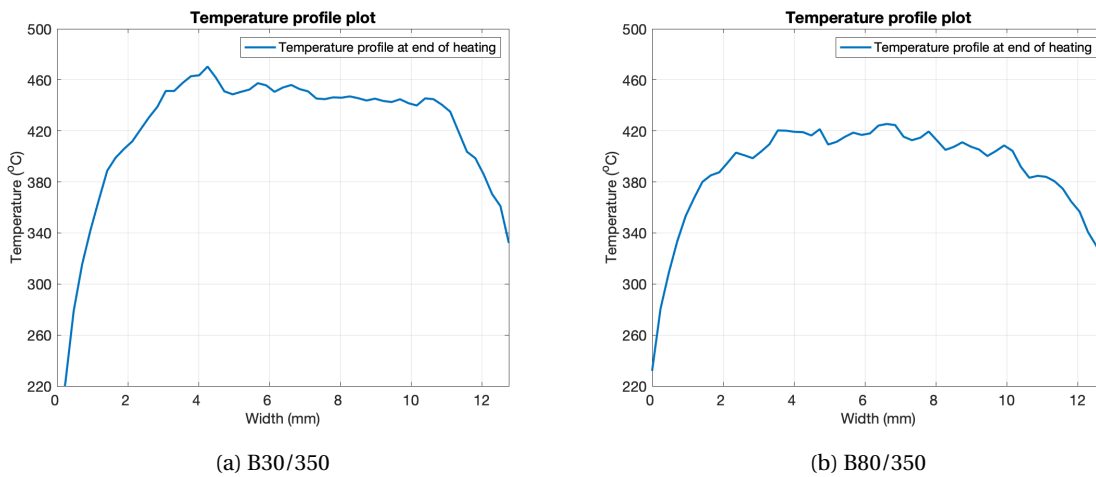


Figure 6.13: Temperature distribution in the nip-point at the end of heating

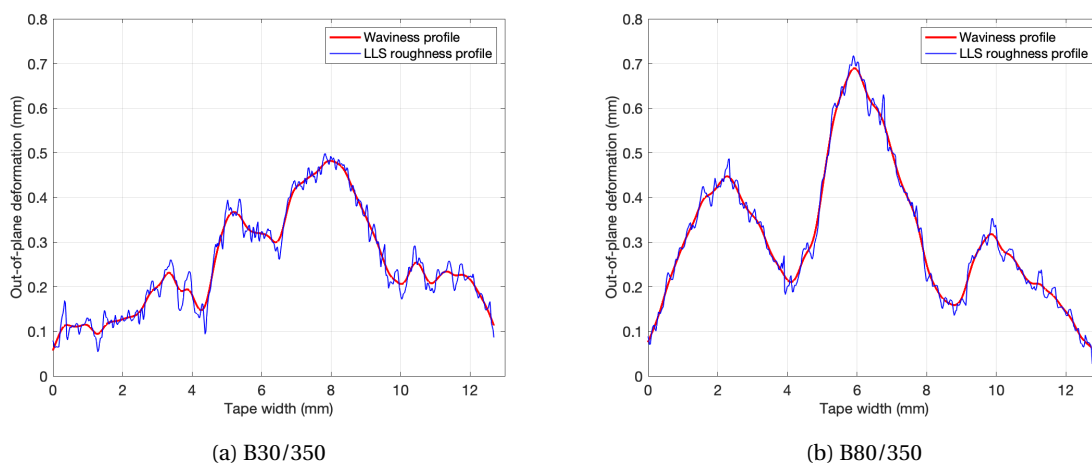


Figure 6.14: Out-of-plane deformation and waviness profile fitted (end of heating)

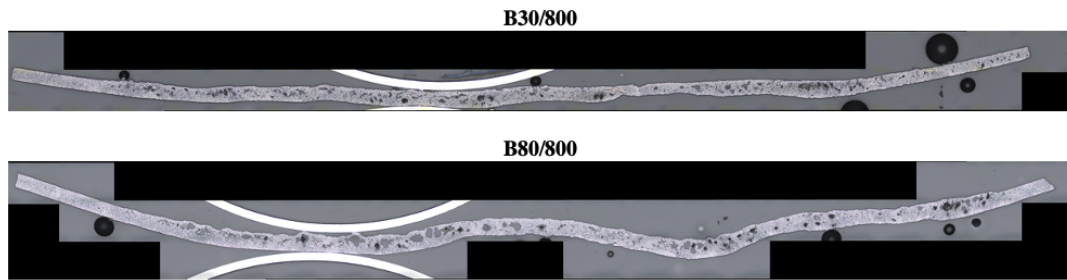


Figure 6.15: Increasing warpage with heated spot length for a heating time of 800ms

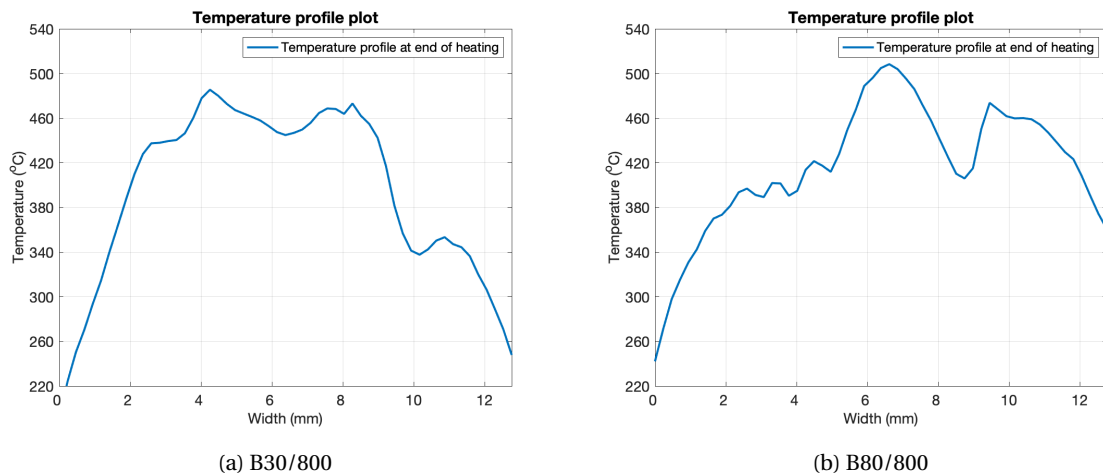


Figure 6.16: Temperature distribution in the nip-point at the end of heating

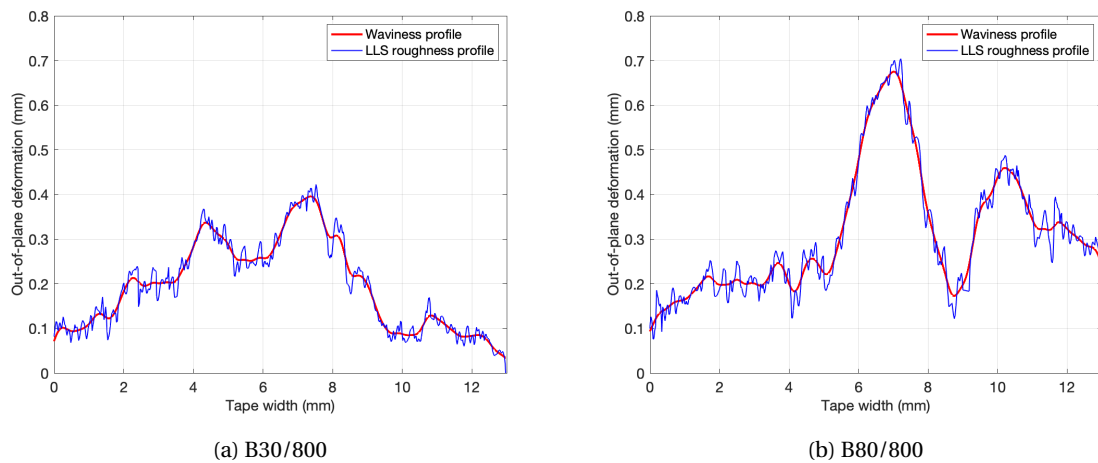


Figure 6.17: Out-of-plane deformation and waviness profile fitted (end of heating)

### 6.3.3. Void content

Figure 6.18 shows the results in terms of final void content. As can be seen for most configurations resin-rich samples exhibit higher final void content than resin-poor samples, only configuration 30/800 seems to show the same void content. Three important phenomena (explained in the next 3 paragraphs), different from deconsolidation effects, have been observed which can affect the final void content. This means that the data is inconclusive since the magnitude of the different phenomena has not been measured. No conclusion can be made with respect to the effect of resin-rich tapes on void content development only.

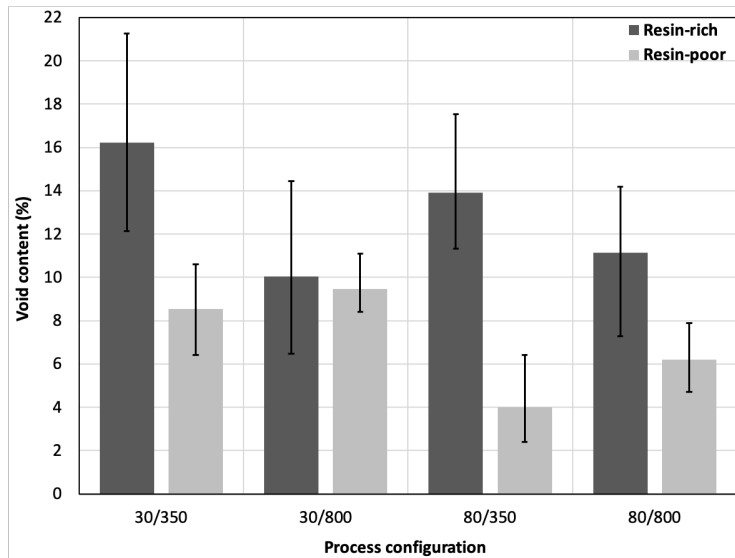


Figure 6.18: Effect of resin-richness on void content

First of all, a resin-rich layer was observed in the middle (through-the-thickness) of the resin-rich tape. In figure 6.19 the resin-rich layer in the middle of the tape can clearly be seen. As a result, less heat will be transferred into the middle of the material due to a lower fiber volume content since fibers absorb the heat. On the other hand, less resistance against void formation in the middle of the material is present when the temperature is above the melting temperature due to lower fiber volume content. Therefore, voids are mainly observed in the middle of the tape (through-the-thickness) as could be observed from the cross-sections in figures 6.12 and 6.15.



Figure 6.19: Resin-rich layer in the middle of the tape (seen through-the thickness), low local fiber volume content

Secondly, large scatter in the measurements for resin-rich samples exist which are caused by minor parts of the tape not heated above the melting temperature. Parts of the tape with locally a temperature below the melt do not show a representative amount of void content which results in a lower global void content. It was observed that this mainly occurred for configurations B30/800 and B80/800 samples as can be seen in figure 6.20.

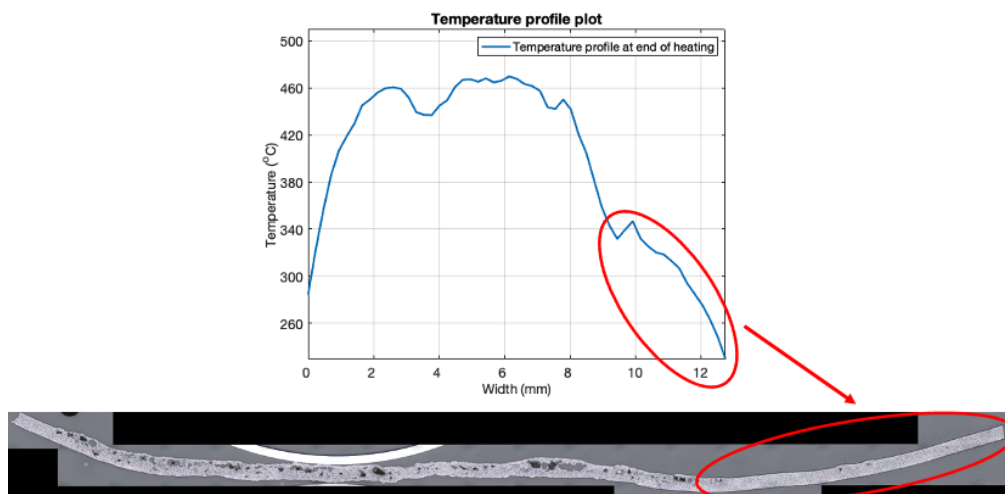


Figure 6.20: Temperature below the melting temperature results in no void formation, sample B80/800

Thirdly, from figure 6.21 it can be seen that variation exists in the initial void content for resin-rich tapes. In the top image it can be seen that low initial void content is already present while in the bottom image no initial void content is present. Scatter in the initial state of the tape will also lead to scatter in the results for the final void content after heating. If a low initial void content is already present in the as-received state of the tape this can cause higher void content after heating. Voids already present in initial state will grow as a result of thermal expansion as was also observed by Choudhary [19]. The initial void content could however not be measured on the actual test samples, since this involves a destructive measurement technique (sample needs to be cut at nip-point location). It is therefore an assumption which is based on void content measurements performed on samples which are similar to test samples used for the actual research.

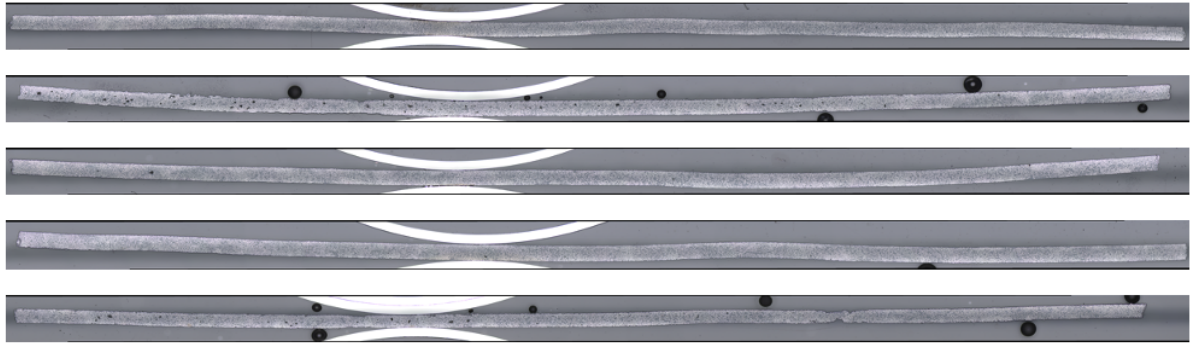


Figure 6.21: As-received resin-rich Suprem samples showing scatter in initial void content

From figure 6.22a it can be seen that the resin-rich samples show a decreasing dependency with heating time. This is interesting since so far only trends with heated spot length were observed. Upon further investigation it became clear that this can be explained by the second phenomenon described above: scatter exist in the results due to parts of the tape not heated above the melting temperature. This explains the lower global void content for, in particular, samples with a heating time of 800ms. No significant trend with heated spot length was found for resin-rich samples.

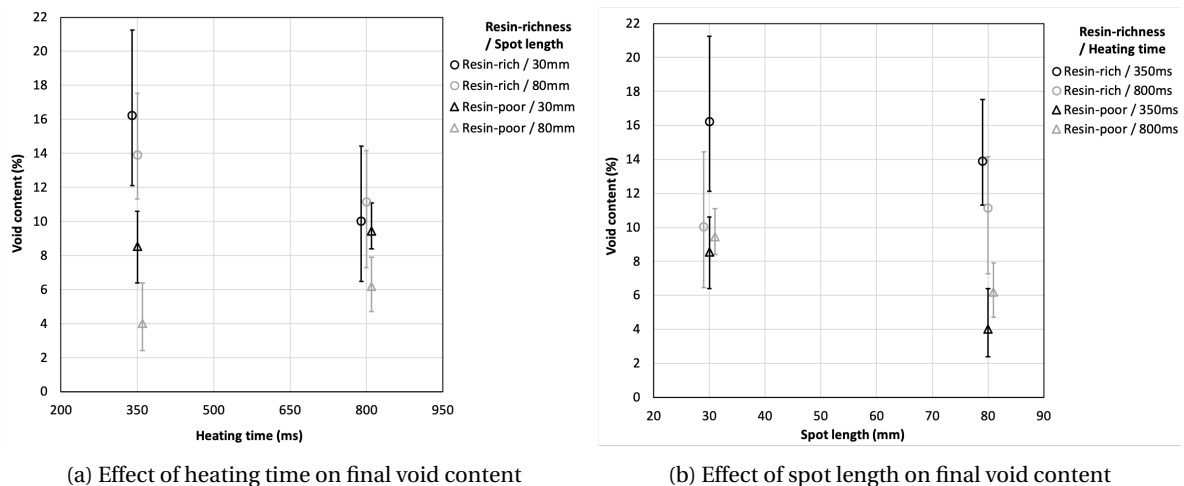


Figure 6.22: Effect of resin-richness on void content for several process configurations

### 6.3.4. Thickness increase

In the previous section the results regarding the void content were presented. The results for thickness increase seem to relate to void content as can be seen in figure 6.23. The most important observation here is that the same trends are observed as for void content (see figure 6.18). Resin-rich samples show more thickness increase and a significant decrease with heated spot length, with again the exception for configuration 30/800. The relation between void content and thickness increase will be further discussed in detail in section 6.4.

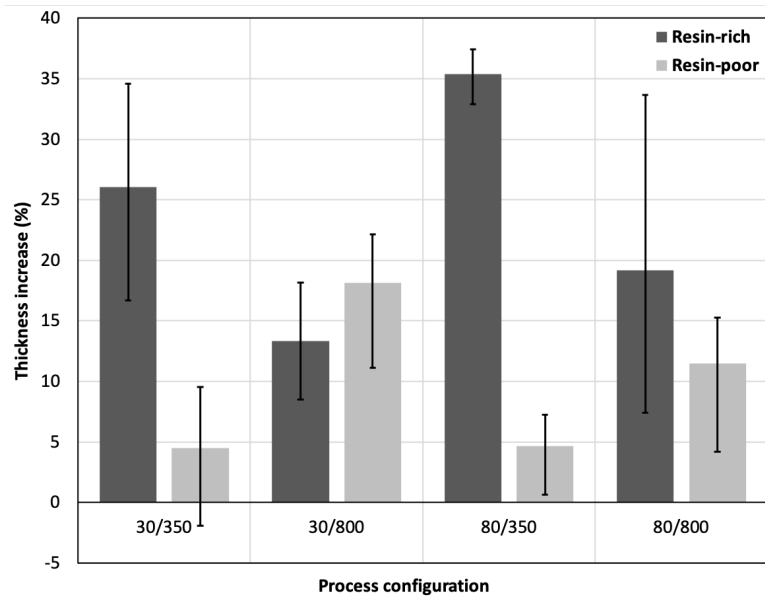


Figure 6.23: Effect of resin-richness on thickness increase

In figure 6.24 the trends with respect to heating time and heated spot length can be observed. It can be noticed that for resin-rich tapes the thickness is decreasing with heating time due to the same reason as was discussed for void content. Parts of the tape are not heated above the melting temperature and do not show significant void content. As a results less thickness increase will be measured at those locations, in particular for samples with a heating time of 800ms.

Due to large error bars it can not be concluded from figure 6.24b that a significant trend with respect to spot length is present. The large error bars are a results of large variations in thickness over the width and sections of the tape without any voids present. Since thickness is locally measured this can therefore affect the results because the thickness can be measured at a local minimum or maximum, see figure 6.25.

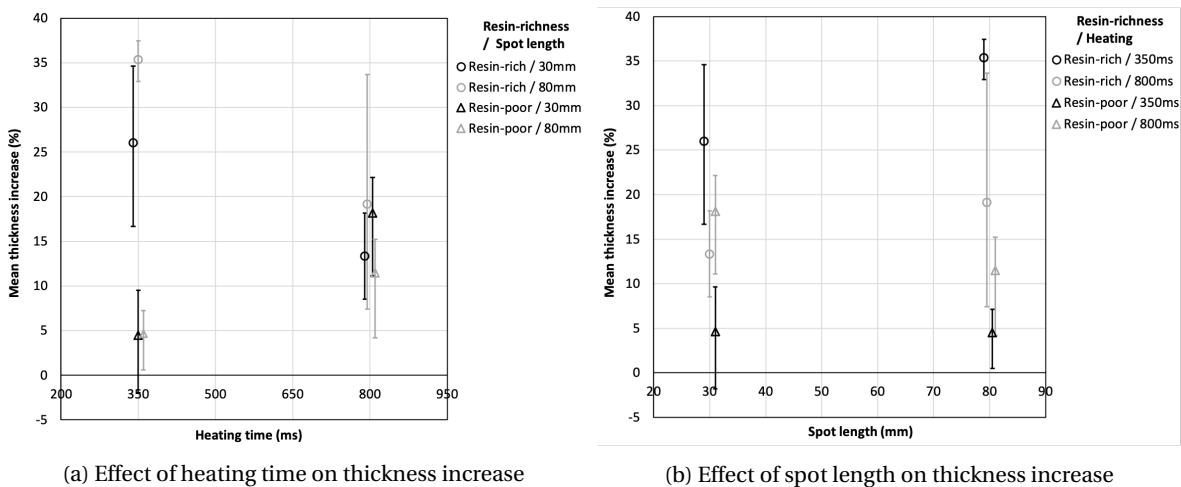


Figure 6.24: Influence on thickness increase for several process configurations

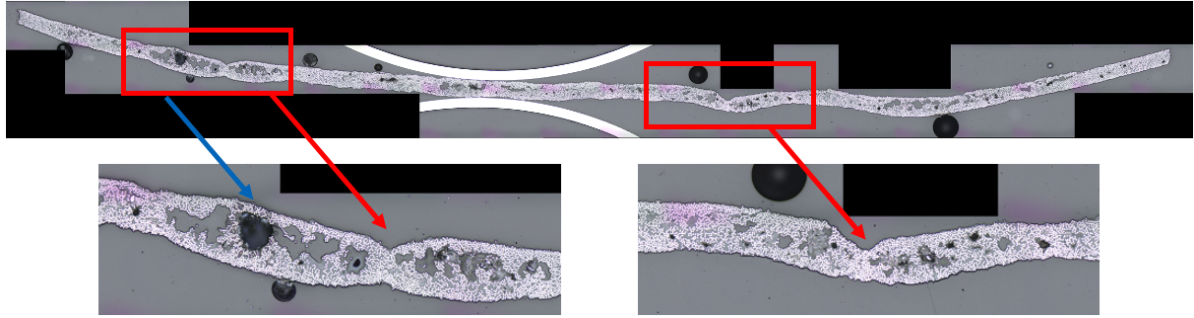


Figure 6.25: Local maximum indicated by blue arrow around 20% width, local minimums indicated by red arrows around 20% and 60% width, sample B80/800

### 6.3.5. Arc-length increase

Arc-length increase is a measure to express the increase in tape dimension in width direction as a result of thermal deconsolidation. It is determined from the arc-length of the out-of-plane waviness curve. Figure 6.26 shows the results for the increase in arc-length. It can be concluded that resin-rich samples show less arc-length increase. It was seen before, for the resin-rich samples, that the out-of-plane deformation was significantly lower. Based on earlier obtained results it is expected that multiple phenomena affect the arc-length increase: out-of-plane deformation, void content development and polymer matrix movement in the melt phase. This will be further discussed in section 6.4.

In figure 6.27a a decreasing trend with heating time can be seen. As was seen before for void content and thickness increase similar decreasing trends with heating time are present. An increasing trend with heated spot length is visible, in figure 6.27b, which is more severe for short heating times. For the resin-rich samples, the out-of-plane deformation was also higher for larger heated spot lengths. All the interaction effects of the five response variables will be further discussed in the next section.

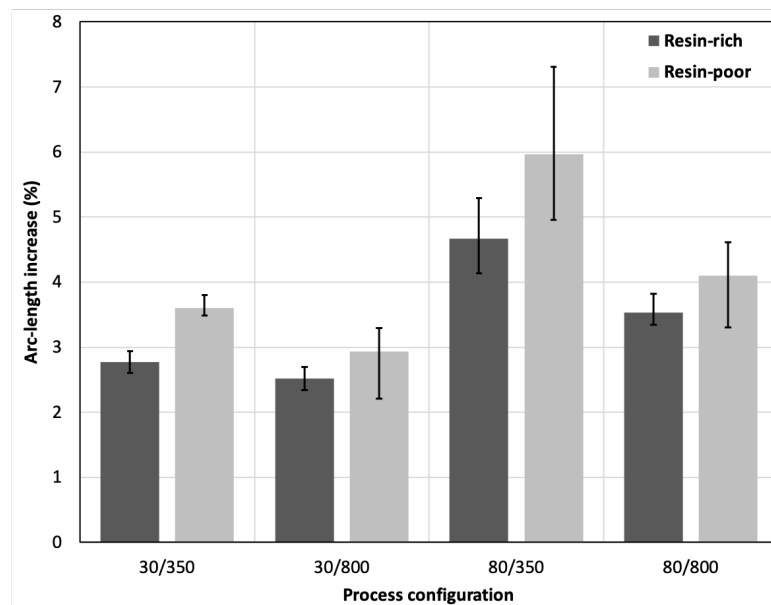


Figure 6.26: Effect of resin-richness on arc-length increase

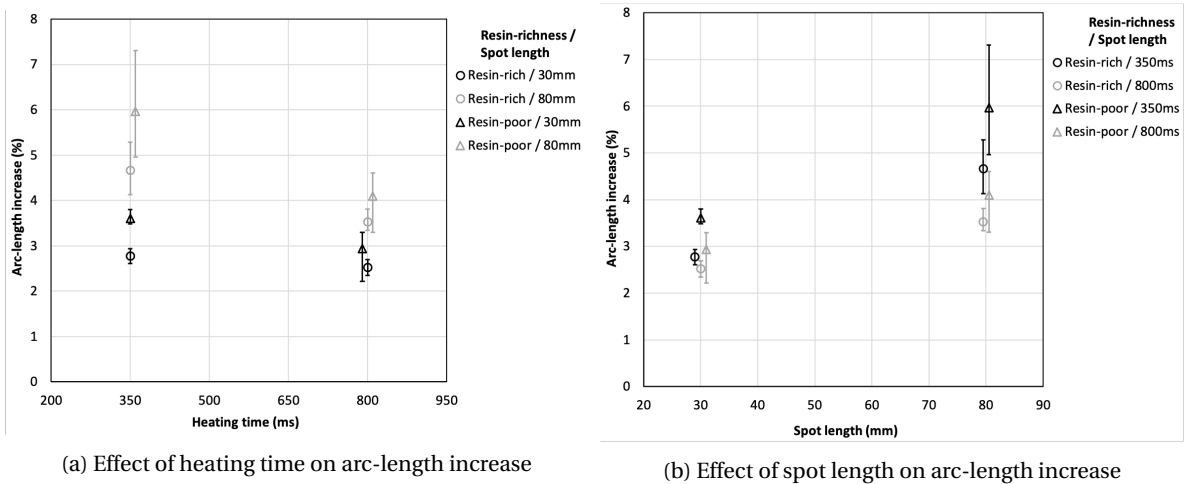


Figure 6.27: Influence on arc-length for several process configurations

### 6.4. Discussion

The hypothesis for surface roughness: "as-received prepreg tapes with a more resin-rich surface will result in a smoother surface (less surface roughness compared to a resin-poor surface) after rapid heating" is confirmed by the results. It is expected that this has to do with the heat input into material. In general, the fibers absorb the heat and transfer the heat towards the resin. Since the fibers are not directly on the outer surface and are surrounded by resin the heat can be more easily dissipated. This is the main reason for the higher laser power that was needed (in comparison with resin-poor tapes) to heat the tape to the processing temperature. The resin-rich surface will cause the fibers to stay into the resin and no fibers popping out-of-plane were observed as was shown in figure 6.10. As a result, the surface roughness after rapid heating remained lower and no rough and fiber-rich surface was developed as was seen for resin-poor samples.

Surface roughness and out-of-plane deformation are linked to the same underlying mechanisms: decompaction in the out-of-plane direction. In contrast to resin-poor samples, the heat input for resin-rich samples is different due to the resin-rich surface as just explained in the section above. No fiber movement in the out-of-plane direction occurred and as a result the less surface roughness was observed and the out-of-plane deformation remained lower. The hypothesis: "A resin-rich surface facilitates a smoother surface resulting in less decompaction of the fiber reinforcement hence less maximum out-of-plane deformation will be measured." seems to hold based on the results.

However, more warpage is observed in general for resin-rich samples, see figure 6.28. The fact that resin-rich samples show more warpage in general can be explained by the fact that variation in resin-richness exists in width direction. The presence of a resin-rich top surface has an effect on the temperature introduction into the material. Since the fibers mainly absorb the heat it is expected that the temperature will locally be higher at locations without a resin layer on the top surface. Therefore temperature variations will exist along the nip-point. This can be confirmed by the temperature profiles at the end of heating, see for example figure 6.16. Out-of plane deformations will therefore locally also be varying which causes warpage of the tape.

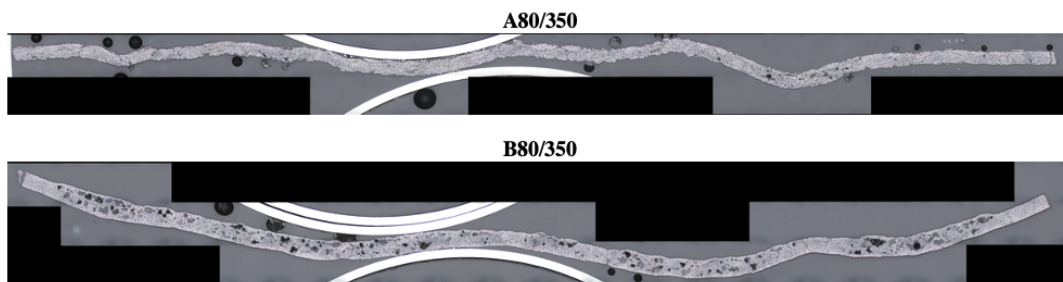


Figure 6.28: More warpage observed for resin-rich sample with the same configuration 80mm/350ms

Next to that, the temperature is decreasing towards the ends of the resin-rich tapes. Due to waviness formation sections of the tape will move closer to the laser heater and therefore these sections will absorb more heat resulting in increased non-uniformity of the temperature distribution. As can be seen in figures 6.12-6.14 and 6.15-6.17 resin-rich samples show a significant amount of warpage and the largest out-of-plane deformation in the center of the width. Therefore, the center of the tape will absorb most of the heat and reaches the highest temperature while the far ends obtain the lowest temperatures. Sections of the tape will remain in solid state if the temperature stays below the melting temperature. These parts of the tape show therefore less surface roughness, out-of-plane deformation and almost no void formation (see figure 6.20). This does also contribute to increased warpage towards the ends of the tape.

The hypothesis on void content: *"resin-rich surface tapes will show a lower final void content at the heated surface of the tape due to less out-of-plane deformation compared to the reference tape (resin-poor tape)"* includes a few elements that were tested and is not supported by the data. First of all, the final void content for resin-rich tapes is larger. The explanation for this was already provided in section 6.3.3. The main reasons for a higher void content are a higher initial void content of the tape. Next to that, a resin-rich layer in the middle of the material resulting is less resistance against void formation when the temperature is above the melting temperature. The observed decompaction for resin-rich samples is less and no fibers popping out-of-plane were observed. Therefore, out-of-plane decompaction does not seem to contribute to the final void content of resin-rich samples.

In section 6.3.3 it was described that less resistance against void formation is present in the middle of the tape when the temperature is above the melting temperature due to a lower fiber volume content. Since the matrix is in a liquid state above the melting temperature and the viscosity will decrease as a result. Next to this, it is expected that warpage of resin-rich tapes results in local fiber movements. This introduces local stresses in the micro-structure of the tape which can tear the material apart, hence local void formation will occur. Out-of-plane deformation due to release of residual stresses was already described by Choudhary [19] as a mechanism for void formation due to traction and cavitation in the material.

Based on the results, void content increase has a major contribution to thickness increase. This is also what the hypothesis suggests: *void content increase is the main contributor to thickness increase, however less thickness increase is expected to be observed for resin-rich surface tapes due to a lower final void content.* However, the second part of the hypothesis is not supported by the results. It was already observed in section 6.3.3 on void content that resin-rich tapes show higher final void content compared to resin-poor tapes.

In order to explain the relation between thickness increase and void content better, figures 6.29-6.30 are shown below. Including the temperature profile at the end of heating because void content development, hence thickness increase also relates to the temperature achieved at the nip-point. As can be seen in the top image of figure 6.29 voids mainly exist on the right-hand side of the cross-section (part between bracket). This can be directly related to the temperature achieved in the material. As can be seen in figure 6.30 the temperature was only above the melt from 3.5 - 12 mm of the width. New voids will be created when the temperature is above the melting temperature and this leads to an increase in thickness. The major contribution of void content development on thickness increase can clearly be seen in the close-up image on the bottom of figure 6.29. It has to be pointed out that voids are created at this part of the tape which has not been above the melting temperature. This can be explained by the fact that voids already present in the as-received material will grow as a result of thermal expansion which starts at  $T_g$ .

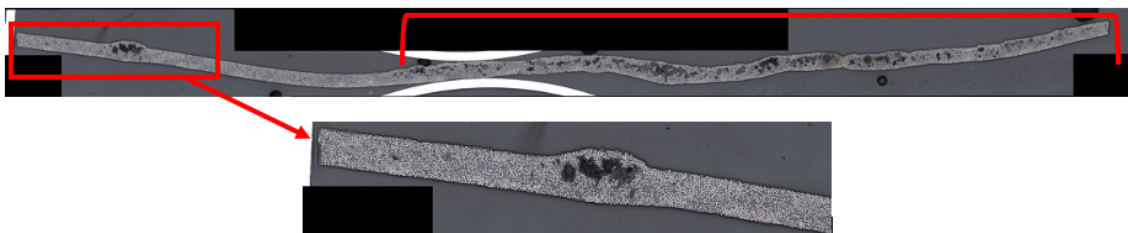


Figure 6.29: Cross-sectional image (B30/800). Void formation can be seen mainly at the right-hand side (between bracket). In the close-up image below the effect of voids on thickness increase

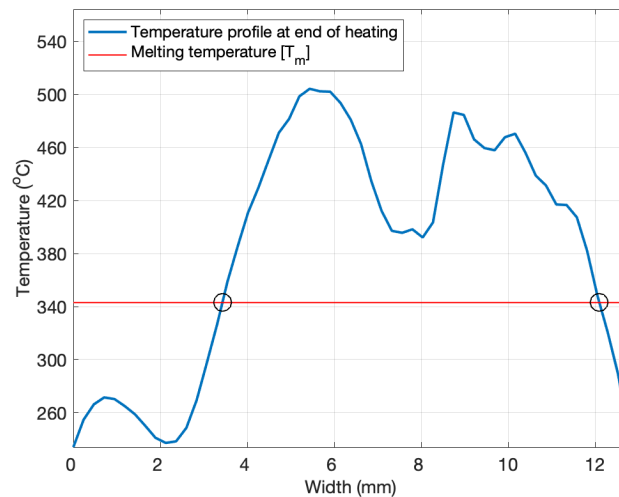


Figure 6.30: Temperature profile at the end of heating for the corresponding sample (B30/800) shown in Fig.6.29

As was seen from figures 6.18, 6.23 and 6.26 similar trends are observed for resin-rich tapes. This indicates that the void content development has a contribution to both thickness increase and arc-length increase. The hypothesis suggests that: *arc-length increase will occur mainly due to polymer matrix movement in the melt phase and to a lesser extent as a result of void content increase, and next to that, less arc-length increase will be observed for resin-rich tapes due to a lower fiber volume fraction at the heated surface.* The latter is not supported by the data since higher void content was measured for resin-rich samples while less arc-length increase was measured.

The fact that less arc-length increase is observed for resin-rich tapes can be clarified by a combination of less out-of-plane deformation and lower fiber volume content in the middle (through-the-thickness) of the material, see figures 6.31 and 6.32. Since fibers absorb and transport the heat, it is expected that a lower fiber volume content in the middle of the material will cause the temperature to be locally lower. As a result the viscosity of the matrix will remain higher, hence less polymer matrix movement can occur. It has to be emphasized that this is only an assumption because the temperature in the middle of the tape (through-the-thickness) was not measured.

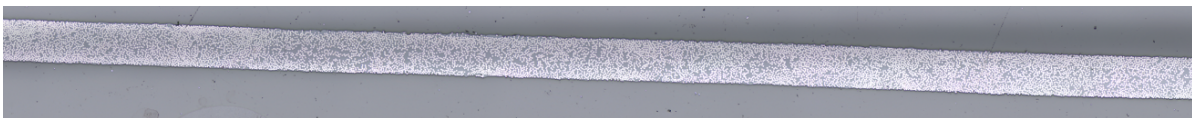


Figure 6.31: Resin-poor Toray-Ten Cate material fibers evenly distributed through-the-thickness of the cross-section

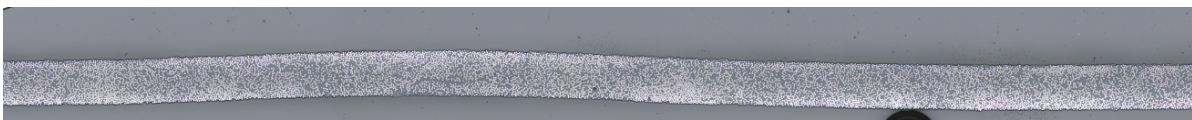


Figure 6.32: Resin-rich Sumprem material lower fiber volume content in the middle, seen through-the-thickness of the cross-section

Polymer matrix movement in the melt phase (towards the ends of the tape) is expected to occur less for resin-rich tapes in comparison to resin-poor tapes. This can also be confirmed from cross-sectional images, see for example figures 6.15-6.17. As was stated before, resin-rich samples show less out-of-plane deformation and lower temperatures towards the ends of the tape. Once the temperature remains below the melting temperature, polymer matrix movement can not occur. This contributes to less arc-length increase.

Next to that, void content, thickness increase and arc-length increase show a decreasing effect with heating time. The lower amount of arc-length increase for longer heating times was already observed by Choudhary

[19]. This was mainly attributed to the fact that void coalescence can take place for the longer heating times. Small voids will coalesce together into larger voids and this results in less arc-length increase. However, the decrease in arc-length in case of the resin-rich samples can be mainly attributed to the lower final void content for the longer heating time as was seen before in section 6.3.3. It was seen before, for the resin-rich samples, that the out-of-plane deformation was higher for larger heated spot lengths due to larger warpage in width direction. As a result, the increase in arc-length that is measured will also be higher. A similar trend for larger heated spot lengths seems also be present in the results of chapter 5.

## 6.5. Conclusion

The effect of a resin-rich surface on the deconsolidation response during the heating phase of LAFP was investigated. The results showed that the laser heating input variables (heating time, heated spot length and resin-richness) have an effect on the deconsolidation response through various interlinked mechanisms. However, it has been demonstrated that the mechanisms affecting the deconsolidation response are different due to the presence of a resin-rich surface. Deconsolidation was quantified through the following response variables (output): surface roughness, maximum out-of-plane deformation, void content, thickness increase and arc-length increase.

It can be concluded that surface roughness and out-of-plane deformation both occur less severe for resin-rich samples, these response variables are interlinked through the following mechanism: decompaction in the out-of-plane direction. However, the heat input in the material is different due to the resin-rich surface. It has been shown that samples with a resin-rich surface show less surface roughness after the heating phase than resin-poor samples. The initial surface roughness (before heating) does not play a role here because it does not seem to be significantly different from resin-poor samples. Dry fibers popping-out of the heated surface were not observed for resin-rich samples as a result of decompaction because the fibers are surrounded by resin. A significantly lower maximum out-of-plane deformation was measured for resin-rich samples.

Samples with a resin-rich surface do show significantly more warpage, especially for 80mm heated spot length. The increased amount of warpage does contribute to out-of-plane deformation and was explained to occur as a result of variation in resin-richness across the width of the resin-rich tape. This will lead to waviness formation, hence a more non-uniform temperature distribution for resin-rich samples at the end of heating. As a result, sections of the tape with locally a lower temperature (below  $T_m$ ) show less surface roughness, out-of-plane deformation and void content.

Void content was demonstrated to be affected by voids already present in the as-received tape, lower fiber volume content in the middle of the tape, minor sections of the tape not heated above  $T_m$ . It was found the out-of-plane decompaction did not contribute to large void formation near the heated surface. On the other hand, it is expected that warpage leads to local fiber movements which will introduce local stresses in the tape. As a result, void formation will occur mainly in the middle of the tape where the fiber volume content was found to be lower. The magnitude of each of the contributions was not measured, this means that no conclusion can be drawn with respect to the mechanism leading to void content increase. In general it can be stated that, a larger void content was measured (except for configuration 30/800) for samples with a resin-rich surface. It has to be emphasized that, the data is inconclusive to demonstrate only the effect of a resin-rich surface on the final void content after heating.

The thickness increase for resin-rich samples was found to be larger than for resin-poor samples. Based on the results it can be concluded that thickness increase occurs mainly due to an increase in void content and this is linked to the temperature achieved in the nip-point. A minor contribution to the final void content is due to thermal expansion of voids already present in the as-received tape which starts at  $T_g$ . Since thickness increase is closely interlinked to void content, the data is inconclusive to demonstrate the effect of the resin-rich surface only.

Arc-length increase was demonstrated to occur due to a combination of effects: out-of-plane deformation, polymer matrix movement in the melt phase, void content increase. Resin-rich samples do show less arc-length increase mainly due to lower out-of-plane deformation. Next to this, based on the shown cross-sectional images it is assumed that polymer matrix movement occurs less severe for resin-rich samples, but

it is expected that this has only a minor contribution in comparison with the lower amount of out-of-plane deformation observed. It can therefore be concluded that a resin-rich surface will lead to less arc-length increase.

To conclude, the research into the effect of a resin-rich surface on deconsolidation revealed that Suprem thermoplastic tapes with a resin-rich top surface have a great potential to be used for the LAFP-process. Less decompaction of the fiber reinforcement network was observed for Suprem resin-rich surface tapes. As a result, the increase in surface roughness remained lower. The smoother and more resin-rich surface (compared to Toray-Ten Cate resin-poor) which were observed after rapid heating are beneficial for intimate contact development. It is therefore expected that a higher degree of effective intimate contact can be reached with Suprem resin-rich surface tapes, hence a higher final laminate quality (compared to Toray-Ten Cate resin poor tapes).

It has to be noted that Suprem resin-rich tapes were found to be more prone to warpage across the width. As explained, this occurred due to variation in resin-richness of the material (off-spec Suprem tapes) across the width of the tape which gave rise to undesired non-uniform heating. It is therefore assumed that for on-spec resin-rich surface tapes this effect of warpage will be diminished.

The obtained results in this chapter contribute to the goal of diminishing deconsolidation effects during the heating phase of LAFP in order to fully commercialize the process. It provides an understanding of the deconsolidation behavior of resin-rich surface tapes. The results can be used as input for an intimate contact model in order to predict the consolidation quality of resin-rich tapes.



# 7

## Results: effect of tape pre-tension on deconsolidation

Chapter 7 will present the results on the effect of the level of tape pre-tension on the deconsolidation behavior of thermoplastic prepreg tapes. This chapter will provide an answer to the third research question: "*What are the main deconsolidation mechanisms in thermoplastic prepreg tapes during the rapid heating phase of LAFP influenced by tape pre-tension?*". The main goal of this chapter is to show the effect of tape pre-tension on the deconsolidation behavior and to compare the different pre-tension levels. The test matrices for the experiments performed during this of the research will be given in section 7.1. Experiments were performed on Toray-Ten Cate tapes with three different levels of tape pre-tension: 5N, 10N and 15N. The results regarding the five deconsolidation response variables and a comparison between pre-tension levels will be presented in section 7.2. At last, the interaction between the five deconsolidation response variables and the driving mechanisms for deconsolidation will be discussed in section 7.3 and the conclusion will follow in section 7.4.

### 7.1. Test matrix

For the third research question 30mm and 80mm heated spot length were used and for the heating time 350ms and 800ms. These variables were again chosen such that the extreme configurations (in terms of heating time and heated spot length) were captured. The main input variable here is the tape pre-tension level. The influence of heating time and heated spot length are of secondary importance again.

In tables 7.1, 7.2, and 7.3 the process configurations can be seen for each of the pre-tension levels. Two repetitions were performed for each of the process configurations. Initially it was aimed again for the same processing temperature (360 - 400 °C). However as can be noticed from the tables below, the total laser power had to be significantly increased for the higher pre-tension levels to achieve this. It is expected that the tool will act as a heat sink due to improved contact between the tape and the surface of the tool as a result of higher pre-tension levels. This will be further discussed in section 7.3. Nevertheless, due to the effect of tape pre-tension (in particular 10N and 15N) it was impossible to achieve the average nip-point temperature of 360 - 400 °C without overheating parts of the tape. In sections 7.2 and 7.3 it will be discussed what exactly could have caused this. To capture the deconsolidation effect it was ensured that at least a part of the tape reached processing temperature.

Table 7.1: Configuration settings experimental research 0.5" Ten Cate prepreg tapes, pre-tension: 5N

<b>Process configuration</b>	<b>C30/350/5</b>	<b>C30/800/5</b>	<b>C80/350/5</b>	<b>C80/800/5</b>
Spot length (mm)	30	30	80	80
Heating time (ms)	350	800	350	800
Pre-tension force (N)	5	5	5	5
VCSEL zones activated	4-6	4-6	1-11	1-11
Power per zone (%)	100	44	54	36
Total power (W)	600	264	1188	792

Table 7.2: Configuration settings experimental research 0.5" Ten Cate prepreg tapes, pre-tension: 10N

Process configuration	C30/350/10	C30/800/10	C80/350/10	C80/800/10
Spot length (mm)	30	30	80	80
Heating time (ms)	350	800	350	800
Pre-tension force (N)	10	10	10	10
VCSEL zones activated	4-6	4-6	1-11	1-11
Power per zone (%)	100	80	62	45
Total power (W)	600	480	1364	990

Table 7.3: Configuration settings experimental research 0.5" Ten Cate prepreg tapes, pre-tension: 15N

Process configuration	C30/350/15	C30/800/15	C80/350/15	C80/800/15
Spot length (mm)	30	30	80	80
Heating time (ms)	350	800	350	800
Pre-tension force (N)	15	15	15	15
VCSEL zones activated	4-6	4-6	1-11	1-11
Power per zone (%)	100	85	70	50
Total power (W)	600	510	1540	1100

## 7.2. Deconsolidation response of Ten Cate pre-tensioned tapes

In the five subsections below the results are presented for the tape pre-tension research. The results are given in a separate subsection for each single deconsolidation response variable. Bar diagrams will be shown with the main results. The error bars represent the minimum and maximum of the 2 repetitions, except for the void content since the void content is given as a range from a minimum to a maximum threshold per sample. The discussion of all the results together follows in section 7.3 since all five response variables interact with each other.

### 7.2.1. Out-of-plane deformation

In figure 7.1 it can be seen that different pre-tension levels behave differently in terms of maximum temperature along the nip-point. The left figure shows the case for 5N. As can be seen a major part of the width (77%) of the tape was above the melting temperature (red horizontal line in the graph). In the middle graph of figure 7.1 a totally different scenario for 10N can be observed. Only a small portion of the width (14%) was above the melting temperature. It has to be mentioned here that only the left peak (part indicated between 2 black circles) in figure 7.1 is taken into account here, since only this part contributes to the maximum out-of-plane deformation at corresponding location in figure 7.2. In the right graph of figure 7.1 another case is shown for 15N. Here it is only a portion at the right-hand side (26%) of the tape that was above the melting temperature. Only this portion is contributing to the maximum out-of-plane deformation, see corresponding right figure in figure 7.2.

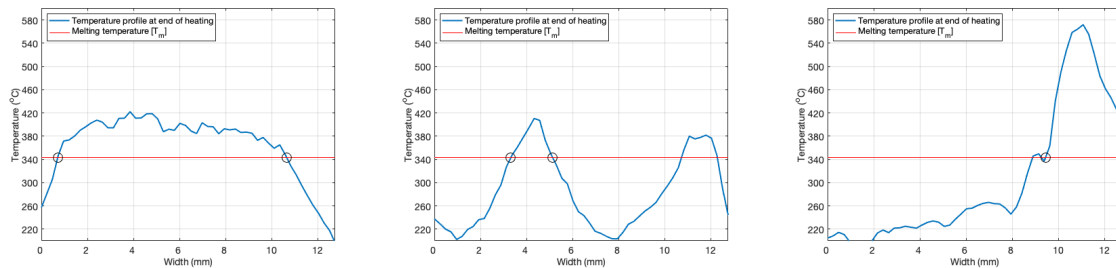


Figure 7.1: Variation in temperature profiles at the end of heating. Heated spot length = 30mm, heating time = 800ms  
Left: pre-tension = 5N; Mid: pre-tension = 10N; Right: pre-tension = 15N

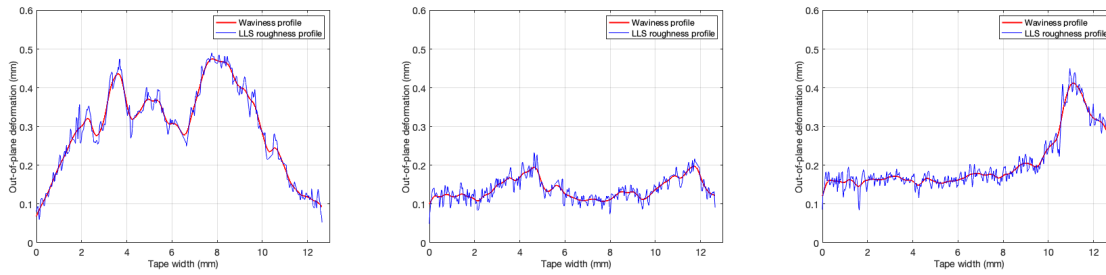


Figure 7.2: Out-of-plane deformation diagrams corresponding to the same samples as in Figure 7.1. Left: pre-tension = 5N; Mid: pre-tension = 10N; Right: pre-tension = 15N

An additional normalization factor was applied for out-of-plane (OOP) deformation because a large variation in maximum nip-point temperature over the width of the tape was seen. As explained in the previous paragraph, samples are present with only minor parts of the tape heated above the melting temperature (in particular samples for 10N and 15N). Therefore, the normalization factor (NF) was determined as a ratio of the width that has been above the melting temperature over the total tape width, see equation 7.2.

$$\text{normalized OOP deformation} = \frac{\text{maximum OOP deformation}}{NF_{OOP}} \tag{7.1}$$

$$NF_{OOP} = \text{OOP normalization factor} = \frac{\text{width of contributing tape section above } T_m}{\text{total tape width}} \tag{7.2}$$

The normalized maximum out-of-plane deformation was calculated using equation 7.1. In figure 7.3 a bar diagram with the normalized results for the maximum out-of-plane deformation (expressed in  $\mu\text{m}$  per unit width) can be seen. Three different pre-tension levels are shown directly next to each other. The 4 different sets on the x-axis correspond to the different configurations for heated spot length and heating time. The only important observation that can be made here is that the maximum out-of-plane deformation increases towards 10N and 15N. Furthermore, no clear distinction between 10N and 15N can be observed due to large error bars. Also, no obvious interaction effects can be observed with respect to heating time and spot length.

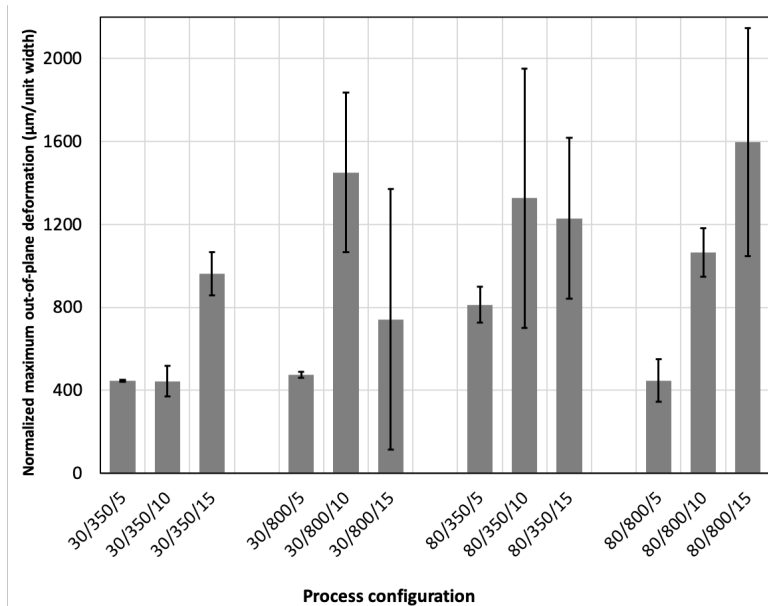


Figure 7.3: Normalized maximum out-of-plane deformation for several tape pre-tension levels and process configurations

The increasing results towards 10N and 15N can be explained by the presence of local out-of-plane deformations. In other words, local peaks are present in the waviness curve however with limited width. Peaks with a small width (above  $T_m$ ) result in a small normalization factor ( $NF_{OOP}$ ) leading to a larger contribution to the normalized out-of-plane deformation. The material behavior causing this effect will be discussed further in section 7.3.

### 7.2.2. Surface roughness

The surface roughness results are shown in the bar diagram in figure 7.4. The results for 5N, 10N and 15N are plotted directly next to each other and the as-received surface roughness is included as well. The 4 process configurations in terms of heated spot length and heating time are divided over the x-axis. The main observation here is that an increase in surface roughness is measured for all configurations and that the surface roughness is significantly higher for 5N compared to 10N and 15N. No clear distinction can be made between the surface roughness for 10N and 15N. Next to this, no significant trends with respect to heated spot length and heating time were observed.

Figure 7.5 shows surface roughness as a function of temperature. This was investigated since large variations exist in the maximum nip-point temperature over the width and the surface roughness was measured at 4 distinct locations. The individual local data points are plotted separately as a function of temperature at that specific location.

In general, a large range in roughness can be observed in figure 7.5. The larger mean surface roughness for 5N samples (figure 7.4) can be explained by the fact that higher roughness is measured for all the individual data points. This can be seen in figure 7.5 by the data points for 5N (black dots) which show in general higher RMS roughness values compared to 10N and 15N. However, both observations are not a result of temperature since no trend with temperature is observed.

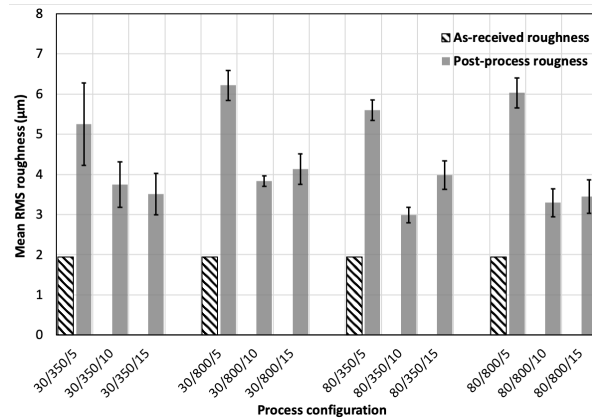


Figure 7.4: RMS roughness for several process configurations

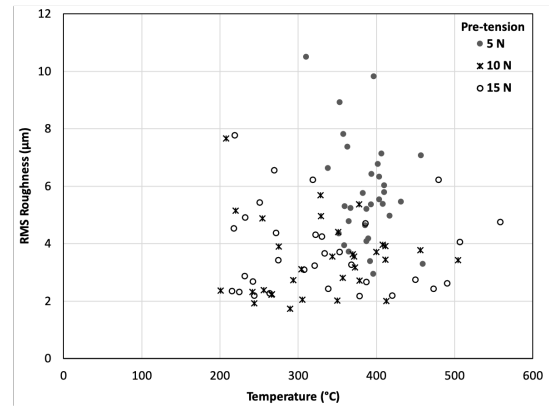


Figure 7.5: RMS roughness as a function of temperature

### 7.2.3. Width increase

In contrast to chapters 5 and 6, the arc-length was not used here as a measure to determine the increase in width dimension. The arc-length of the waviness curve was driven by local peaks in out-of-plane direction, as was seen for example in figure 7.6. This is not a representative measure for the dimensional changes of the tape in width direction. Alternatively width increase was measured, i.e. the increase in tape distance from edge-to-edge transverse to the fiber direction. Figure 7.6 shows the measured distance before and after heating, the edges of the tape (the most outer data points) are indicated by the black circles in the graphs.

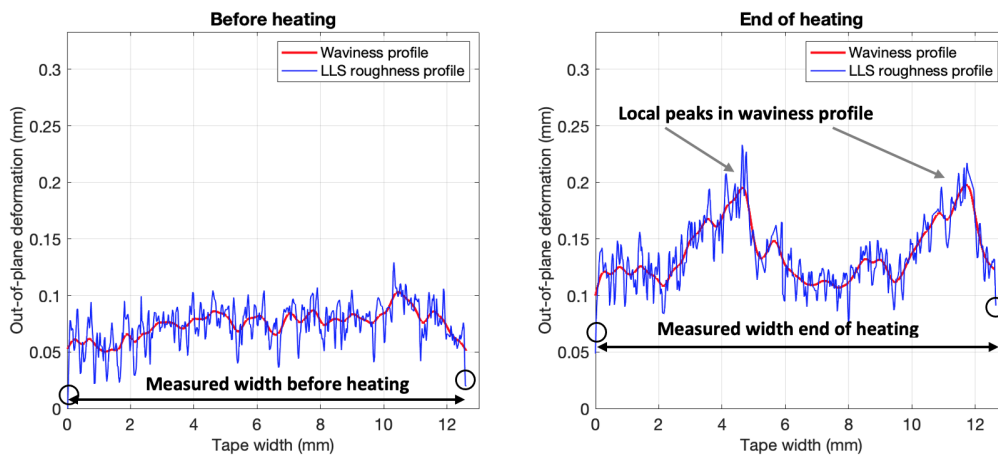


Figure 7.6: Width increase measured before and after heating, sample from config. C30/800/10

In figure 7.7 the results are shown in a bar diagram. In general, it can be stated that for all configurations a small increase in width is observed. The results show average values around  $1\% \pm 0.5\%$  for all configurations. The maximum width increase calculated is  $<2\%$  which corresponds to an absolute increase in the order of magnitude of around 0.1-0.2 mm.

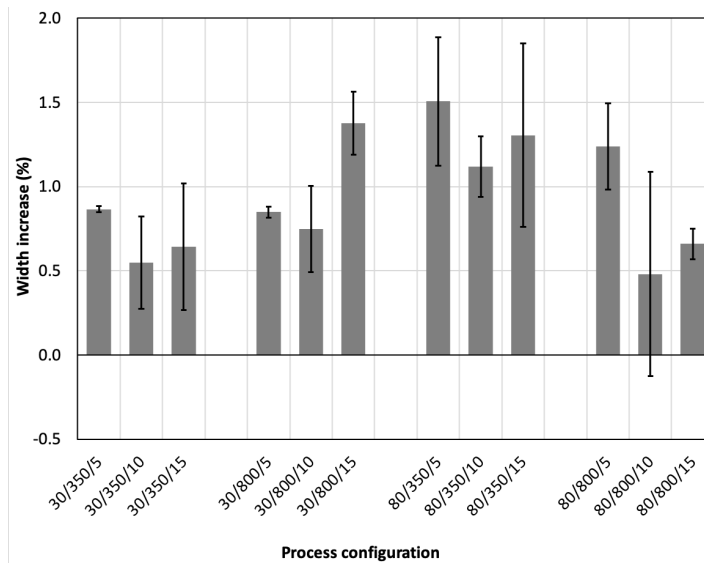


Figure 7.7: Width increase for several pre-tension levels and process configurations

The selection of the edge data points of the tape introduces a certain error within the width measurements. In the left image of figure 7.8 a screenshot of the raw LLS data can be seen. The data points within the green box correspond to the surface of the tape, these are the data points selected for analysis. In the right image of figure 7.8 a schematic overview of the data points around the edge of the tape is given. As can be seen several data points are present close to each other around the edge. The threshold for selection of the best data point is given by the center data point. One of the data points on the right-hand side of the center give the best representation of the actual edge data point. Hence, the selection of the data point designated to the edge introduces an absolute error of around 0.1mm. This means that no significant difference can be noticed between different process configurations as a results of the measurement error.

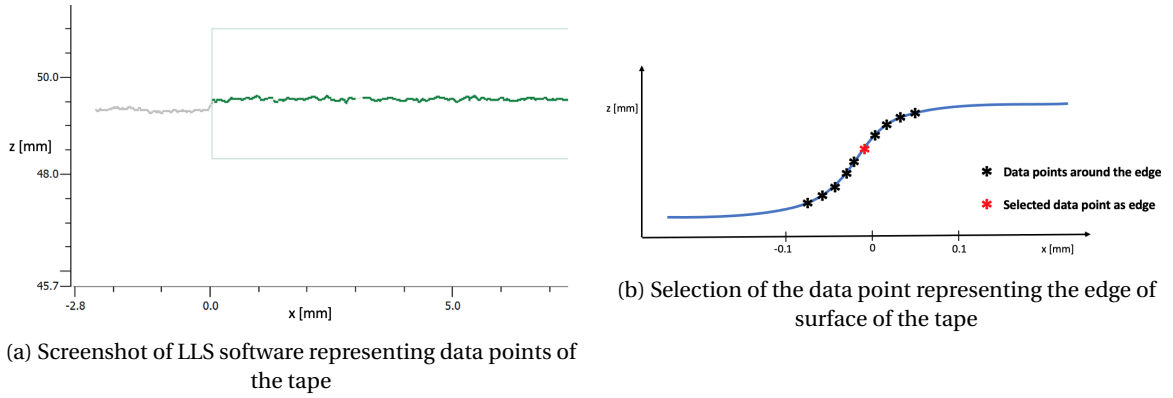


Figure 7.8: Schematic representation of the edge of the tape

### 7.2.4. Void content

As was already mentioned before in section 7.2.1, large variations in the maximum nip-point temperature exist. It was observed that higher void content is present only at locations with a temperature above the melt. In figure 7.9 two regions can be observed where the temperature exceeds  $T_m$ . In figure 7.10 it can be observed that voids are mainly present at these corresponding locations. As can be seen regions which remained below the melt hardly show any void content.

A normalization factor was therefore applied to the void content results. As described by the methodology in section 4.3.5 the void content is determined globally per sample. However, voids are not present over the entire width of the tape but mainly at regions where the temperature was above  $T_m$ . Therefore, equations 7.3 and 7.4 are applied to calculate the normalized void content per sample.

$$\text{normalized void content} = \frac{\text{total global void content}}{NF_{void}} \quad (7.3)$$

$$NF_{void} = \text{void normalization factor} = \frac{\text{total width above } T_m}{\text{total tape width}} \quad (7.4)$$

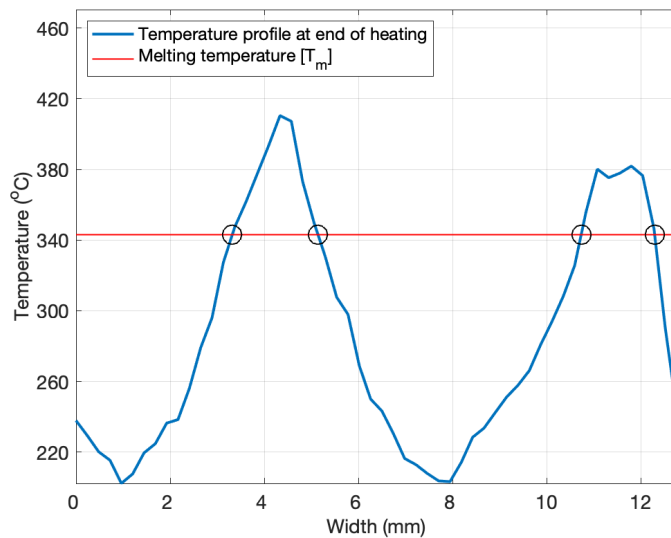


Figure 7.9: Temperature profile of config. C30/800/10

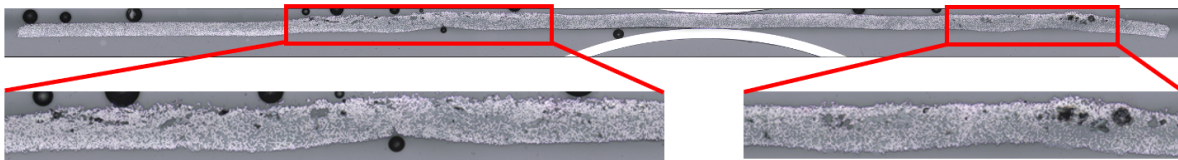


Figure 7.10: Higher void content present at locations where temperatures above  $T_m$  were reached, config. C30/800/10

Figure 7.11 shows the results for the normalized void content. Except for configuration 30/800/10 all the average results show values between 4-9% void content. Since the void content is given as a range (approximation of a minimum and maximum void content per sample), no significant distinction can be made between different pre-tension levels or process configurations. It can be stated that pre-tensioned samples show a normalized void content of 4-9% on average, regardless of the pre-tension level. With an exception for 30/800/10 that shows an average void content of 16%. This can be explained by a relatively large void content for the portions of the tape above  $T_m$ . Moreover, the void normalization factor is relatively small (only 26%, see figure 7.10) which contributes to a large normalized void content. To summarize, there is no direct effect of different pre-tension levels on the void content. Temperature seems to play a dominant role here, this will be further discussed in section 7.3.

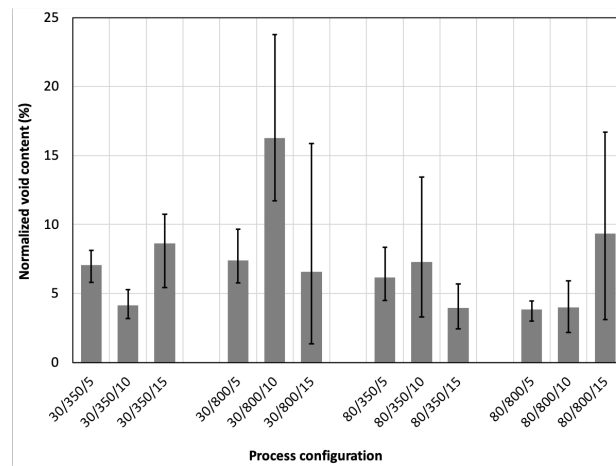


Figure 7.11: Normalized void content for several pre-tension levels and process settings

### 7.2.5. Thickness change

The results for thickness change can be observed in figure 7.12. Positive values represent a thickness increase, while negative values represent a thickness decrease. As can clearly be seen significant thickness increase is present for samples with 5N pre-tension. Furthermore, the most important observation is that almost no thickness increase is measured for 10N and 15N samples.

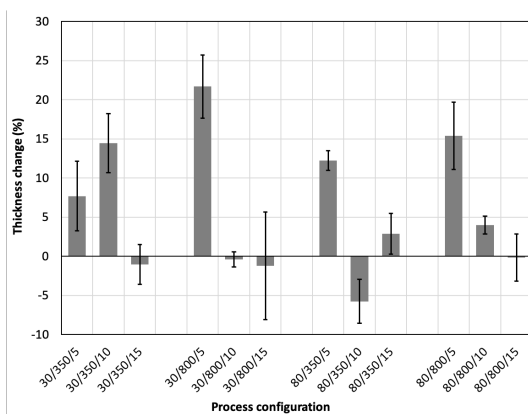


Figure 7.12: Thickness increase for different levels of pre-tension

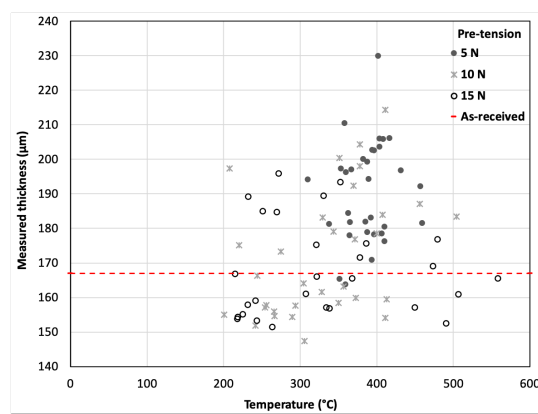


Figure 7.13: Measured thickness as a function of temperature

In figure 7.13 the relation between the thickness measurements and temperature can be seen. The thickness was measured locally at 4 distinct locations (20%, 40%, 60% and 80% of the width). Each individual thickness measurement is directly related to the temperature achieved at that specific location. A few important observations can be made with respect to different pre-tension levels. First of all, it can be seen that almost all 5N data points are above the as-received state which means that an increase in thickness is measured. Secondly, the measured thickness for 5N is in general larger than for 10N and 15N samples. Next to that, a slightly increasing trend with temperature can be observed for the 5N data points. For 10N and 15N no trend with temperature seems to be present at all. Pre-tension seems to play the major role here since no significant trend with respect to temperature can be observed from figure 7.13.

As already observed from the scatter plot the temperature does not seem to play a role in the thickness change results. This can be proven by figure 7.14. In this graph thickness change results normalized with temperature can be seen, expressed in percentage thickness change per degree Celsius. For the normalization the thickness change is divided by the temperature above the glass transition temperature ( $T_g$ ), see equation 7.5.

$$\text{normalized thickness change} = \frac{\text{thickness change}}{\text{measured temperature} - T_g} \quad (7.5)$$

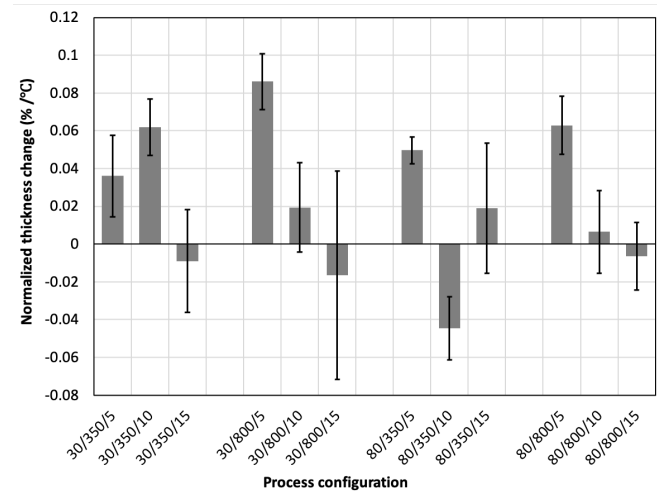


Figure 7.14: Normalized thickness change for several pre-tension levels and process settings

### 7.3. Discussion

Based on the results it is assumed that due to applying tape pre-tension contact between the tape and the surface of the tool will improve. Heat that is initially absorbed by the fibers can conduct through the tape towards the tool. The tool will act subsequently as a heat sink. To the authors knowledge this is the main reason why increased laser power was needed for higher tape pre-tension levels while keeping heating time and heated spot length constant. Heating the tape to the processing temperature did become increasingly difficult as the level of pre-tension increased.

It can be stated that for higher pre-tension levels (10N and 15N) a highly non-uniform temperature distribution exists over the width of the tape. Severe local out-of-plane deformation is mostly present due to locally higher temperatures above the melting temperature. The first hypothesis: *"for higher tape pre-tension a more uniform temperature distribution in width direction is expected to be seen at the nip-point location and the amount of out-of-plane deformation is expected to be less severe"* does not seem to hold. In contrast to the hypothesis, the results show an increase in out-of-plane deformation and a less uniform temperature distribution for higher pre-tension levels.

Global out-of-plane deformation is hindered since the temperature will not rise uniformly above the melting temperature. Due to tape pre-tension and improved contact between the tape and the surface of the tool,

heat is dissipated towards the tool. Formation of local peaks in waviness curve (for 10N and 15N pre-tension samples) occurs as a result and can be explained by local areas taking more heat due to presence of fiber clusters, see figure 7.15. The contact between the tape and the surface of the tool will decrease locally. Once a local area starts to heat up more than the surrounding area, locally more out-of-plane deformation will occur. Therefore, that particular section of the tape will come closer to the VCSEL module and in turn the local heat flux will increase resulting in further increase of the local temperature. This will exacerbate the effect of out-of-plane deformation and cause large local peaks in the out-of-plane deformation curve and a highly non-uniform temperature distribution, as was seen in figures 7.1 and 7.2. Based on the results, it is expected that this effect increases as the level of tape pre-tension increases.

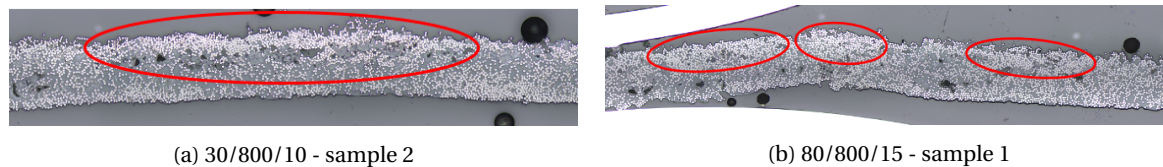


Figure 7.15: Fiber clusters located at the heated surface causing locally high temperatures, hence out-of-plane deformation

It was hypothesized that the locally measured temperature at the measurement points (4 distinct locations) for surface roughness had an influence on surface roughness. However, the data showed no trend between the local measured surface roughness and temperature values. As can be seen in figure 7.15, dry fibers are popping-out of the surface. The heated surface showed a larger surface roughness at locations with a large out-of-plane deformation which corresponds to the peaks in the temperature distribution across the width. Hence, out-of-plane decompaction of the fiber reinforcement network does seem to play a role in large local surface roughness formation. This implies that large peaks in the temperature distribution correlate to increased surface roughness.

It was hypothesized that: *"increased tape pre-tension will diminish the surface roughness due to less out-of-plane decompaction of the fiber reinforcement network and a more uniform temperature distribution"*. The hypothesis suggest that less out-of-plane deformation will lead to lower surface roughness as the tape pre-tension level will increase. Higher local out-of-plane deformation was observed for higher pre-tension levels. At these locations higher surface roughness was observed. If surface roughness is globally assessed, the results show a decreasing surface roughness for higher pre-tension levels. However, this has to do with the fact that only a minor part of the tape was heated above  $T_m$  as was shown by the normalized out-of-plane deformation results. An increasing out-of-plane deformation with higher pre-tension levels was shown by the normalized results, based on this, the hypothesis does not seem to hold. However, the fact that surface roughness is locally measured at four pre-defined locations prohibits to draw solid conclusions on the effect of tape pre-tension on surface surface due to local heat absorption. In order to draw more solid conclusions it would be required to measure the surface roughness at the exact location where the local heat absorption occurs.

The results for the width increase results show for all configurations values of around 1% on average. This means that no effect of different tape pre-tension levels is measured. Next to that, no interaction with out-of-plane decompaction can be noticed as the hypothesis tested: *"more width increase will be observed for pre-tensioned prepreg tapes since out-of-plane decompaction will be hindered. If the tape can deform less in the out-of-plane direction then it should deform in width direction."* Global out-of-plane deformation is hindered for higher pre-tension levels, as was seen before, however no significant effect on width increase is measured as a result of this. The fact that such a small width increase was measured that this was not found to be significant with respect to the measurement accuracy was already discussed in section 7.2.3.

Based on the results for normalised void content, the fourth hypothesis: *"void content development is expected to become less with increasing pre-tension force since the tape will be hindered to decompact"* does not seem to hold. On average the normalised void content was measured within the range of 4-9% for all configurations (with an exception for 30/800/10) and no correlation with tape pre-tension levels. It was observed that global decompaction is hindered as a result of higher pre-tension levels. However, the locally observed fiber decompaction still seems to correlate with local void content development. Void formation near the heated surface

does mainly occur in the melt phase and as a result of decompaction of the fiber reinforcement network. Therefore, voids can be observed from cross-sectional images at locations where severe out-of-plane deformation does also occur. It has to be noted that the methods for normalization of the results for maximum out-of-plane deformation and void content are not exactly the same. For normalised maximum out-of-plane deformation only the section that contributes to the local maximum peak in the out-of-plane deformation is taken into account while for the normalised void content the section of the tape above  $T_m$  was taken into account. This discrepancy makes it hard to draw solid conclusions (based on measurement data) on void formation due to out-of-plane decompaction. Finally, void formation does also occur due to void thermal growth. This can start already from glass transition temperature ( $T_g$ ). It is expected that this will have a minor contribution to the final void content and it is proposed that this will have similar contribution for all test samples since all the temperature distributions show values above  $T_g$  for the entire width.

The following hypothesis was tested with regards to thickness change: *"thickness increase will be expected to be less severe since less void content development is expected for higher tape pre-tension levels"*. Based on the results of figures 7.11 and 7.12 it is hard to notice any interaction between void content and thickness increase. This has to do with the fact that the thickness was measured at four local points along the width and the void content was measured globally. The highly non-uniform temperature distribution across the width caused difficulties in comparing the results and drawing conclusions on the contribution of void content to thickness increase. For a pre-tension level of 5N, the samples do seem to be slightly dependent on the measured temperature. The thickness seems to be increasing with higher temperature. This is an indication that temperature, hence fiber decompaction and as a result void formation does contribute to thickness increase. Therefore, it is expected that for 5N samples void content development is the main contributor to thickness increase.

For higher pre-tension levels (10N and 15N) almost no significant thickness change was observed. As can be seen from figure 7.13, no trend for thickness change with respect to temperature could be observed for 10N and 15N pre-tension measurements. Next to that, normalization was applied to the thickness change results. This had however no significant effect and implies that the highly non-uniform temperature distribution, which is a result of increased pre-tension, does not have any impact on the thickness change results. Therefore, no effect of increased tape pre-tension on thickness change was measured.

## 7.4. Conclusion

The effect of tape pre-tension on the deconsolidation response during the heating phase of LAFP was investigated. The results showed that the laser heating input variables (heating time, heated spot length and tape pre-tension) have an effect on the deconsolidation response through various interlinked mechanisms. However, it has been demonstrated that the mechanisms affecting the deconsolidation response are different as a result of tape pre-tension. Deconsolidation was quantified through the following response variables (output): surface roughness, maximum out-of-plane deformation, void content, thickness increase and arc-length increase.

It can be concluded that increasing the level of tape pre-tension improved the contact between the tape and the surface of the tool. The tool worked as a heat sink in this case and as a result it became more difficult to heat the material to the processing temperature at the nip-point location. It was shown that local heat absorption occurred only at locations where fiber clusters were present. Large out-of-plane deformation was observed only locally for increased tape pre-tension with a highly non-uniform temperature distribution as a result.

It was expected that a correlation between out-of-plane deformation and width increase would exist. However, the data showed no significant effect of out-of-plane deformation on width increase. No effect of tape pre-tension was measured on width increase as the results show a width increase of around 1% on average, despite the pre-tension level.

Out-of-plane decompaction of the fiber reinforcement network seems to play a role in large local surface roughness formation. For higher pre-tension levels, large local out-of-plane deformation occurred and at these locations higher surface roughness was observed. This implies that large peaks in the temperature dis-

tribution correlate to increased surface roughness. However, surface roughness was measured locally at four distinct locations. This will, together with the local heat absorption, prohibit to draw solid conclusions on the effect of tape pre-tension on surface roughness. Local surface roughness measurements at the location of the local heat absorption would help to draw better conclusions.

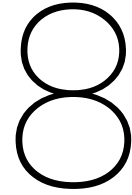
The results for the normalised void content showed no effect of tape pre-tension. On average the normalised void content was measured in the range of 4-9% for all configurations and tape pre-tension levels. Increased void content was mainly observed at locations where severe out-of-plane deformation did occur. Therefore, locally observed fiber decompaction still seem to interact with local void formation. However, the discrepancy between normalized out-of-plane deformation data based on the very local heat absorption and the normalised void content data (global data) makes it difficult to draw solid conclusions on void formation as a result of out-of-plane decompaction.

No solid conclusions can be made on the contribution of void content (measured globally) to thickness change (measured locally). The highly non-uniform temperature distribution caused difficulties in comparing the measurements for void content and thickness change. For 5N tape pre-tension an increasing trend of thickness with respect to temperature was seen. This result showed that void formation did contribute to thickness increase. For higher pre-tension levels no thickness change was observed. Normalization was applied to the thickness change results, but this did not show any change in the results. To conclude, no effect of increased tape pre-tension on thickness change was measured.

To conclude, this research into the effect of tape pre-tension on deconsolidation revealed that the most important mechanism at play is decompaction of the fiber reinforcement network. The results showed that the normalized maximum out-of-plane deformation is increasing with higher pre-tension levels as a result of decompaction. Next to that, decompaction is the main mechanism responsible for large local out-of-plane deformation and surface roughness.

To achieve a high degree of effective intimate contact it is required that an average processing temperature of around 360 °C across the simulated nip-point is reached during the heating phase and an as uniform as possible temperature distribution. Next to that, a low out-of-plane decompaction and low surface roughness are beneficial for intimate contact development. Therefore, it does not seem to be advantageous to increase the tape pre-tension level towards 10N and 15N for the LAFP-process. Moreover, the temperature data showed a highly non-uniform temperature across the simulated nip-point (for 10N and 15N) which is also unfavorable for intimate contact development during the consolidation phase of the LAFP-process. Therefore, it is expected that the optimum pre-tension level lies around 5N. Based on the results, it is assumed that the global out-of-plane decompaction and global surface roughness increase will remain lower as a result of pre-tension application. This remains however to be more extensively investigated in future research.





## Conclusion

The influence of varying the heating time and heated spot length on the deconsolidation response during the heating phase of LAFP was investigated and compared to an earlier performed study by Choudhary [19]. Next to that, an experimental investigation on the effect of a resin-rich surface and tape pre-tension on the deconsolidation response during the heating phase of LAFP was performed. The results show that the laser heating input variables (heating time, heated spot length, resin-richness and tape pre-tension) have an effect on the deconsolidation response through various interlinked mechanisms. However, it has been demonstrated that the deconsolidation response was different due to the presence of a resin-rich surface or tape pre-tension. Deconsolidation was quantified through the following response variables (output): surface roughness, maximum out-of-plane deformation, void content, thickness increase and arc-length (width) increase.

For the research into the influence of heating time and heated spot length and the research into the effect of a resin-rich surface on deconsolidation, the experimental setup of Choudhary [19] was rebuilt. For the research into the effect of tape pre-tension on deconsolidation, a new experimental setup was developed and built with which force controlled tape pre-tension could be applied and measured. Tape pre-tension was applied at one end of the tape using a pre-defined subset of weights. At the other end of the tape, a load cell was attached to the tape to be able to measure tape pre-tension.

Resin-richness was defined during this research as: the resin area content on the top surface of CF/PEEK prepreg tapes. It was characterized from top surface micrographs captured with a LSCM. A novel methodology to assess the resin-richness from top surface micrographs of tape specimens was developed, which was based on the DEIC method described in the work of Celik [42].

### **Influence of heating time and heated spot length**

It can be concluded that out-of-plane decompaction is the mechanism behind surface roughness development and out-of-plane deformation. Next to that, it contributes to void content development and thickness increase, mainly for the short heated spot length of 30mm. No significant effects of heating time and heated spot length were found on surface roughness and maximum out-of-plane deformation. The temperature achieved at the nip-point has been shown to be the most dominant factor causing out-of-plane deformation and surface roughness. The non-uniform temperature profile at the end of heating is caused by waviness formation, peaks in the temperature profile do correspond to peaks in the waviness profile and larger roughness was found at local peaks in the waviness curve.

Void content development has shown two possible mechanisms of void formation: void formation due to traction and cavitation and void thermal growth of voids already present in the as-received material. Next to that, void coalescence can occur for larger heating times. Void content development was found to contribute to arc-length increase and thickness increase. No significant trend of heating time on void content was measured and larger void content was found for shorter heated spot length. The latter is a result of decompaction which plays an important role in void formation for short heated spot lengths of 30mm for which heat flux is higher (total amount of power per unit spot length).

Various mechanisms were found to contribute to arc-length increase. Since arc-length is determined by the waviness profile, it is expected that the variation in waviness is the main contributor. Next to that, it was demonstrated that void coalescence and polymer matrix movement can play a role however the magnitude of each contributions could not be determined from the measurement data. The data has shown that increasing heating time has a decreasing effect on arc-length, while increasing the heated spot length has an increasing effect on arc-length. It is expected that these observed trends occur mainly due to global waviness formation.

Thickness increase occurs primarily due to void content increase however out-of-plane decompaction does also contribute to thickness increase. It can not be concluded from the data that significant effects of heating time and heated spot length exist which affects thickness increase due to large scatter.

Waviness formation and out-of-plane decompaction of the fiber reinforcement network are the main deconsolidation mechanisms. To emphasize the relevance, waviness formation is undesirable because it will lead to non-uniform heating across the simulated nip-point causing locally higher out-of-plane decompaction and a rough fiber-rich surface. Mainly, the fiber-rich surface with an increased surface roughness is disadvantageous for the LAFP-process. A tape with an increased surface roughness (at the end of the heating phase) will lead to a lower degree of effective intimate contact, which is required for a good bond strength and a high final laminate quality, during the consolidation step in the LAFP-process.

The results gathered during this research did contribute to a better understanding of the heating phase of LAFP. The outcome of this research can be used as input for an intimate contact model for the consolidation phase of LAFP, since models found in literature did not include the fact that the tape will undergo a change in consolidation state during the heating phase. With an improved model the material behaviour during the consolidation phase and the final quality of LAFP-manufactured laminates could be better predicted.

#### **Effect of a resin-rich surface**

Surface roughness and out-of-plane deformation both occur less severe for resin-rich surface tapes, these response variables are interlinked through the following mechanism: decompaction in the out-of-plane direction. It has been shown that samples with a resin-rich surface show less surface roughness and significantly lower maximum out-of-plane deformation after the heating phase. Because the fibers are surrounded by resin, no dry fibers popping-out of the heated surface were observed as a result of decompaction .

Samples with a resin-rich surface do show significantly more warpage, especially for 80mm heated spot length. The increased amount of warpage does contribute to out-of-plane deformation and was explained to occur as a result of variation in resin-richness across the width of the resin-rich tape. This will lead to waviness formation, hence a more non-uniform temperature distribution for resin-rich samples at the end of heating.

Void content was demonstrated to be affected by voids already present in the as-received tape, lower fiber volume content in the middle of the tape, minor sections of the tape not heated above  $T_m$ . It was found the out-of-plane decompaction did not contribute to large void formation near the heated surface. On the other hand, it is expected that warpage leads to local fiber movements which will introduce local stresses in the tape. As a result, void formation will occur mainly in the middle of the tape where the fiber volume content was found to be lower. In general it can be stated that, a larger void content was measured (except for configuration 30/800) for samples with a resin-rich surface. However, the data is inconclusive to demonstrate only the effect of a resin-rich surface on the final void content after heating.

The thickness increase for resin-rich samples was found to be larger than for resin-poor samples. It can be concluded that thickness increase occurs mainly due to an increase in void content and this is linked to the temperature achieved at the nip-point location. A minor contribution to the final void content is due to thermal expansion of voids already present in the as-received tape which starts at  $T_g$ . As for void content, the data is inconclusive to demonstrate the effect of the resin-rich surface only.

Arc-length increase was demonstrated to occur due to a combination of effects: out-of-plane deformation, polymer matrix movement in the melt phase, void content increase. Resin-rich samples do show less arc-

length increase mainly due to lower out-of-plane deformation. Next to this, it was shown that polymer matrix movement occurs less severe for resin-rich samples, but it is expected that this has only a minor contribution in comparison with the lower amount of out-of-plane deformation observed. It can therefore be concluded that a resin-rich surface will lead to less arc-length increase.

Suprem thermoplastic tapes with a resin-rich top surface have a great potential to be used together with the LAFP-process. Less decompaction of the fiber reinforcement network resulting in less increase in surface roughness were observed after rapid heating. To emphasize the relevance of these findings, the smoother and more resin-rich surface (compared to Toray-Ten Cate resin-poor) are beneficial for intimate contact development. It is therefore expected that a higher degree of effective intimate contact can be reached with Suprem resin-rich surface tapes, hence a higher final laminate quality (compared to Toray-Ten Cate resin poor tapes).

The promising results contribute to the goal of diminishing deconsolidation effects during the heating phase of LAFP in order to further commercialize the process. It provides an understanding of the deconsolidation behavior of resin-rich surface tapes. Furthermore, the results can be used as input for an intimate contact model. Hence, the model can be further improved and extended to be widely applied and to predict the consolidation quality of resin-rich tapes.

### **Effect of tape pre-tension**

Laser heating experiments were performed with three levels of tape pre-tension: 5N, 10N and 15N. Increasing the level of tape pre-tension improved the contact between the tape and the surface of the tool. The tool worked as a heat sink in this case. It was shown that local heat absorption occurred only at locations where fiber clusters were present. Large out-of-plane deformation was observed only locally for increased tape pre-tension with a highly highly non-uniform temperature distribution as a result.

No effect of tape pre-tension was measured on width increase as the results show an increase in width of around 1% on average, despite the pre-tension level. It was found that out-of-plane deformation does not have a significant effect on width increase.

Out-of-plane decompaction of the fiber reinforcement network seems to play a role in large local surface roughness formation. For higher pre-tension levels, large local out-of-plane deformation occurred and at these location higher surface roughness was observed. This implies that large peaks in the temperature distribution correlates to increased surface roughness. Due to local heat absorption and locally measured surface roughness (at four distinct locations), no solid conclusions could be drawn to the effect of tape pre-tension on surface roughness.

The results for the normalised void content showed no effect of tape pre-tension. On average the normalised void content was measured in the range of 4-9% for all configurations and tape pre-tension levels. Higher void content was mainly observed at locations where severe out-of-plane deformation did occur. Therefore, locally observed fiber decompaction still seem to interact with local void formation. No solid statements on void formation (globally measured) as a result of out-of-plane decompaction (local behaviour) can be made.

For 5N tape pre-tension an increasing trend of thickness with respect to temperature was seen. This showed that void formation did contribute to thickness increase. For higher pre-tension levels no thickness change was observed. Normalization of the thickness change results did not show any change in the results. Therefore, no effect of increased tape pre-tension on thickness change could be measured.

The obtained results during this research are relevant for the LAFP-process. It is expected that the optimum pre-tension level lies around 5N. Increasing the tape pre-tension level towards 10N and 15N seem to be disadvantageous for the LAFP-process. The temperature data showed a highly non-uniform temperature across the simulated nip-point (for 10N and 15N) which is unfavorable for intimate contact development during the consolidation phase of the LAFP-process. Next to this, the local heat absorption caused large local out-of-plane decompaction of the fiber reinforcement network. This is the main mechanism responsible for out-of-plane deformation and a large local surface roughness.

Based on the results, it is assumed that the global out-of-plane decompaction and global surface roughness increase will remain lower as a result of low (5N) pre-tension application. It would therefore be interesting to investigate the deconsolidation response of Suprem resin-rich tapes together with a pre-tension force of 5N applied. Since Suprem resin-rich tapes facilitated a smoother surface (less decompaction, hence less increase in surface roughness) after rapid heating it would be interesting to see if the deconsolidation response can be further diminished with the application of a low (5N) pre-tension force. This remains to be experimentally investigated in future research.

# 9

## Recommendations

In this chapter the recommendations for future research will be provided. First of all, general suggestions will be provided for the LAFP-process. Next to that, since the focus in this research was on the effect of a resin-rich surface and tape pre-tension on the deconsolidation response, further propositions will be provided in these research directions.

### **LAFP-process**

During this research it became clear that resin-rich surface tapes are beneficial in order to diminish deconsolidation effects. The next step is that it should be investigated what the effect is on the consolidation phase and the final quality (mechanical performance) of LAFP-manufactured laminates. This could be done through modeling of the consolidation phase with the results gained during this research as input. However, the behavior of *deconsolidated* resin-rich tapes during the consolidation step of the LAFP-process should be confirmed by experimental research. Moreover, it would be valuable to quantify the difference in response between resin-poor tapes and resin-rich tapes during the consolidation phase and the effect on the final laminate quality.

To further commercialize the LAFP-process a step (in either processing, materials or both) should be made with regards to the deposition rate. During the current research production rates within the range of 37.5 - 228 mm/s were simulated. To qualify the process for industry it would be required to reach deposition rates within the range of 400 - 800 mm/s (2-4x current rate) with still the same quality. It remains for future research whether this is feasible and how this could be achieved without losing quality.

### **Heating phase of LAFP**

For further research into the heating phase of LAFP it is advised to make use of resin-rich surface tapes since the results are promising with respect to decreasing the deconsolidation response. This is beneficial for intimate contact development and the final quality of LAFP-manufactured laminates. Next to that, it is expected that with an applied tape pre-tension force of 5N the deconsolidation effects can be further reduced. Less out-of-plane decompaction and surface roughness are expected. Therefore, a repetition of the research on tape pre-tension (only for 5N) is needed in combination with the use of resin-rich tapes.

### **Resin-rich surface tapes**

In general, further solid research could be performed on resin-rich surface tapes. Since the material used during the current study showed variation in resin-richness across the width (material is off-spec), effects were measured which were not necessarily a result of deconsolidation. For instance, a larger void content was measured for resin-rich tapes compared to resin-poor tapes. However, the data was inconclusive to demonstrate only the effect of a resin-rich surface on void content. One of the most critical parameters (in aerospace industry) for the final product quality is void content, therefore a deeper understanding of the deconsolidation mechanisms affecting void content is needed.

**Thickness of the resin-rich layer on the top surface**

Additional research can be performed on quantifying the thickness of the resin-rich layer (for instance with Scanning Electron Microscopy) on the top surface. During the current study the resin-richness measurements were based on top surface micrographs. This provided 2D data and information on whether a resin-rich surface was present or not. A qualitative comparison was made between the resin-richness observed from top surface micrographs and cross-sectional micrographs. It could be seen from the cross-sectional micrographs that resin-rich areas shows a thicker resin-rich layer on the top surface. It is expected that variation in the thickness of the resin-rich layer across the width at the nip-point location will affect the heat absorption into the tape. Further investigation into the effect of the thickness of the resin-rich layer on the top surface is needed. This will help in understanding the mechanisms that will cause deconsolidation for resin-rich surface thermoplastic CF/PEEK tapes.

**Data analysis tape pre-tension research**

Increasing the level of tape pre-tension showed formation of a highly non-uniform temperature distribution across the width at the nip-point location. As a result of the current measurement methodologies the data showed inconclusive results. Surface roughness and thickness change were only measured locally at four distinct locations. Void content and the change in width were measured globally. The local heat absorption makes it hard to draw solid conclusions on the effect of tape pre-tension on the deconsolidation response. Re-processing the temperature together with the data from the LLS can provide additional information on the deformation of the tape in out-of-plane direction and width direction during the heating phase. Additionally, the methodologies for surface roughness and thickness change measurements can be further optimized by also measuring at the exact locations where the local heat absorption does occur.

**Tape pre-tension force**

For higher pre-tension levels (10N and 15N) the uniformity of the temperature distribution across the width decreased. Since for a tape pre-tension of 5N a more uniform temperature distribution was shown, it is expected that an optimum tape pre-tension force exist around 5N. This corresponds to low tape pre-tension used in actual LAFP placement machines [11]. Further investigation is needed in optimization of the tape pre-tension level (in the range of  $5N \pm 3N$ ) in an attempt to minimize the effect of deconsolidation.

# A

## Conceptual design of a pre-tension setup

A preliminary design of the pre-tension setup is sketched in Figure A.1.

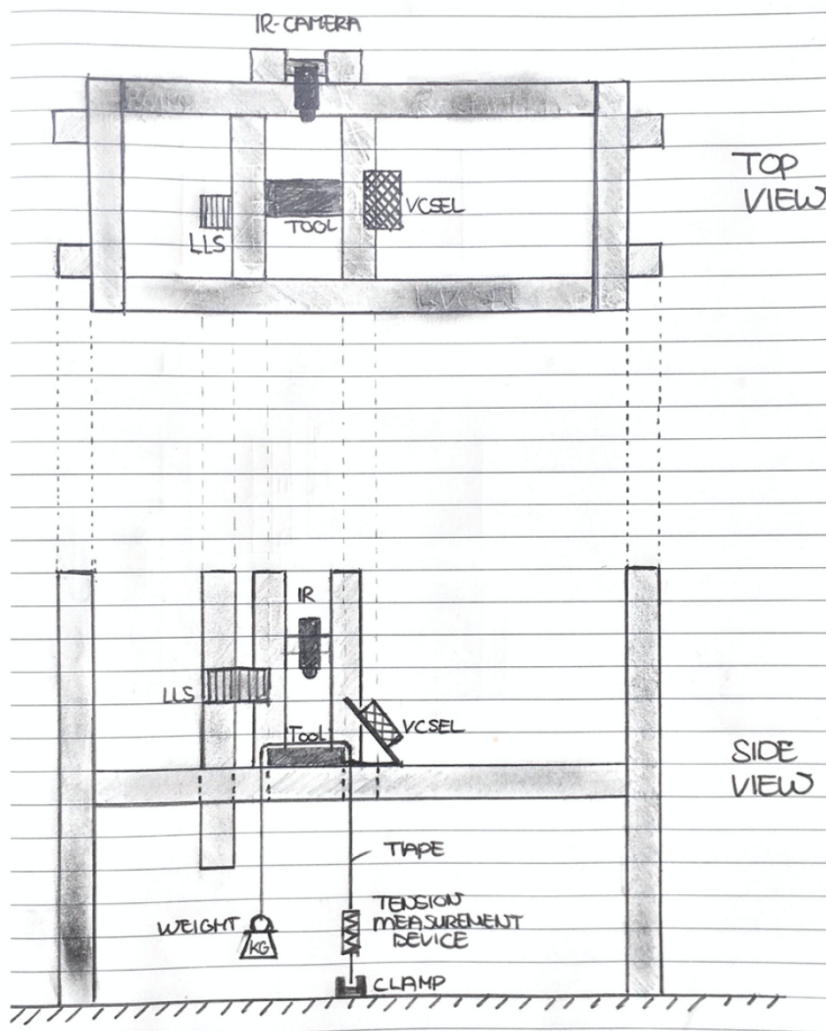


Figure A.1: Schematic preliminary design of pre-tension setup, top and side view

The proof-of-concept of the pre-tension setup is shown in Figure A.2.



Figure A.2: Proof-of-concept tape pre-tension setup

# B

## Load cell calibration

An in-house made load cell was used to measure the pre-tension in thermoplastic prepreg tapes prior to the rapid heating phase. The load cell was part of the static pre-tension experimental setup and was therefore calibrated before. The calibration itself was performed by using weights, since the pre-tension applied to the thermoplastic prepreg tapes was force driven. In Figure B.1 the load cell calibration setup is shown. A chain attached via a loop to a horizontal beam made it possible to hang the load cell free from the surroundings in the air. The upper side of the load cell was connected to the chain. On the lower side a mass holder was connected on which disk masses could be applied.

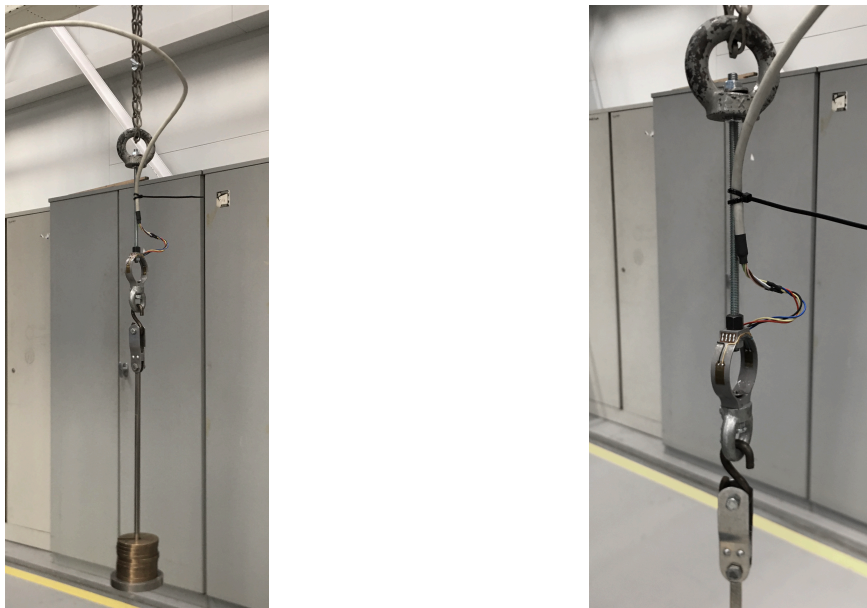


Figure B.1: Load cell calibration setup

Before the calibration was started the exact mass of the weights were determined using a scale. Three calibration runs were performed subsequently for which the total mass applied to the load cell was increased step-by-step towards 40 Newton and subsequently released again. In Figure B.2 the jumps in the graph could clearly be noticed and indicate an increase in weight of approximately 5 Newton. The total weight is increasing with decreasing output signal ration as indicated in Figure B.2. Around the jump to the next weight level disturbances could be observed in the graph, therefore 20 data points in the middle were taken such that the peaks caused by manually adding weight were excluded.

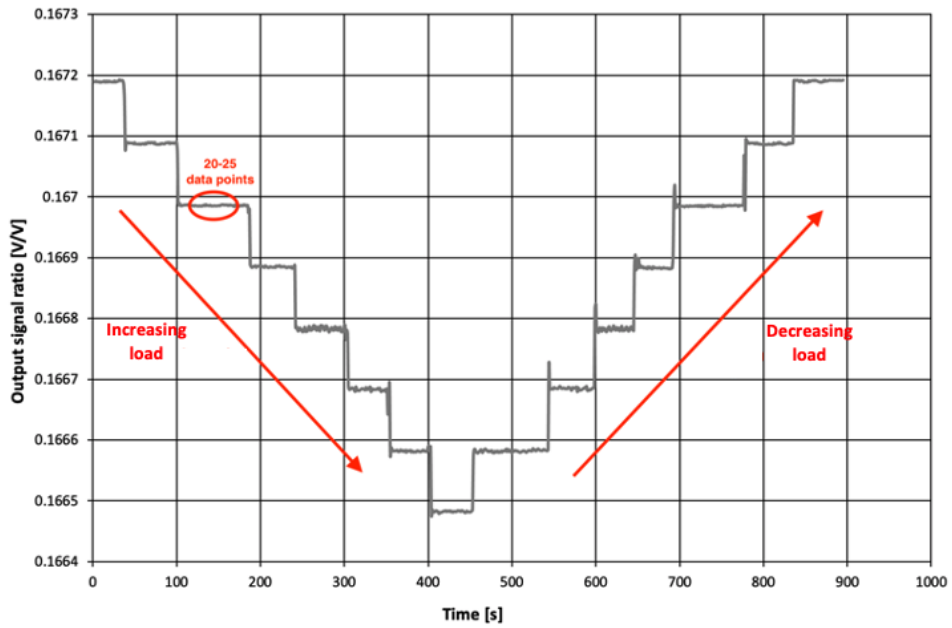


Figure B.2: Load cell calibration run

The output signal ratio per weight level was averaged over the 20 data points. For three calibration runs the average data points were plotted together in one graph as can be seen in Figure B.1. A linear regression curve was fitted to the given data. The linear relationship between output signal ratio and the force can be described by the following equation:

$$y = -48941x + 8188 \quad (B.1)$$

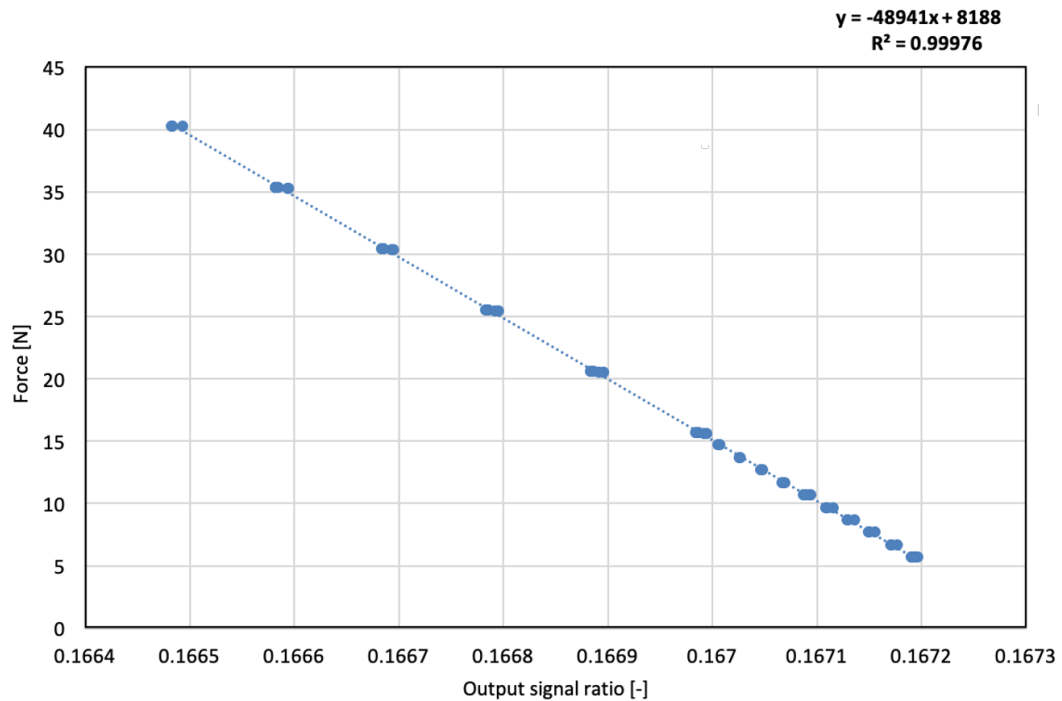


Figure B.3: Load cell calibration curve

# C

## IR-camera calibration

A calibration setup consisting of a VCSEL, IR-camera and tool (including tape specimen) was used to calibrate the IR-camera. The VCSEL was positioned perpendicular to the tape, by doing this, 2 separate zones in the tape could be heated as equally as possible and with the same distance to the VCSEL. The IR-camera was positioned at an inclination angle of  $55^\circ$  with respect to the tape as can be seen in figure C.1.

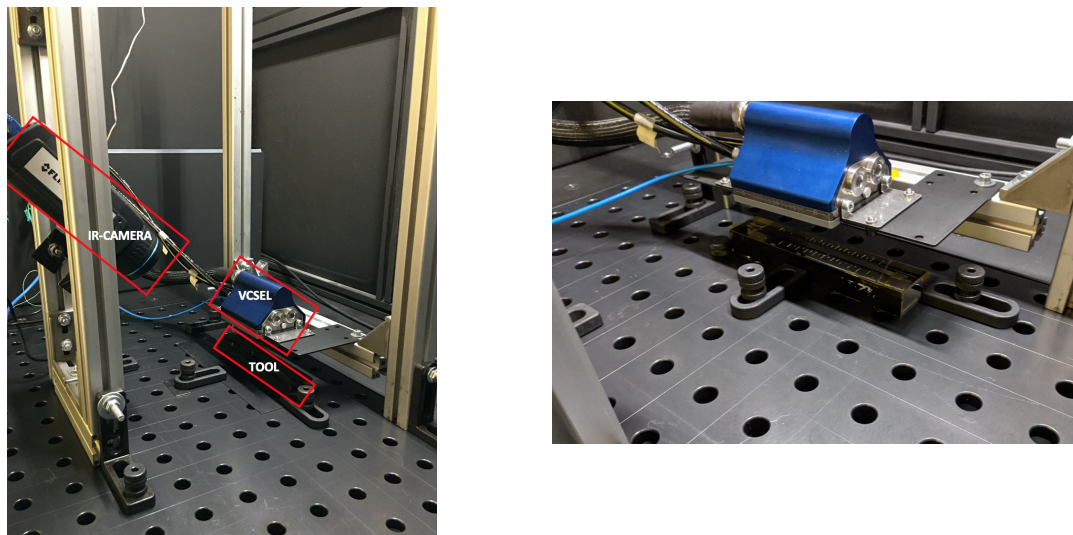


Figure C.1: Calibration setup, VCSEL positioned orthogonal w.r.t. tool surface

The calibration of the FLIR A655sc IR-camera was based on ASTM Standard E1933 [66] and the methodology similar to Choudhary [19]. The experiments were performed in parallel with Bussink[67]. In order to determine the emissivity of CF/PEEK thermoplastic prepreg material the VCSEL laser was used to heat two separate zones. Zones 5-6 (left) and 10-11 (right) were activated, at the location of the left zone a K-type thermocouple was attached by ultrasonic spot welding to the thermoplastic prepreg tape. Laser heating experiments were performed and the temperatures were measured by the thermocouple at the left zone and with the IR-camera at the right zone respectively. The IR-camera captured the temperature at the right zone as an average over 3x3 pixels. By adjusting the emissivity value in the FLIR software, the IR-camera reading was matched. The distance from the IR-camera to the specimen was set to 0.25m. All calibration measurements were performed at 200W laser power equally divided over the zones and 500ms heating time. The maximum temperature reached here was  $200^\circ\text{C}$  due to problems with the thermocouple reading at higher temperatures. Above the glass transition temperature the thermoplastic prepreg tape starts to deform which caused the thermocouple to become unattached from the tapes' surface. Assumption is made here that emissivity stays constant over the entire heating phase. The emissivity calibration experiments were performed using both Toray/Ten Cate material (see Figure C.3) as well as Suprem material (see Figure C.4). For Toray/Ten Cate

thermoplastic prepreg CF/PEEK material an average emissivity of 0.80 was found over 4 calibration experiments. For Suprem CF/PEEK thermoplastic prepreg an average emissivity of 0.81 was found over 4 calibration experiments.

In previous research of Choudhary and Celik et al. [19, 29] an emissivity of 0.84 was found for CF/PEEK and 0.855 for CF/PEKK however processing temperature was reached during these experiments. Celik et al [68] found an emissivity of 0.85 for CF/PEKK material for which the calibration was performed around 220 °C. According to M. Di Fransesco et al. [69] the apparant emissivity was found to be 0.80 for CF/PEEK material in a temperature range from 350-450 °C. A methodology according to the ASTM E1933 standard was used here.

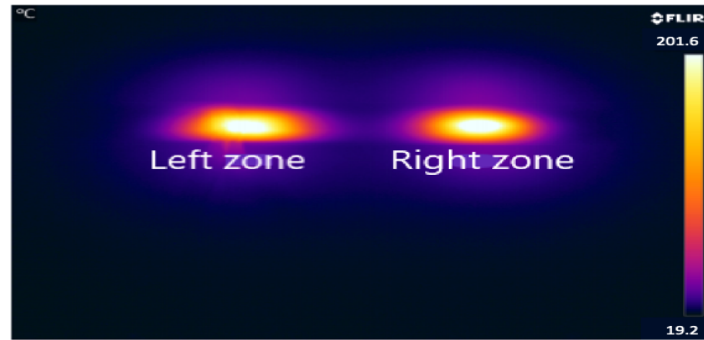
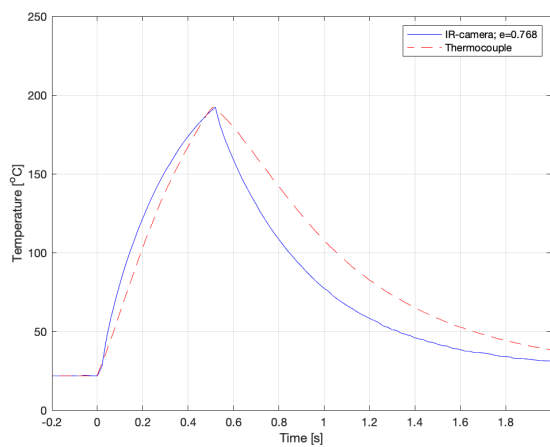
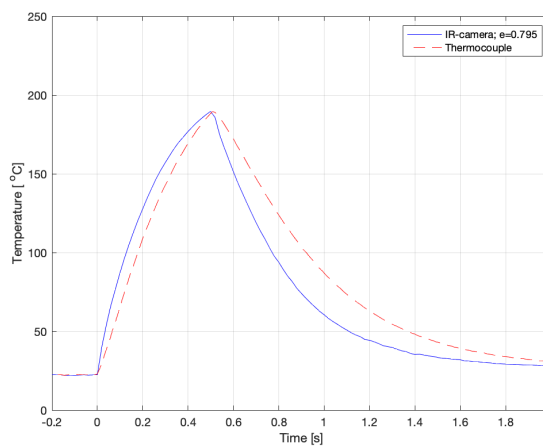


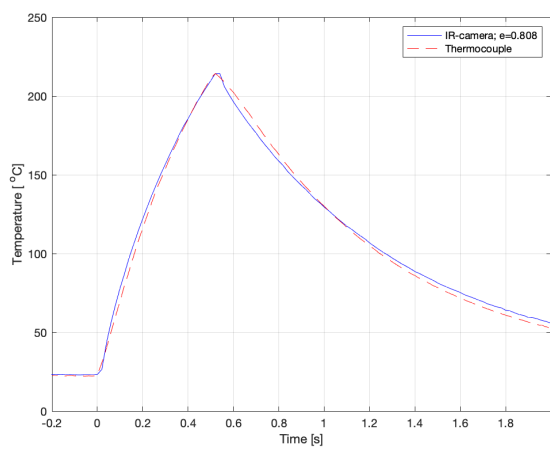
Figure C.2: Thermal image captured by IR-camera during emissivity calibration



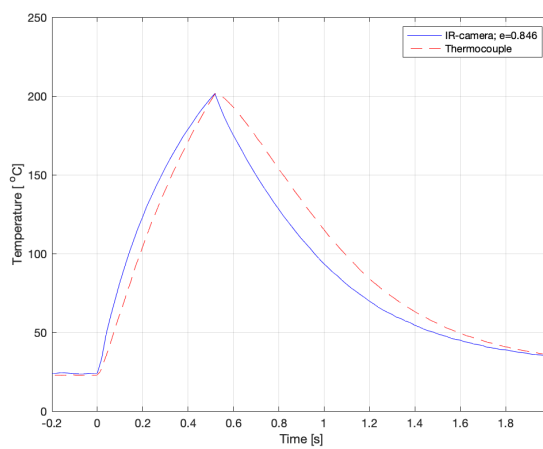
(a) Emissivity calibration - Toray/Ten Cate - Sample 1



(b) Emissivity calibration - Toray/Ten Cate - Sample 2

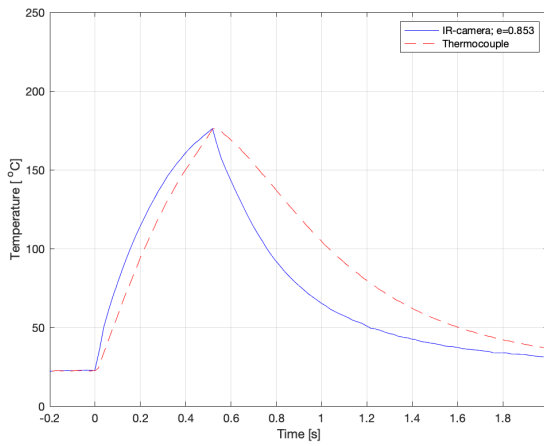


(c) Emissivity calibration - Toray/Ten Cate - Sample 3

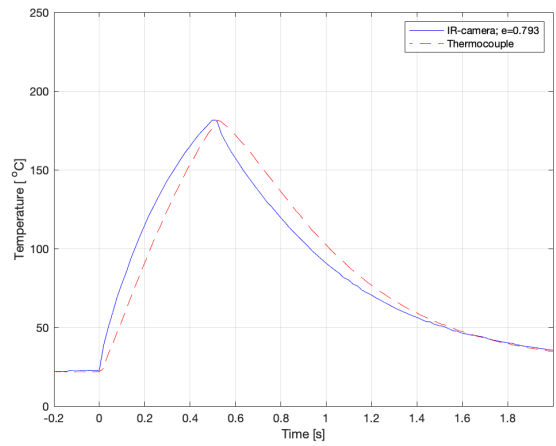


(d) Emissivity calibration - Toray/Ten Cate - Sample 4

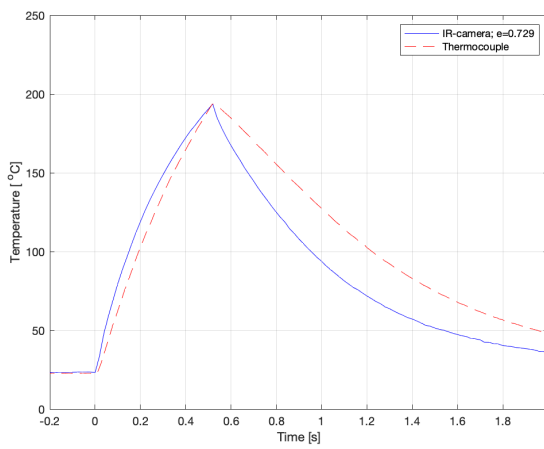
Figure C.3: Emissivity calibration curves Toray/Ten Cate thermoplastic prepreg CF/PEEK



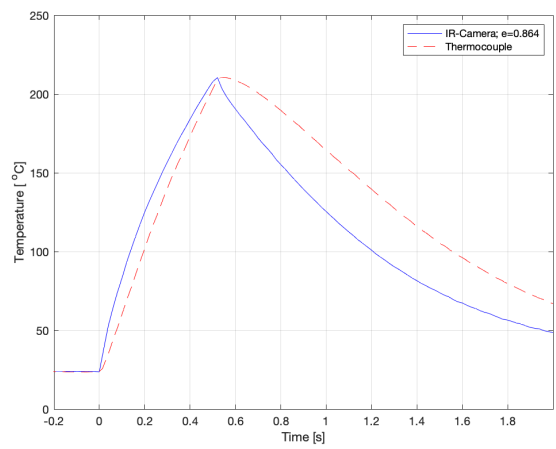
(a) Emissivity calibration - Suprem - Sample 1



(b) Emissivity calibration - Suprem - Sample 2



(c) Emissivity calibration - Suprem - Sample 3



(d) Emissivity calibration - Suprem - Sample 4

Figure C.4: Emissivity calibration curves Suprem thermoplastic prepreg CF/PEEK

# Bibliography

- [1] C. Kukla et al. "Joining of Thermoplastic Tapes with Metal Alloys Utilizing Novel Laser Sources and Enhanced Process Control in a Tape Placement Process". In: *Procedia CIRP* 66 (2017), pp. 85–90. DOI: 10.1016/j.procir.2017.03.307.
- [2] E. Oromiehie et al. "Automated fibre placement based composite structures: Review on the defects, impacts and inspections techniques". In: *Composite Structures* 224 (2019), p. 110987. DOI: 10.1016/j.compstruct.2019.110987.
- [3] R. Schledjewski. "Thermoplastic tape placement process - In situ consolidation is reachable". In: *Plastics, Rubber and Composites* 38.9-10 (2009), pp. 379–386. DOI: 10.1179/146580109X12540995045804.
- [4] Composites World. *Evolving AFP for the next generation*. URL: <https://www.compositesworld.com/blog/post/evolving-afp-for-the-next-generation>. Accessed: 05-09-2019.
- [5] Airbus. *Global Market Forecast 2018-2037*. URL: <https://www.airbus.com/content/dam/corporate-topics/publications/media-day/GMF-2018-2037.pdf>. Accessed: 05-09-2019.
- [6] Composites World. *I want to say two words to you: thermoplastic tapes*. URL: <https://www.compositesworld.com/articles/i-want-to-say-two-words-to-you-thermoplastic-tapes>. Accessed: 05-09-2019.
- [7] C. Brecher et al. "Innovative manufacturing of 3D-lightweight components: New insights in the processing of continuous fibre-reinforced thermoplastic prepregs". In: *Laser Technik Journal* 8.5 (2011), pp. 36–40. DOI: 10.1002/latj.201190057.
- [8] C.M. Stokes-Griffin and P. Compston. "The effect of processing temperature and placement rate on the short beam strength of carbon fibre-PEEK manufactured using a laser tape placement process". In: *Composites Part A: Applied Science and Manufacturing* 78 (2015), pp. 274–283. DOI: 10.1016/j.compositesa.2015.08.008. URL: <http://dx.doi.org/10.1016/j.compositesa.2015.08.008>.
- [9] E. Beyeler, W. Phillips, and S. I. Güçeri. "Experimental Investigation of Laser-Assisted Thermoplastic Tape Consolidation". In: *Journal of Thermoplastic Composite Materials* 1 (1988), pp. 107–121. DOI: 10.1177/089270578800100109.
- [10] A.J. Comer et al. "Mechanical characterisation of carbon fibre-PEEK manufactured by laser-assisted automated-tape-placement and autoclave". In: *Composites Part A: Applied Science and Manufacturing* 69 (2015), pp. 10–20. DOI: 10.1016/j.compositesa.2014.10.003.
- [11] D.B. Miracle and S.L. Donaldson. *ASM Handbook: Volume 21, Composites*. ASM International, 2001. Chap. 60. Fiber Placement. DOI: 10.1361/asmhba0003410.
- [12] F C Campbell. "Thermoset Composite Fabrication". In: *Structural Composite Materials* (2010), pp. 119–182.
- [13] M.A. Khan and R. Schledjewski. "Influencing factors for an online consolidating thermoplastic tape placement process". In: *ICCM International Conferences on Composite Materials* (2009).
- [14] M.A. Khan, P. Mitschang, and R. Schledjewski. "Identification of Some Optimal Parameters to Achieve Higher Laminate Quality Through Tape Placement Process". In: *Advances in Polymer Technology* 29 (2010), pp. 98–111. DOI: 10.1002/adv.20177.
- [15] O Celik. *Consolidation during laser assisted fiber placement Heating, compaction and cooling phases*. 2021. DOI: 10.4233/uuid:375598ed-f138-471c-9a1e-e28ee3820855.
- [16] Mahoor Mehdikhani et al. "Voids in fiber-reinforced polymer composites: A review on their formation, characteristics, and effects on mechanical performance". In: *Journal of Composite Materials* 53.12 (2019), pp. 1579–1669. DOI: 10.1177/0021998318772152.
- [17] T. Kok. *On the consolidation quality in laser assisted fiber placement: the role of the heating phase*. University of Twente, Netherlands, 2018. DOI: 10.3990/1.9789036546065.

- [18] T. Kok et al. "Quantification of tape deconsolidation during laser assisted fiber placement". In: *3rd International Symposium on Automated Composites Manufacturing, ACM* (2017). DOI: 10.1017/CB09781107415324.004.
- [19] A. Choudhary. *Thermal deconsolidation of thermoplastic prepreg tapes during Laser-Assisted Fiber Placement*. Delft University of Technology, 2019.
- [20] R. Schledjewski and A. Miaris. "Thermoplastic tape placement by means of diode laser heating". In: *International SAMPE Symposium and Exhibition (Proceedings)* 54 (May 2009).
- [21] W.J.B. Grouve et al. "Weld strength assessment for tape placement". In: *International Journal of Material Forming* 3.SUPPL. 1 (2010), pp. 707–710. DOI: 10.1007/s12289-010-0868-z.
- [22] W.J.B. Grouve et al. "On the weld strength of in situ tape placed reinforcements on weave reinforced structures". In: *Composites Part A: Applied Science and Manufacturing* 43.9 (2012), pp. 1530–1536. DOI: 10.1016/j.compositesa.2012.04.010.
- [23] D. Ray et al. "Fracture toughness of carbon fiber/polyether ether ketone composites manufactured by autoclave and laser-assisted automated tape placement". In: *Journal of Applied Polymer Science* 132.11 (2015), pp. 1–10. DOI: 10.1002/app.41643.
- [24] E.N. Cogswell. *Thermoplastic Aromatic Polymer Composites*. Butterworth-Heinemann Ltd, Oxford, 1992. Chap. 4.
- [25] S. Gao and J. Kim. "Cooling rate influences in carbon fibre/PEEK composites. PartII:interlaminar fracture toughness". In: *Composites Part A: Applied Science and Manufacturing* 32 (6 2001), pp. 763–774. DOI: 10.1016/S1359-835X(00)00188-3.
- [26] Zhi Bin Wang et al. "A review of tensioner for automated fiber placement". In: *Advanced Materials Research* 740 (2013), pp. 183–187. DOI: 10.4028/www.scientific.net/AMR.740.183.
- [27] Jolie Frketic, Tarik Dickens, and Subramanian Ramakrishnan. "Automated manufacturing and processing of fiber-reinforced polymer (FRP) composites: An additive review of contemporary and modern techniques for advanced materials manufacturing". In: *Additive Manufacturing* 14 (2017), pp. 69–86. DOI: 10.1016/j.addma.2017.01.003.
- [28] Yi Liu, Qiang Fang, and Yinglin Ke. "Modeling of Tension Control System with Passive Dancer Roll for Automated Fiber Placement". In: *Mathematical Problems in Engineering* 2020 (2020). DOI: 10.1155/2020/9839341.
- [29] O. Celik et al. "Deconsolidation of thermoplastic prepreg tapes during rapid laser heating". In: *Composites Part A: Applied Science and Manufacturing* 149 (2021). DOI: doi.org/10.1016/j.compositesa.2021.106575..
- [30] C. M. Stokes-Griffin and P. Compston. "A combined optical-thermal model for near-infrared laser heating of thermoplastic composites in an automated tape placement process". In: *Composites Part A: Applied Science and Manufacturing* 75 (2015), pp. 104–115. DOI: 10.1016/j.compositesa.2014.08.006.
- [31] R. Funck and M. Neitzel. "Improved thermoplastic tape winding using laser or direct-flame heating". In: *Composites Manufacturing* 6.3-4 (1995), pp. 189–192. DOI: 10.1016/0956-7143(95)95010-V.
- [32] C.M. Stokes-Griffin et al. "Thermal modelling of the laser-assisted thermoplastic tape placement process". In: *Journal of Thermoplastic Composite Materials* 28.10 (2015), pp. 1445–1462. DOI: 10.1177/0892705713513285.
- [33] C.M. Stokes-Griffin et al. *Modelling the Automated Tape Placement of Thermoplastic Composites with In-Situ Consolidation*. 2012, pp. 61–68. DOI: 10.1007/978-3-642-24145-1\_9.
- [34] T. Weiler et al. "Optical modelling of VCSEL-assisted thermoplastic tape placement". In: *ECCM 2016 - Proceeding of the 17th European Conference on Composite Materials* June 2016 (2016).
- [35] H. Moench et al. "High-power VCSEL systems and applications". In: *High-Power Diode Laser Technology and Applications XIII* 9348.March (2015), 93480W. DOI: 10.1117/12.2076267.
- [36] H. Moench and G. Derra. "High Power VCSEL Systems". In: *Laser Technik Journal* 11.2 (2014), pp. 43–47. DOI: 10.1002/latj.201400024.

- [37] TRUMPF Photonic Components GmbH. *High Power Infrared Sources for Industrial Heating*. URL: [https://www.trumpf.com/filestorage/TRUMPF\\_Master/Products/Photonic\\_Components/Broschures/TRUMPF-Photonics-Components-Flyer-High-Power-Infrared-Sources-for-Industrial-Heating.pdf](https://www.trumpf.com/filestorage/TRUMPF_Master/Products/Photonic_Components/Broschures/TRUMPF-Photonics-Components-Flyer-High-Power-Infrared-Sources-for-Industrial-Heating.pdf). Accessed: 25-10-2019.
- [38] J.M. Haake. "High power diode laser-assisted fiber placement of composite structure". In: *24th International Congress on Applications of Lasers and Electro-Optics, ICALEO 2005 - Congress Proceedings* 907 (2005), pp. 437–443. DOI: 10.2351/1.5060524.
- [39] M. Narnhofer and R. Schledjewski. "Simulation of the Tape-Laying Process for Thermoplastic Matrix Composites". In: *Advances in Polymer Technology* 32.S1 (2013), E705–E713. DOI: 10.1002/adv.21312.
- [40] C.M. Stokes-Griffin and P. Compston. "Laser-Assisted Tape Placement of Thermoplastic Composites: The Effect of Process Parameters on Bond Strength". In: *Sustainable Automotive Technologies 2013* (2013), pp. 133–141. DOI: 10.1007/978-3-319-01884-3\_13.
- [41] T. Weiler. *Thermal Skin Effect in Laser-Assisted Tape Placement of Thermoplastic Composites*. Apprimus Verlag, Aachen, 2019. DOI: 10.18154/RWTH-2019-06638.
- [42] Ozan Çelik et al. "Intimate contact development during laser assisted fiber placement: Microstructure and effect of process parameters". In: *Composites Part A: Applied Science and Manufacturing* 134 (2020), p. 105888. ISSN: 1359835X. DOI: 10.1016/j.compositesa.2020.105888.
- [43] W.J.B. Grouve et al. "Optimization of the tape placement process parameters for carbon-PPS composites". In: *Composites Part A: Applied Science and Manufacturing* 50 (2013), pp. 44–53. DOI: 10.1016/j.compositesa.2013.03.003.
- [44] K. Yassin and M. Hojjati. "Processing of thermoplastic matrix composites through automated fiber placement and tape laying methods: A review". In: *Journal of Thermoplastic Composite Materials* 31 (2018), pp. 1676–1725. DOI: 10.1177/0892705717738305.
- [45] M.A. Lamontia and M.B. Gruber. "Remaining developments required for commercializing in situ thermoplastic atp". In: *International SAMPE Symposium and Exhibition (Proceedings)* 52 (2007).
- [46] Z. Qureshi et al. "In situ consolidation of thermoplastic prepreg tape using automated tape placement technology: Potential and possibilities". In: *Composites Part B: Engineering* 66 (2014), pp. 255–267. DOI: 10.1016/j.compositesb.2014.05.025.
- [47] M. Di Francesco et al. "Influence of laser power density on the mesostructure of thermoplastic composite preforms manufactured by Automated Fibre Placement". In: *International SAMPE Technical Conference* January 20 (2016).
- [48] C. M. Stokes-Griffin et al. "Manufacture of steel-CF/PA6 hybrids in a laser tape placement process: Effect of first-ply placement rate on thermal history and lap shear strength". In: *Composites Part A: Applied Science and Manufacturing* 111.May (2018), pp. 42–53. DOI: 10.1016/j.compositesa.2018.05.007.
- [49] J. Wolfrath, V. Michaud, and J.-A.E. Manson. "Deconsolidation in glass mat thermoplastic composites: Analysis of the mechanisms". In: *Composites Part A: Applied Science and Manufacturing* 36.12 (2005), pp. 1608–1616. DOI: 10.1016/j.compositesa.2005.04.001.
- [50] L. Ye et al. "De-consolidation and re-consolidation in CF/PPS thermoplastic matrix composites". In: *Composites Part A: Applied Science and Manufacturing* 36.7 (2005), pp. 915–922. DOI: 10.1016/j.compositesa.2004.12.006.
- [51] F. Henninger, L. Ye, and K. Friedrich. "Deconsolidation behaviour of glass fibre-polyamide 12 composites sheet material during post-processing." In: *Plastics Rubber and Composites Processing and Applications* 28.6 (1998), pp. 287–292.
- [52] A. Beehag and L. Ye. "Role of cooling pressure on interlaminar fracture properties of commingled CF/PEEK composites". In: *Composites Part A: Applied Science and Manufacturing* 27A.3 (1996), pp. 175–182. DOI: 10.1016/1359-835X(95)00027-Y.
- [53] C. Ageorges, L. Ye, and M. Hou. "Experimental investigation of the resistance welding of thermoplastic-matrix composites. Part II: optimum processing window and mechanical performance". In: *Composites Science and Technology* 60.8 (June 2000), pp. 1191–1202. DOI: 10.1016/S0266-3538(00)00025-7.

- [54] M. Brzeski and P. Mitschang. "Deconsolidation and its interdependent mechanisms of fibre reinforced polypropylene". In: *Polymers and Polymer Composites* 23.8 (2015), pp. 515–524. DOI: 10.1177/096739111502300801.
- [55] L. Ye, M. Lu, and Y. W. Mai. "Thermal de-consolidation of thermoplastic matrix composites-I. Growth of voids". In: *Composites Science and Technology* 62.16 (2002), pp. 2121–2130. DOI: 10.1016/S0266-3538(02)00144-6.
- [56] R.M. Ogorkiewiz. *Thermoplastics – properties and design*. London, New York, Wiley, 1974.
- [57] J.D. Ferry. *Viscoelastic properties of polymers*. New York, Wiley, 1980.
- [58] M. Lu, L. Ye, and Y.W. Mai. "Thermal de-consolidation of thermoplastic matrix composites-II. "Migration" of voids and "re-consolidation"". In: *Composites Science and Technology* 64.2 (2004), pp. 191–202. DOI: 10.1016/S0266-3538(03)00233-1.
- [59] M.A. Khan, P. Mitschang, and R. Schledjewski. "Tracing the void content development and identification of its effecting parameters during in situ consolidation of thermoplastic tape material". In: *Polymers & Polymer Composites* 18.1 (2010), pp. 1–16. DOI: 10.1177/096739111001800101.
- [60] T. Kok et al. "Intimate contact development in laser assisted fiber placement". In: *ECCM 2016 - Proceeding of the 17th European Conference on Composite Materials* June (2016).
- [61] S. Ranganathan, S.G. Advani, and Mark A. Lamontia. "A Non-Isothermal Process Model for Consolidation and Void Reduction During In-Situ Tow Placement of Thermoplastic Composites". In: *Journal of Composite Materials* 29.8 (1995), pp. 1040–1062. DOI: 10.1177/002199839502900803.
- [62] F Yang and R Pitchumani. "A fractal Cantor set based description of interlaminar contact evolution during". In: *Journal of Materials Science* 36 (2001), pp. 4661–4671.
- [63] R. Pitchumani et al. "Analysis of transport phenomena governing interfacial bonding and void dynamics during thermoplastic tow-placement". In: *International Journal of Heat and Mass Transfer* 39.9 (1996), pp. 1883–1897. DOI: 10.1016/0017-9310(95)00271-5.
- [64] Toray advanced composites. *Aerospace advanced composite materials selector guide*. URL: [https://www.toraytac.com/media/99290c4d-4856-49e5-8ca7-d338c8f144f5/rfj7rQ/TAC/Documents/Selector%20Guides/Aerospace%20selector%20guides/Toray\\_Aerospace-Advanced-Composite-Materials\\_Selector-Guide.pdf](https://www.toraytac.com/media/99290c4d-4856-49e5-8ca7-d338c8f144f5/rfj7rQ/TAC/Documents/Selector%20Guides/Aerospace%20selector%20guides/Toray_Aerospace-Advanced-Composite-Materials_Selector-Guide.pdf). Retrieved on: 09-10-2019.
- [65] Suprem. *Suprem T Technical Facts*. URL: <https://www.suprem.ch/suprem-t-wide/>. Accessed: 23-09-2021.
- [66] *ESTM E1933 - 14. Standard Practice for Measuring and Compensating for Emissivity Using Infrared Imaging Radiometers. Standard, American Society for Testing and Materials*. 2018.
- [67] T. Bussink. *Effect of Rapid Laser Deconsolidation on Intimate Contact Development*. Delft University of Technology, 2019.
- [68] O. Celik et al. "Deconsolidation of thermoplastic prepreg tapes during rapid laser heating". In: *Composites Part A: Applied Science and Manufacturing* 134.105888 (2020). DOI: 10.1016/j.compositesa.2020.105888..
- [69] M. Di Francesco et al. "Deconsolidation of thermoplastic prepreg tapes during rapid laser heating". In: *Composites Part A: Applied Science and Manufacturing* 101 (2017), pp. 408–421. DOI: doi.org/10.1016/j.compositesa.2017.06.015.